The assessment of UAV-based multispectral imagery to monitor lichen-dominated biological soil crusts response to fog and disturbances, Central Namib

Ailly Nanguloshi Nambwandja

Thesis submitted in partial fulfillment of the requirements for the degree of Master of Natural Resources Management at the Namibia University of Science and Technology

NAMIBIA UNIVERSITY OF SCIENCE AND TECHNOLOGY

Supervisor: Professor Ben Strohbach
(Namibia University of Science and Technology)
Co-Supervisor: Dr Nichola Knox
(Namibia University of Science and Technology)

October 2022

Declaration

I, *Ailly Nanguloshi Nambwandja*, hereby declare that the work contained in the thesis entitled: *The assessment of UAV-based multispectral imagery to monitor lichen-dominated biological soil crusts response to fog and disturbances, Central Namib* is my own original work and that I have not previously in its entirety or in part submitted it at any university or higher education institution for the award of a degree.

Signature:……………………………………………… Date: …………………………….

Retention and Use of Thesis

I, *Ailly Nanguloshi Nambwandja*, being a candidate for the degree of *Master of Natural Resource Management* accept the requirements of the Namibia University of Science and Technology relating to the retention and use of theses deposited in the Library and Information Services.

In terms of these conditions, I agree that the original of my thesis deposited in the Library and Information Services will be accessible for purposes of study and research, in accordance with the normal conditions established by the Librarian for the care, loan or reproduction of theses.

Signature:……………………………………………… Date: …………………………….

Table of Contents

List of Figures

List of Tables

List of Acronyms

DN: Digital Numbers

GIS: Geographic Information Systems

VI: Vegetation Indices

NDVI: Normalized Difference Vegetation Index

NDRE: Normalized Difference Red-Edge Index

SAVI: Soil-Adjusted Vegetation Index

AOI: Area of Interest

UAV: Unmanned Aerial Vehicle

RS: Remote sensing

GPS: Global Positioning System

ND: Digital Number

GCP: Ground Control Point

DSM: Digital Surface Model

GLONASS: Globalnaya Navigazionnaya Sputnikovaya Sistema

RGB: Red Green Blue

RE: Red edge

NIR: Near Infrared

BRDF Bidirectional Distribution Function

NOAA: National Oceanic and Atmospheric Administration

Acknowledgements

First and foremost, I want to express my sincere thanks to my mentor and supervisor, Dr. Ben Strohbach, for all of his academic advice and support over the course of this project. I am appreciative of the chance to collaborate with such an academic on everything from proposal writing through data gathering, analysis, and report writing. I also want to thank Dr. Knox Nichola as my academic co-supervisor for guiding me through the writing process. I would also like to give thanks the Gobabeb-Namib Research Institute and its local and international associates for the support and guidance. I most specifically want to express my gratitude to Mr. Eugene Marais as my research supervisor at Gobabeb, and for her help with field data gathering. I also give many thanks to Dr. Gillian Maggs-Kolling for support, guidance and advice. I am grateful to everyone who helped me while completing my research at various phases, including Eric Norton, Nataniel Ndeilenga, Iipinge Ndelimona, Ulrich, Leandri Wessels, all of my friends, and everyone else. This work was funded by the German Federal Ministry of Education and Research under the “Support for SASSCAL Science Services – Module B: SASSCAL Biodiversity Monitoring 2.0 – Harvesting the products of 17 years of biodiversity observation combined with capacity development and transfer to African partners” project, Commission number (FKZ) 01 LG 1201 N. Therefore, I am especially appreciative of the support from the Southern African Science Service Centre for Climate Change and Adaptive Land Management (SASSCAL - Work package SP2 WP3), which paid for both the tuition and the entire research project. And the NNF/Go-Green Netbank for co-funding.

Dedication

My mother, my big sisters and my deceased grandmothers are honored in this thesis. Even though grand ma Ndapewa and Frieda, you were unable to watch me become successful. I am certain that you would have been pleased with the woman I have grown into. There isn't a day that goes by that I don't think of you. I appreciate the woman in my life. This thesis is ours

Abstract

Lichen-dominated biological soil crusts (BSCs or biocrusts) are a major contributor to biodiversity and ecosystem services of desert environments. There appropriate monitoring of lichen fields of the hyper-arid coastal Namib Desert is important to understanding their greater ecological functions, such as vital CO_2 sinks, and for management of socio-economic land use practices (i.e. mining, tourism, off-road tracks) which destroy the endemic, fragile and slow recovering lichens. Thanks to advanced remote sensing techniques such as the use of Unmanned Aerial Vehicles (UAVs or drones), lichen fields can be monitored, whilst minimising the environmental impact of traditional ground-based ecological research, as well as overcoming challenges in monitoring lichens with the satellite datasets, piloted aircraft. The objectives of this study was to assess the effects of hourly sunshine intensity on the use of UAV-based multispectral imagery for monitoring lichen-dominated biological soil crusts in the hyper-arid Central Namib Desert. We then assess the applications UAV-based NDVI to observe lichen photosynthetic activity response to moisture input, topography and disturbances, as well as to assess the influence of micro-topography and disturbances in off-road tracks on lichen coverage.

We tested the performance of UAV-based Parrot Sequoia multispectral sensor by acquiring time series flights from 08:00 to 17:00 during a fog day. Time series of radiometrically and atmospherically corrected and uncorrected multispectral image datasets (i.e. reflectance images and vegetation indices) were compare it to solar elevation. Influence of brightness effects in sample plot on image values was tested with one-way ANOVA and Tukey HSD pot-hoc test for pairwise comparisons. There was statistical significant difference in means of the sample plots with $p < 0.05$. We also gathered time series UAV-based NDVI images on fog and non-fog day derived the temporal patterns of lichen photosynthetic activity in responding to wet and dry conditions, overtime. These UAV observations were supported with ground cover observation of lichens. Statistical analysis was performed to determine presence of significant differences of lichen cover and NDVI response between micro-topographic habitats (i.e. ridges, windward and leeward sides of the relief), and as well in landforms such as plains, river washes and tracks. The one-way ANOVA and Student-test (t-tests), were considered significant at $p < 0.05$ for both UAV and ground observations. Polynomial regression analysis of the relationship between elevation and ground lichen cover and NDVI was significantly correlated with p-values of < 0.05.

Well illuminated good quality images can be captured at low solar elevation, in morning images at 08:00 and in the later afternoon at 17:00. Midday images taken between 10:00 and 15:00 at higher solar elevation are heavily impacted by brightness effects. The radiometrically corrected images and NDVI were more accurate than the raw uncorrected images. UAV-based NDVI can estimate photosynthetic activity when lichens are hydrated by fog or higher air humidity, as opposed to when they are desiccated and photosynthetic activity is inhibited. Elevation is good predictor lichen cover and photosynthetic activity. Lichen cover is heavily impacted by off-road tracks. The topographic attribute influence the distribution of lichen cover and lichen species diversity. This research study has provided insights into a means to monitor these sensitive environments. It also enables informed decision making to manage natural resource and regulate socio-economic land-use.

Keywords: Unmanned Aerial Vehicle (UAV) remote sensing, biological soil crusts (BSCs), Namib Desert Lichen fields, multi-spectral imagery, fog-driven ecosystems, off-road driving disturbance

Chapter 1: General Introduction

1.1 Background

1.1.1 Lichen Biota in Coastal Fog Deserts

The hot, hyper-arid deserts have limited resources to support vascular vegetation growth. Within the coastal fog zone, however, conditions often favour the growth of non-vascular lichen communities. Lichens form part of the biological soil crusts (BSCs or bio-crusts) composed of photosynthesizing organisms, such as cyanobacteria, lichens, green algae, as well as heterotrophic fungi and bacteria (Karnieli *et al.* 2003, Loris *et al.* 2009, Wirth *et al.* 2010a, Belnap *et al.* 2016). This group of ground-dominating microbial organisms make up a major part of biodiversity not just in the hyper-arid Namib Desert, but also in other coastal subtropical deserts, such as the Atacama in South America and Baja California in Mexico and California (Wirth *et al.* 2010a). In the Namib Desert, over 120 lichen species are known, of which many are endemic, and others show similarities between the Namib and other world fog deserts (Michael *et al.* 2010, Wirth *et al.* 2010a). Therefore it should be our aim to preserve the Namibia's remaining lichen bio-crusts with appropriate management, for which regular monitoring accurate is necessary.

These lichen ecosystems are important bio-indicators of environmental change because they are easily impacted by disturbances, such as land use activities. Additionally, lichens and other BSCs also fulfil ecological functions similar to those performed by vascular plants by assisting in the cycling of nutrients, controlling water flow, preventing soil erosion, offering secure locations for the growth of vascular plant and sheltering small animals (Lalley and Viles 2005, Elseroad *et al.* 2009). Most importantly, through photosynthesis, they extract atmospheric carbon dioxide and convert it into organic carbon (Schultz 2006, Lange *et al.* 2008, Rodríguez-Caballero *et al.* 2017). As a result, carbon sequestration is an essential but less understood ecosystem service of the lichen fields in Central Namib. In addition, knowledge on their role to global carbon sinks is mostly lacking. Hence this current research aimed to assess monitoring tools necessary to protect lichen flora as a vital carbon sink and to promote land degradation neutrality.

In the Central Namib Desert, a great diversity of epilithic lichens are restricted to the rocky gravel plains colonizing soil particles and rock surfaces and unevenly distributed following a fog gradient to drive photosynthetic processes (Lange *et al.* 1994, Loris *et al.* 2009). The morphology of lichens varies greatly within desert ecosystems with ranging temperatures and degree of aridity. As a result, lichens are grouped into three morphological growth forms of crustose, fructose, and foliose lichen communities, with to regard to their water requirements (Wessels and van Vuuren 1986a, Lange *et al.* 2008, Michael *et al.* 2010). Lichens are a symbiotic growth of fungi and algae working together to complete life's essential tasks. The fungal part of a lichen provides support and inorganic nutrients, while the algae, through photosynthesis, provide organic food (Michael *et al.* 2010, Wirth *et al.* 2010b). They are divided into three growth types, crustose, fruticose, and foliose lichens, which range in color from orange to grey to green to brown to black, due to their morphological variation and resilience to aridity. (Wirth *et al.* 2010a).

These lichens are highly favoured by weather conditions fluctuating from hyper-aridity to high relative air humidity and frequent fog precipitation from persistent inversion of air temperature caused by the upwelling of cold water in the Benguela Current that flows from Antarctica; when the air above the sea causes the water to get cold, water vapour condenses, and the resulting fog bank is drawn onto the land (Michael *et al.* 2010, Wirth *et al.* 2010a). This results in lichens developing more successfully than higher plants due to their ability to equilibrate (poikilohydric) to the water status of these fog desert environments (Karnieli *et al.* 2003, Lange *et al.* 2008, Loris *et al.* 2009, Michael *et al.* 2010, Wirth *et al.* 2010a). This desert adaptive mechanism used by lichens to survive in hostile environments demonstrates what greater functions lichens serve in dryland ecosystems devoid of vascular high plants.

1.1.2 Disturbances on Central Namib Lichen Fields

Lichen bio-crusts composition of the Central Namib is strongly disturbed by both climate and human-induced changes. This reduces their functionality and often causes more land degradation. The lichen fields are influenced by natural changes such as reduced fog occurrence and hot dry bergwind ("eastwind") conditions (Daneel 1992, Lalley and Viles 2006, Schultz 2006). The Health and stability of this fragile ecosystem is known to be negatively impacted by potential changes in fog regime brought on by climate change (Schieferstein and Loris 1992, Schultz 2006, Maphangwa *et al.* 2012). Even though studies have extensively proven that fog is a key driver for lichen survival, this is still a relatively unexplored field of research to understand how the endemic lichen biodiversity in the Namib is responding to global change. Thus it is crucial to develop monitoring systems for the dynamics of lichen fields driven by impacts of climatic events (i.e. hot dry strong bergwinds), and the impacts of long-term climatic changes (i.e. reduced fog events) as well as human land use activities (i.e. off-road driving).

Central Namib ground-dwelling (terricolous) lichen communities are particularly vulnerable to and threatened by land-use changes, such as expanding mineral exploration, uranium mining activities, increasing tourism, filming crews, road constructions, and extensive vehicle off-road driving (Daneel 1992, Lalley and Viles 2005). Studies have shown that the lichens have a slow growth recovery rate, usually ranging from years to decades, after disturbance and because of the hard desert conditions and their structure (Lalley and Viles 2008, 2005, 2006). The fragile nature of lichen communities, makes damage during traditional, ground-based ecological surveys also a problem, not only to the health of lichens, but also to conservation (Schultz 2006, Hinchcliffe *et al.* 2017). Owing to that, this creates the need for adopting technologically advanced research tools which cause less intrusion not just in monitoring lichen dynamics response to change, but also in other environmental research applications. Therefore, this study focused on assessing the feasibility of using time series of Unmanned Aerial Vehicles (UAVs or Drones) multispectral imagery to monitor lichens photosynthetically respond to fog moisture input, and disturbance from off-road driving in the Central Namib Desert. This provides minimal environmental harm, while generating rapid, robust, and meaningful data for conservation and resource management.

1.1.3 Remote Sensing of Lichen Biodiversity Monitoring

Lichen monitoring is necessary to achieve restoration because it offers the crucial baseline against which future changes may be evaluated. Remote sensing data and techniques had been utilized due to their time-saving and cost-effective nature compensating for research carried out in inaccessible areas, as well as in ecosystems fragile to disturbance (Karnieli *et al.* 2003). In light of the increasing recognition of lichen ecological services and damage from natural and artificial disturbances (i.e. off-road driving trampling actions), a large number of researchers have utilized satellite imagery to monitor lichen distribution and investigating their spectral characteristics, not only in the Namib Desert (Wessels and van Vuuren 1986b, Schultz 2006, Hinchcliffe *et al.* 2017), but elsewhere (Karnieli *et al.* 2003, Knox 2004, Maphangwa *et al.* 2012, Casanovas *et al.* 2015, Rodríguez-Caballero *et al.* 2017, Macander *et al.* 2018, Rieser *et al.* 2021). These satellite-based remote sensing studies had proven to be useful in monitoring lichens. However, their coarse spatial and temporal resolutions tend to overlook the presence of lichens because their distribution can vary at very small spatial scales (Casanovas *et al.* 2015, Collier 2019). Additionally, data that correspond to the resolution of the feature under observation and the related processes are necessary for the measurement of environmental changes (Whitehead and Hugenholtz 2014). As a result, precise assessment of the degree of lichen ecosystem changes and consistent monitoring continue to be conservation-related challenges.

UAV aerial imagery with a considerably finer spatial and temporal resolutions has grown in popularity for environmental applications and has the ability fill the spatial data gap between conventional ground ("in situ") observations, piloted aircraft, and satellite datasets (Assmann *et al.* 2019, Stow *et al.* 2019). Therefore studies have used this advanced research solutions for a variety of environmental research applications, such as topographic mapping (Zietara 2017, Trajkovski *et al.* 2020), precision agriculture (Rasmussen *et al.* 2016, Tu *et al.* 2018, Stow *et al.* 2019), phenology (Rasmussen *et al.* 2016, Adler 2018, Tu *et al.* 2018), forestry (Brede *et al.* 2015, Oldeland *et al.* 2017), welands (Gray *et al.* 2018), and conservation. Despite, the growing number of environmental studies adopting the use of UAV imagery, there have been only a few attempts to demonstrate the ability of UAV aerial imagery to map lichens and other biocrusts (Casanovas *et al.* 2015, Macander *et al.* 2018, Collier 2019), but none so far particularly in the Central Namib. This created the need to assess the performance of the UAVs accompanied by a multispectral sensor to monitor the spatial distribution and photosynthetic activity of lichens. Furthermore, it has been determined that one of the top priorities in the field of lichen monitoring research is the use of very high-resolution UAV imagery (Belnap *et al.* 2016, Collier 2019, Rieser *et al.* 2021).

In addition, to assess the impact of meteorological conditions on biocrust ecosystems, remotely sensed vegetation indices (VI), such as the Normalised Difference Vegetation Index (NDVI), are used as a proxy for lichen metabolic activity (Román *et al.* 2019, Chen *et al.* 2020, Rieser *et al.* 2021). However, there has not been much research done in Central Namib that uses UAV-based multispectral data to observer changes in lichen photosynthetic activity. In order to successfully monitor the response of lichens to moisture availability in the Central Namib, this study evaluates the feasibility of using UAV remotely sensed vegetation indices in supported with ground-based ("in situ") measurements. It also serves as a proof of concept for further monitoring of this phenomenon using UAV technology.

Chapter 2: Literature Review

In this section, previous work on monitoring the dynamics of lichen and other BSCs utilizing ground-based ("in situ") observations, remote sensing technologies, a geographic information systems (GIS) technique to retrieve data, and the use of UAV technology for natural resource management were discussed.

2.1 Lichen Dynamics in the Central Namib

2.1.1 Ground-Based Observations of Temporal Patterns of Lichen Photosynthetic response

Lichens absorb moisture from both air humidity and the precipitating fog that makes up the majority of the water in the Namib. They possess the ability to desiccate when dry and become inactive, and to hydrate when wet (active state) (Michael *et al.* 2010, Wirth *et al.* 2010a). Water interactions on net photosynthesis and carbon dioxide exchange of ground and epiphytic lichen species on the coastal gravel plain of the Namib Desert were described in studies by Lange *et al.* (2007). The weather and the level of hydration affect the Namib lichens' daily photosynthetic activity (Lange *et al.* 2006). In general, lichen species showed a similar pattern of hydration from fog or dew soaking, increasing their water content in the second half of the night to a maximum between 06.00 and 09.30 h, then rapidly dehydrating and going dormant when dry (Lange *et al.* 1994a, 2007, 2008). They also illustrated three phases of CO_2 exchange, which were (1) an increased respiratory CO_2 loss between 05h00 and 07.00 h, hour immediately before sunrise; (2) possible extensive rates of positive net photosynthesis only immediately after sunrise from 07.30 to 10.30 h; and (3) then the lichens dried and almost completely inactive until sunset (Lange *et al.* 1994). In the third phase, they discovered a trend for hydration to rise later in the afternoon as a result of water vapour intake at increasing air humidity, while on some days a brief window of low rates of photosynthesis just before sunset was made possible by this increased hydration. (Lange *et al.* 1994b, 2007). Owing to that, UAV imagery flights were prioritised from 08h00 to 10h00, and then later in the afternoon from 15h00 to 17h00. Although the photosynthetic rates of soil-crust lichens moistened naturally by fog or dew were similar to those of fruticose and foliose lichens in the same habitat (Lange *et al.* 1994b), many factors such as structure, colour, and thermal properties could affect the moisture yield and length of the hydrated period of the lichen crusts (Lange *et al.* 1994b). This study is a special focus to habitats dominated by mainly crustose lichens, from coast to inland fog gradient.

2.1.2 Impacts of Off-Road Tracks on Adjacent Lichen Communities

Driving over the lichen fields essentially destroys the crusts. Ox wagon tracts from over a century ago are still clearly visible, as are more recent tracks of exploration vehicles in the 1970s and recent tracks by off-road driving enthusiast (Daneel 1992, Lalley and Viles 2006). Large movie productions like The Flight of the Phoenix and Mad Max have also left their scars, even though the film companies spent millions on post-production rehabilitation. The regrowth of the lichens is extremely slow estimates indicate over 50 years for full rehabilitation to occur naturally (Daneel 1992, Lalley and Viles 2006, 2008, Lalley *et al.* 2006). The success of artificial rehabilitation attempts is doubtful. At the same time, however, the lichen fields are known to reduce carbon dioxide (CO^2), thus lichen is a major controlling factor in global climate change (Daneel 1992, Karnieli *et al.* 2003, Schultz 2006, Lalley and Viles 2008, Michael *et al.* 2010, Maphangwa *et al.* 2012). Previous studies show that the lichens only photosynthesize and grow during fog events and that the thallus desiccates to a dormant stage soon after the fog has lifted and the sun is shining (Lange *et al.* 1994b, Lalley *et al.* 2006, Loris *et al.* 2009, Michael *et al.* 2010, Wirth *et al.* 2010a). Understanding of the average daily growing period, and the actual annual growth rate and carbon fixation rate are currently small. Thus, enhanced information regarding lichen dynamics in the coastal desert can inform the development of long-term monitoring protocols when applying for drone permits for this protected area, but can also serve to demonstrate the efficacy and relevance of this technology in other locations.

2.2 Previous research in monitoring lichen using remote sensing

2.2.1 Satellites- Versus UAV-Based Remote Sensing

Monitoring biological soil crusts with satellite-based remote sensing imagery has proven effective by providing a wide spatial extent and high spectral resolution (Wessels and van Vuuren 1986a, Knox 2004, Schultz 2006, Casanovas *et al.* 2015, Rodríguez-Caballero *et al.* 2017, Rieser *et al.* 2021). One of the earliest satellite-based remote sensing studies on monitoring lichen in the Central Namib Desert was carried out by Wessels and Van Vuuren (1986). To distinguish lichens from other land cover features and assessed the spread of lichen cover, they employed 1981 space-borne multispectral Landsat MSS data (Wessels and van Vuuren 1986b). Similar to this, Schultz (2006) examined the spatial patterns of lichen colonies in the Central Namib Desert using multispectral LANDSAT 7 ETM+ and LANDSAT 5 TM satellite images. Satellite imageries are a useful tool for mapping Namib Desert lichen vegetation at a large landscape scale, however extensive fieldwork for ground-truth data are needed to accurately distinguish lichens in satellite images (Schultz 2006, Gray *et al.* 2018). Moreover, these traditional airborne remote sensing studies had been limited by the fact that satellite platforms produce untimely and coarse spatial resolution images that often provide insufficient detail to monitor lichen biocrusts distribution varying at very small spatial scales (Casanovas *et al.* 2015, Collier 2019). For example, maps generated from Landsat 8 imagery with a temporal resolution of 16 days re-visit and a coarse-spatial resolution of 30 m (i.e. pixel size) are likely to overlook lichen biocrusts (Casanovas *et al.* 2015, Collier 2019).

Thanks to emerging advancements in remote sensing technologies, low-altitude UAV platforms and associated sensors, can offer finer spatial resolution (up to 1 cm/pixel) and temporal resolution in comparison to conventional space-borne remote sensing tools (Turner *et al.* 2014). Additionally, the utilization of UAV aerial imagery can reduce the amount of time spent in the field and the environmental impact (Gray *et al.* 2018). Furthermore, it was concluded that UAV data can validate satellite data due to the observed similarity in overall accuracy agreement of 96 percent and negligible difference between

UAV and field-based assessments (Gray *et al.* 2018). However, other research supported their findings with *in-situ* Spectro-radiometer hyperspectral measurements on the lichens. These measurements ranged from 325 to 1075 nm, covering the visible and near-infrared spectrum (Schultz 2006, Hinchcliffe *et al.* 2017). They suggested that detailed coverage of lichen communities may be achieved by using UAV platforms and sensors with higher spectral and spatial resolutions (Hinchcliffe *et al.* 2017).

2.2.2 UAV Sensors

Another essential component is having sufficient spectral resolution, especially when monitoring vegetation because it has a high degree of spectral variability in the NIR (near-infrared) range (Turner *et al.* 2014). Narrow band multi- or hyper-spectral sensors are needed for in-depth investigation of vegetation structural and metabolic properties (Turner *et al.* 2014, Adler 2018). Fortunately, the field of UAV-based remote sensing is constantly improving in photogrammetry technology with lower costs and improvements of sensors (such as the Parrot Sequoia multispectral sensor and the MicaSense RedEdge) placed on various UAV platforms (e.g. Quadcopters and Fixed-wing drones) (Tu *et al.* 2018, Assmann 2019). The visible red, green and blue (RGB) channels (spectral range 400–700 nm) and the invisible near-infrared (NIR) (spectral range 700 – 1000 nm) portions of the spectrum, which can be used to provide more information about plant health or productivity, are frequently included in the spectral data collected by multispectral sensors (Adler 2018, Assmann 2019) (see Figure 1).

Detecting invisible lichen vegetation biophysical characteristics, such as photosynthetic reflectance, and parameters that can vary over small spatial scales due to the influence of micro-topography or meteorological conditions is a limitation of mapping BSCs that extends beyond the mapping of a small area coverage. The inability to extract precise biophysical data of lichens due to the lack of NIR reflectance information necessitates the use of a multispectral sensor (Turner *et al.* 2014, Adler 2018, Collier 2019). With the availability of the invisible NIR capability of UAV multispectral sensors, it is possible to monitor the vigour of the lichens, as well as the signs of recovery after disastrous events like vehicle passing or severe bergwind (“Eastwind”) conditions. Therefore, this study aimed to make use of UAV platforms plus visible and invisible near-infrared (NIR) wavelength cameras, to measure lichens and other BSCs spectral reflectance characteristics, and to estimate bio-parameters of lichen biocrust cover using vegetation indices (VIs), as such NDVI.

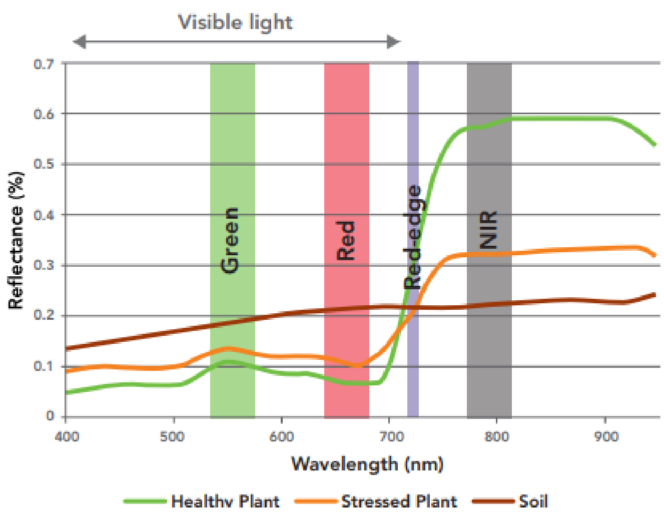

Figure 1: Parrot Sequoia multispectral sensor's band spectral locations in the electromagnetic spectrum, and spectral reflectance signature of plants and soil (Parrot Sequoia manual 2022).

2.2.3 Image Radiometric and Geometric Calibration Techniques

UAVs may be able to provide an alternative to conventional airborne remote sensing, but it is important to consider the quality and efficiency of image correction algorithms when processing the significant volume of high spatial resolution data that a UAV collects (Turner *et al.* 2014). UAV platforms have proven to be very helpful because they frequently fly at such low altitudes that atmospheric effects do not need to be taken into account in the analysis (Adler 2018). As a result, when using UAV imagery, some radiometric corrections requirements similar to those for satellite data are disregarded (Yu *et al.* 2017, Adler 2018). Even though atmospheric attenuation in the low-altitude atmosphere is minimal, it can nonetheless cause a target object's reflectance to be misled (Yu *et al.* 2017, Adler 2018). In situations where correct spectral data is required, it should be removed to improve the ability to analyse datasets of images collected by UAVs (Yu *et al.* 2017). On the other hand, research like Rasmussen et al. (2016)

discovered that the camera (with or without an NIR channel) and spectral indices (ExG, NGRDI, NDVI, and ENDVI) had no significant effects on the capacity to evaluate the overall quantity and vigor of vegetation. Their output results from directly calculating spectral indices utilizing multi-spectral data were questionable due to the lack of atmospheric corrections (Rasmussen *et al.* 2016).

To generate radiometrically, atmospherically and geometrically corrected UAV imagery products, it is crucial to apply basic remote sensing techniques. This enables comparing the 'actual' ground spectral reflectance of surface features over time and space. Geometric rectification is necessary because remote sensing image analysis is frequently done pixel-by-pixel comparison basis (Adler 2018). The pixels in images must depict the same ground features for there to be geometric precision (Adler 2018, Tu *et al.* 2018). Figure 2 illustrates how to employ common ground control points (GCPs) of fixed objects or features present in all images to ensure the correct pixels are overlaid between separate images and get a good geometric match between them (Adler 2018, Tu *et al.* 2018).

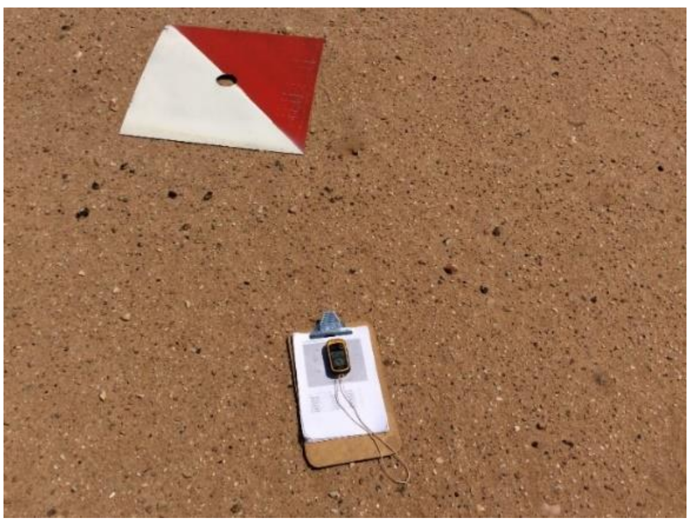

Figure 2: 60 x 60 cm GCP plate used for geo-referencing images, for Utuseb and Swartbank study sitse.

In addition to transforming images from digital numbers (DNs) recorded at each image pixel to surface reflectance, radiometric correction is important for adjusting for environmental factors including variations in lighting and atmospheric impacts on images (Adler 2018). As a result, the images produced by the aforementioned sensor's radiometric calibration must exhibit a radiometric consistency (Adler 2018).

Radiometric calibration of UAV remote sensing imagery differs in research studies depending to the types of UAV sensors applied. The empirical line calibration method developed by Smith and Milton (1999) is the strategy used most frequently for radiometric calibration. The empirical line approach needs the reflectance of the dark and bright plates in the UAV image to be measured *in situ* (Smith and Milton 1999, Adler 2018). The reflectance of image features is then predicted using a linear relationship between these dark and bright plates and digital numbers (DN) (Smith and Milton 1999, Adler 2018). With this technique, field measurements are taken along with each flight to account for the particular lighting conditions, and photos of the calibration plates during the mission are taken. However, the empirical line approach has a number of drawbacks, including the assumption that the surface is composed of Lambertian reflections and that there is constant illumination in the image (Adler 2018, Stow *et al.* 2019). Additionally, illumination might not be consistent due to topographic changes or shadows cast by irregular clouds (as seen in figure 3), which makes atmospheric effects very changeable even over short distances (Assmann 2019).

These presumptions can be challenging to achieve during UAV aerial flights since cloud cover shadows may change throughout the flight and surfaces are not always precisely Lambertian, resulting in the appearance of bi-directional reflectance properties (Adler 2018, Stow *et al.* 2019) (see Figure 3). Because natural surfaces do not reflect equally in all directions, they exhibit anisotropic reflectance, which indicates that viewing and illumination geometries may have an impact on reflectance measurements (Assmann 2019, Stow *et al.* 2019). The interaction between illumination and viewing angles geometry, as described by the sun zenith angles and the sensor at a given pixel, as well as the angular variation in reflectance of a surface, which is described by its bidirectional reflectance distribution function (BRDF), are what lead to variations in apparent reflectance across an image (or anisotropic reflectance effects) (Adler 2018, Gray *et al.* 2018, Assmann 2019, Stow *et al.* 2019).

Figure 3: Fog clouds shadow effects and non-uniform illumination on the ground, Swartbank study site, 06 September 2021.

Some research have combined an ambient light sensor (also known as the sunlight irradiance sensor) with the UAV-mounted Parrot Sequoia multispectral image sensor (Parrot Drones SAS, Paris, France) (Assmann 2019) (see figure 3). In order to calibrate the relationship between the radiances observed at the two sensors, the measurements from the multispectral and ambient light sensors are converted to at-sensor radiances in arbitrary units (Assmann 2019). In addition to that, it has been found that anisotropic reflectance effects are significantly less noticeable in orthomosaics than in individual photos, which suggests that the exact pixel averaging technique in the Pix4D's digital photogrammetry program uses to determine pixel reflectance values is somewhat successful at correcting for these effects (Assmann 2019). However, the ambient light sensor only records one measurement per image, assuming uniform illumination, and it is typically calibrated on the ground, ignoring any effect of flight altitude and potentially introducing errors from atmospheric effects (Assmann 2019). As a result, this does not solve the issues with the empirical line method. Hence, when the sky is entirely overcast and the irradiance changes during a flight, for example, the irradiance sensor is most effective at adjusting for variations in illumination conditions (Assmann 2019). However, they are unable to accurately adjust for partly cloudy days where clouds may cast shadows on some portions of the earth but not the sensor (Assmann 2019).

The UAV imagery requires comparable lighting conditions in order for radiometric calibration to perform well. However, if these parameters are not met, researchers must properly consider the variance in results brought on by different lighting conditions (Adler 2018). Furthermore, the bi-directional reflectance direction function (BRDF) is a minor factor for satellite remote sensing but is magnified for UAV remote sensing (Adler 2018, Fernández-Guisuraga *et al.* 2018). Depending on the viewing angle and solar angle, which is lowered on bigger scales in satellite photography, a scene may have dark or bright areas (Rasmussen et al. 2016, Adler 2018). Local weather conditions can be taken into account when adjusting the UAV flight acquisition time, however some factors must be managed, such as solar strength, UAV orientation with the sun, and consistent cloud conditions for each flight (Rasmussen *et al.* 2016, Adler 2018, Assmann 2019). By avoiding days with scattered clouds, the variation in illumination brought on by cloud shadows can be reduced (Assmann 2019). These alterations might be feasible for brief flights, but they are challenging for lengthy flights and when time series flights are necessary due to the fact that conditions might rapidly change while a flight is in progress.

Despite these limitations, a number of studies have used multispectral sensors to monitor vegetation with success, as radiometric calibration can somewhat correct some of these image distortions (Turner *et al.* 2014, Rasmussen *et al.* 2016, Yu *et al.* 2017, Adler 2018, Tu *et al.* 2018, Assmann 2019). Additionally, issues like fluctuations in illumination, atmospheric distortions, and shadows within the corresponding multispectral reflectance image bands can be reduced with the aid of ratio-based vegetation indices (VI), such as NDVI (Adler 2018). It has also been demonstrated that illumination geometry and flying height have an effect on the retrieval of reflectance values from individual UAV-taken images (Assmann 2019). The results shown that variation in anisotropic reflectance effects between NDVI images is significantly smaller than across individual image bands, suggesting that the use of vegetation indices, such as NDVI, may somewhat normalize these effects (Assmann 2019). Furthermore, I had been recommended that vegetation indices derived from consumer-grade cameras mounted on UAVs can be trusted if three crucial prerequisites are met, including stable ambient light conditions during image acquisition, consideration of angular variation in reflectance during plot cropping in sunny conditions, and testing of digital photogrammetry software for mosaic creation to assess how it handles bidirectional reflectance (Rasmussen *et al.* 2016). These effects depend on fluctuating solar geometry, canopy structure, and possibly atmospheric composition, making them unique to specific flights (Assmann 2019). Therefore, before using UAV-derived multispectral datasets in general, there are certain important considerations.

2.3 Approaches for Extracting Spectral Data

2.3.1 Vegetation Indices (VI)

Earlier remote sensing vegetation studies has looked on the reflectance spectral signature of photosynthesising material. It is necessary to employ a quantifiable metric to track changes in order to determine, for example, the amount of vegetation and its condition over time (Adler 2018). The simplest metric to employ to measure vegetation photosynthetic activity from passive sensors is reflectance, which is the ratio of incoming radiation (irradiance) to outgoing radiation (radiance) (Adler 2018). The portion of incident light that is reflected at a surface's interface is known as reflection (Stow *et al.* 2019). The underlying assumption is that vegetation's spectral reflectance, or reflectance for a particular electromagnetic wavelength, varies depending on a variety of parameters, including the type of plant, its health, its water and chlorophyll content, and its morphology, to mention a few (Adler 2018). However, it could be necessary to examine metrics more closely related to physiological factors as opposed to spectral reflectance signature profile (Adler 2018). When computing this VI, it is frequently necessary to employ two or more wavelength bands in the equation (Adler 2018). While classifications frequently divide images based on these differences, VI enhances the characteristic electromagnetic reflectance signatures of various surfaces (such as bare ground and sparse or dense vegetation) (Assmann 2019, Stow *et al.* 2019).

Figure 1 illustrates the spectral reflectance signature of plants and soil. Vegetation indices (VI) alone can help identify areas with photosynthetically active (or live) vegetation, While NIR data can help distinguish plant species that differ in their reflectance. Using the recovered NIR data, unique spectral signatures of the various plant species can be used as training input data for classification, and use to inform supervised classification (Rasmussen *et al.* 2016)**.**

The greenness, density, health, and biophysical characteristics of the plant cover are estimated using vegetation indices (VI) algorithms as proxies. The normalized difference vegetation index (NDVI), which is a ratio of the chlorophyll-absorbing red (600-700nm) and the reflected near-infrared-NIR (700-1100 nm) bands , is one of the more often utilized VI, as it correlates with vegetation biomass (Adler 2018). The default NDVI equation is as follows:

$$NDVI = ((NIR - Red)/(NIR + Red)) \qquad \textit{Equation 1}$$

Where *NDVI* is the output values ranging from -1 and 1, where -1 represents minimal or no greenness and 1 represents maximum greenness or high amount of vegetation, the *Red* is the reflectance values from the red band and *NIR* is the reflectance values from the NIR band (Adler 2018, Indices gallery-ArcGIS Pro Documentation 2022).

The two other reflectance-based VIs calculated in this study were the Normalized Difference Red-Edge Index (NDREI) and the Soil-Adjusted Vegetation Index (SAVI) to provide biophysical information (Adler 2018). The Soil-Adjusted Vegetation Index (SAVI) approach is a vegetation index that modifies the NDVI with the goal of reducing the influence of soil brightness using a soil-brightness adjustment factor (Huete 1988, Indices gallery-ArcGIS Pro Documentation 2022). It produces values between -1.0 and 1.0 (Huete 1988, Indices gallery-ArcGIS Pro Documentation 2022). This is frequently employed in arid environments with minimal vegetative cover and in situations where the soil is exposed because the reflectance of light in the Red bands is changed, which may affect the outcome (Huete 1988, Canata 2021). The equation of SAVI is as follows:

SAVI = ((NIR - Red) / (NIR + Red + L)) x (1 + L) *(Equation 2)*

Whereby *NIR* is the reflectance values from the near-infrared band, the *Red* is the reflectance values from the near-red band, and the *L* is the soil adjusted factor (Indices gallery-ArcGIS Pro Documentation 2022).

In order to determine how radiometric correction might have influenced another VI that is independent of the red band, the Normalized Difference Red-Edge Index (NDRE) was also computed (Barnes *et al.* 2000, Canata 2021). Only sensors with the "Red Edge" spectral band support NDRE (Barnes *et al.* 2000, Canata 2021). The Red-edge is more sensitive to the amount of chlorophyll and nitrogen in the leaf (Barnes *et al.* 2000, Canata 2021). The equation of NDRE is as follows:

NDRE = (NIR - RE) / (NIR + RE) *(Equation 3)*

Whereby *NIR* is the reflectance values from the near-infrared band, while the *Red-edge* is the reflectance values from the near Red-edge band (Indices gallery-ArcGIS Pro Documentation 2022).

The use of satellite-based NDVI overlooks the presence of lichen biocrusts due to mixed pixels, even if their land cover is extensive, and it is recommended that adapting UAV platforms is an alternative(Casanovas *et al.* 2015, Rieser *et al.* 2021). Moreover, vegetation studies have shown that approach for radiometric correction and image processing give UAV-based NDVI values nearer to the NDVI values determined with the handheld spectrometer (Adler 2018). Similarly, it has been showed that *in-situ* Spectro-radiometer measurements on the lichens, significantly correlated with NDVI (Karnieli *et al.* 1999, Schultz 2006). This created an opportunity to make use of higher spatial resolution UAV-based multispectral spectral indices as good quantitative proxy measure of lichen photosynthetic activity. Research on biocrust NDVI from UAV-derived multispectral imagery is limited. Therefore this current study applied the UAV-borne VI algorithms is to monitor lichen biocrusts on Central Namib gravel plains, based on the principle similar to vegetation and lichen studies that have made use of satellite imagery for mapping vegetation distribution. By using UAV-based multispectral image datasets to analyse time-series of lichen photosynthetic response patterns and determine the major causes of change, it is possible to predict lichen cover regimes and understand the factors that influence them, such as the distribution of fog moisture.

2.4 Research Objectives

2.4.1 Main Research Objective

The main objective is this study was to assess the ability of UAV-derived multispectral time series imagery, as a proxy to observe the photosynthetic activity of lichens' response to fog moisture; as well as to closely observe photosynthesizing lichen vegetation of intact versus damaged lichens (e.g. in off-road tracks), in the Central Namib Desert. The application of this advanced UAV-based multispectral remote sensing system for ecological monitoring of lichens will assist in efforts to determine the best time of day for using UAVs to monitor the health of this fragile, dynamic and productive ecosystem, especially considering threats like climate change and inappropriate land-use practices.

2.4.2 Research Questions

To achieve the overall main objective, this research focused on the following detailed research questions:

1. What are the key effects contributing to uncertainties in the time-series of UAV-based multispectral imagery of Namib lichen fields, and be best accounted for?
2. What is the best time to capture good quality UAV multispectral image observations to monitor lichens' photosynthetic response to fog moisture input?
3. How does lichen photosynthetic activity response change over time in wet and dry conditions?

4. How do spatial variables (i.e. micro-topography and off-road tracks) influence lichen coverage and distribution across space?
5. Do UAV-based observations of lichen NDVI reflectance activity correspond to ground (in-situ) observations of lichen coverage in undisturbed and disturbed areas?

Thesis outline

This thesis is divided into 5 chapters. Chapter 1 covered the General introduction of this research study, which included the Background information of the study. Chapter 2 deals with the literature review which highlights the previous work done, the methods used and their findings which may be associated to this study. It also includes the main research objectives and the associated detailed research questions. Chapter 3 is the first manuscript paper which assessed the effects of hourly sunshine intensity on the use of UAV-based multispectral imagery for monitoring lichen-dominated biological soil crusts in the hyper-arid Central Namib Desert. In provides the introduction, a brief description of the study site and outlines the methods for image data collection, image processing and analysis techniques applied. It also deals with discussion, which interprets and explains the results obtained, as well as the conclusion and recommendations for future research. Chapter 4 is the second manuscript paper which deals the application of UAV multispectral imagery to assess the coverage, disturbance, and fog response of lichen-dominated Biological Soil Crusts in the Central Namib In provides the introduction, a description of the study sites and outlines the methods for UAV image and ground data collection, image processing and analysis techniques applied. Finally, it deals with discussion, which interprets and explains the results obtained, as well as the conclusion and recommendations for future research.

Chapter 3: The effects of hourly sunshine intensity on the use of UAV-based multispectral imagery for monitoring lichen-dominated biological soil crusts in the hyper-arid Central Namib Desert

Manuscript of paper to be submitted to:

International Journal of Remote Sensing (ISSN: 1366-5901)

Remote Sensing of Environment (ISSN: 0034-4257)

Remote Sensing (ISSN: 2072-4292)

3.1 Introduction

In the coastal Namib Desert the growth of higher vegetation is limited, but it is covered by a distinctive and abundant lichen flora (Wessels, 1993). Lichen colonized quartz pebbles and stones from part of the desert pavement and quartz outcrops in the Namib Desert (Wessels, 1989). The bare rocks and desert pavement of the Central Namib fog desert provide ample substrates for colonization by several lichen species (Wessels, 1989). The occurrence of lichen fields is restricted to the stable surfaces in the coastal fog zone, and their density and morphological structure changes with exposure, elevation, and distance from the coastline (Schieferstein & Loris, 1992). Areas of the Namib with dense lichen coverage are considered 'lichen fields' when ground cover exceeded 20% within one square meter (Schieferstein & Loris, 1992). However, in the east distance, approximately 40 km from the coast, lichen density sinks below 20% (Schieferstein & Loris, 1992). The different growth form of lichen species vary in colour and shape, thus their vegetative body sizes with respect to the width (diameter) can be as minimum as 0.5 cm and sometimes a thallus with a diameters up to ~20 cm can be found (Schieferstein & Loris, 1992).

Moreover, lichen communities form a dynamic and productive ecosystem that provides a wide variety of ecosystem services for arid environments. However, climate change and disturbances from land use practices have the potential to degrade those services. Thus undertaking scientific research of the lichen communities is useful in managing these lichens. However, proper management of the lichens had been challenging when using destructive field research methods, which also pose threats to the health and stability of this fragile and slow recovering lichen ecosystem. In addition, the coarse spatial resolution of satellite imagery is a drawback for monitoring the small sized and spared lichen communities. The application of satellite imagery is also a limited by the low temporal resolution (i.e. re-visit days), clouds and other atmospheric effects (Tu *et al.* 2018, Assmann *et al.* 2019).

Alternatively, the use of UAV's can overcome a number of the shortcomings of satellites for monitoring these small scale objects. UAVs platforms providing high temporal resolution and finer spatial resolution (Tu *et al.* 2018, Assmann *et al.* 2019, Collier 2019). However, in lower altitude UAV flights, the bidirectional reflectance distribution function effects (BRDF) become more serious because of increasing sun-surface-view geometry variation, which causes inconsistent illumination in the UAV imagery (Adler 2018, Tu *et al.* 2018). As the spatial resolution increases, so does the variance of observed reflectance (Tu *et al.* 2018). Several empirical studies have provided some insightful information on the UAV Parrot Sequoia multispectral sensor performs. The several factors which affect the UAV-derived reflectance of earth features include viewed area, canopy geometry, terrain, and the viewing geometry between the ground surface, sensor, and the sun (Adler 2018, Tu *et al.* 2018, Assmann *et al.* 2019). Some authors have observed that the BRDF effect which causes brightness variations is highly present for the UAV-derived Parrot Sequoia multispectral imageries due to illumination and solar-sensor-surface geometries variations (Adler 2018, Fernández-Guisuraga *et al.* 2018, Tu *et al.* 2018). Other authors observed that the vignetting present in the Parrot Sequoia multispectral images is the increase in DNs or pixel values from the image centre and an increase that is not circular (Kelcey and Lucieer 2012, Adler 2018). Rasmussen *et al.* (2016) investigated the effects of plot position relative to sun position and found that the angular variation in reflectance emerging in images as a brightness gradient was observed with darker sections in the direction of the incident solar radiation, and brighter sections found opposite the sun. Assmann *et al.* (2019) also observed anisotropic reflectance effects (i.e. variations in reflectance measurements) in both individual multispectral images and orthomosaics over one day, due to the surface, sun angles, and sensor geometries. This affects the quality of UAV imagery data and the accuracy estimation of plants' biophysical properties (e.g. biomass, chlorophyll content, nitrogen content, plant type, water content and morphology to name a few). Although studies had identified which factors (e.g. illumination change, atmospheric effect, viewing geometry, and instrument response characteristics) should be considered for radiometrically correcting UAV multi-spectral imagery in order to analyses plants' biophysical properties and their temporal changes (Tu *et al.* 2018). There is still little to no solution on how to correct for these factors, because proposed radiometric calibration methods used often do not include extreme changes in illumination.

Radiometric correction protocols for satellite images have been well developed and applied, and provide the basis for correcting images for illumination change, atmospheric effect, viewing geometry, and instrument response characteristic (Knox 2004, Schultz 2006). However, techniques for processing UAV multispectral imagery are relatively new, to dealing with the very similar general problems in satellite imagery, even though the scale is much smaller and the details of data are much higher (Tu *et al.* 2018). Moreover, the recommended radiometric correction methods are rather more technical and site-specific. This study, therefore, aimed to provide an optimal way to derive accurate measurements of vegetation's biophysical properties, taking into consideration the inconsistency in reflectance, using a specific focus on non-vascular lichen plants in a low vegetated covered hyper-arid environment.

3.2 Materials and Methods

3.2.1 Study Sites

The study site is located in the Central Namib Desert (23°17'53.15"S, 14°50'32.11"E), on the leeward (east) side of the Swartbank mount. The Central Namib Desert region experiences a coastal subtropical climate, characterized by the coastal fog belt, that reaches t0 ~50km inland, with average annual fog precipitation estimated at 37 mm per annum, occurring on an average of 146 days a year at the coast (Lalley & Viles, 2006). Fog events occur during any month of the year, but the heaviest occurrence is in the winter months of May to September (Daneel, 1992; Lalley, et al., 2006). Rainfall is experienced during the summer months of January to March in short duration and decreases with distance from inland to coastal areas. Conditions of extremely low humidity are fairly uncommon and are normally associated with winter berg winds. The strong easterly "berg" winds are experienced during the winter months from May to August, and characteristically result in hot, dry conditions. Temperature extremes are moderated in the Namib by the presence of the cold Benguela current, but maximum temperatures in the region of 40°C are mainly experienced during February and March.

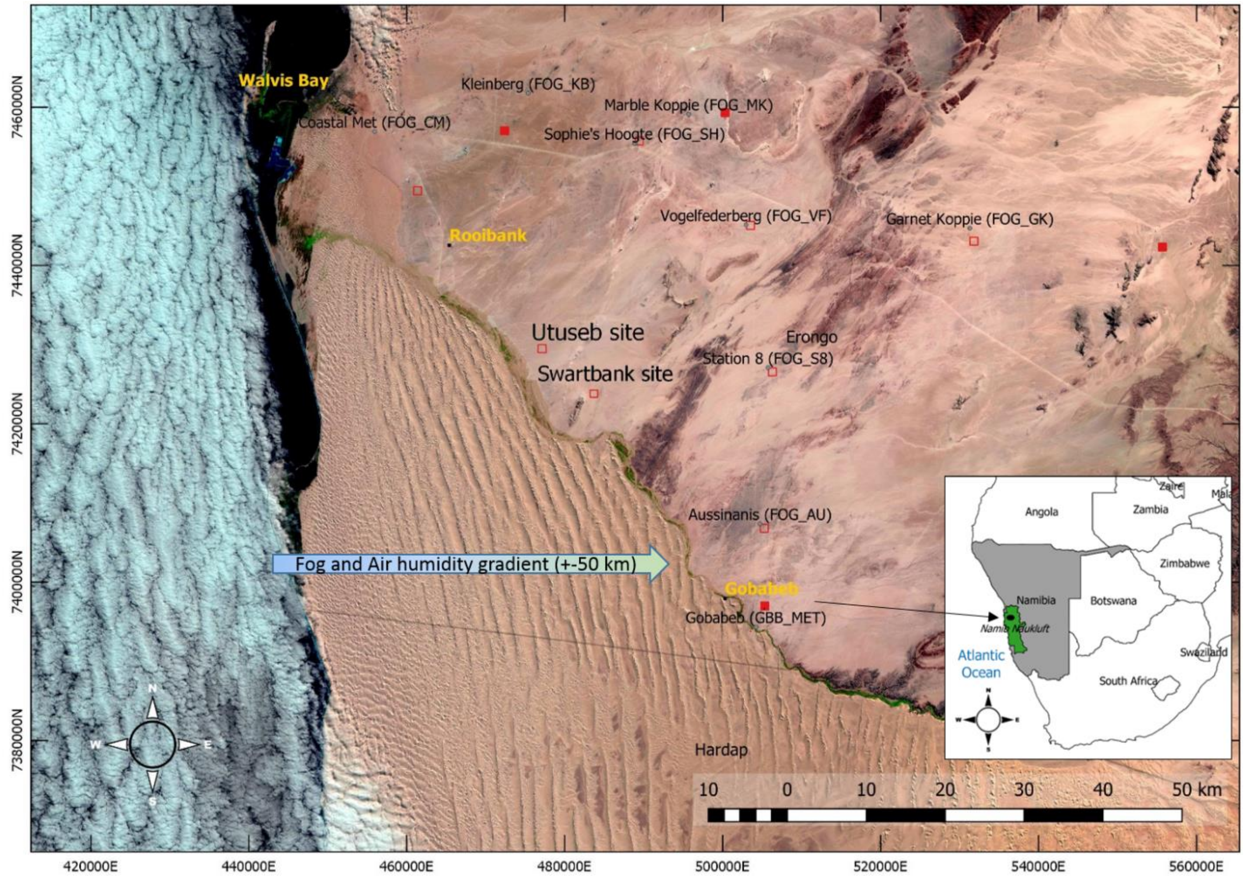

Figure 4. Location of the study area in Central Namib, including the Swartbank study sites, with a flight surveyed areas indicated by the black polygon. Red squares represent the Namibian BIOTA observatories transects, in the Namib Desert Biome (Biodiversity Monitoring Transect Analysis in Africa), around the SASSCAL fognets weather stations. The two photos show that lichen density cover is much higher at the coast, for example at the Kleinberg observatory site, compared to be Swartbank site further inland. The base image is a Sentinal-2 image (2021-07-03) downloaded from the USGS-Earthexplorer, it shows how fog clouds travel from coast to inland, as indicated by the arrow. The focus area for UAV aerial surveying was located along a ridge top including the west and east slopes of the ridge, covering a mission plot that is of 500m long and 200 m wide.

The Swartbank experimental lichen site is 35 km inland from the Atlantic Ocean coast, and 5 km north of the Swartbank Topnaar settlement and along the old Swartbank road, SE of Walvis Bay (Figure 4 and Figure 5) This site is accessible ~30km from the Gobabeb-Namib Research Institute in a southern direction. This site is at a high elevation of approximately 323 m above sea level. It is dominated by fairly dense lichens on exposed soil and quarzitic rock surfaces of gravel plains. The vegetation cover is very sparsely limited to scattered small shrubs in river channels and is typical of the summer rainfall season. There are also drainage channels but without recent dynamics or changing aspects. The gypsum crusts are visible at the soil surface. Land use activity is intensively high, as indicated by the presences on off-road vehicle tracks in high intensity caused by careless drivers, tourism, mining and exploration, constructions and maintenance of services, and filming crews. These disturbance lowers lichen covers and their ecological function.

In addition, the study site is rich in relief, thus the slopes, ridges and rocks induced variation in lichen ground cover and diversity (Figure 5). This is because fog travels at high altitude and from a west to east direction. As a result, the top of the ridge and windward side (west) of the ridge would have more lichen cover than the leeward side (east) (Schieferstein and Loris 1992). This high topographic variations within the site and the sun intensity and elevation, causes lighting effects (i.e. illumination, shading, and shadows) in the UAV aerial imagery.

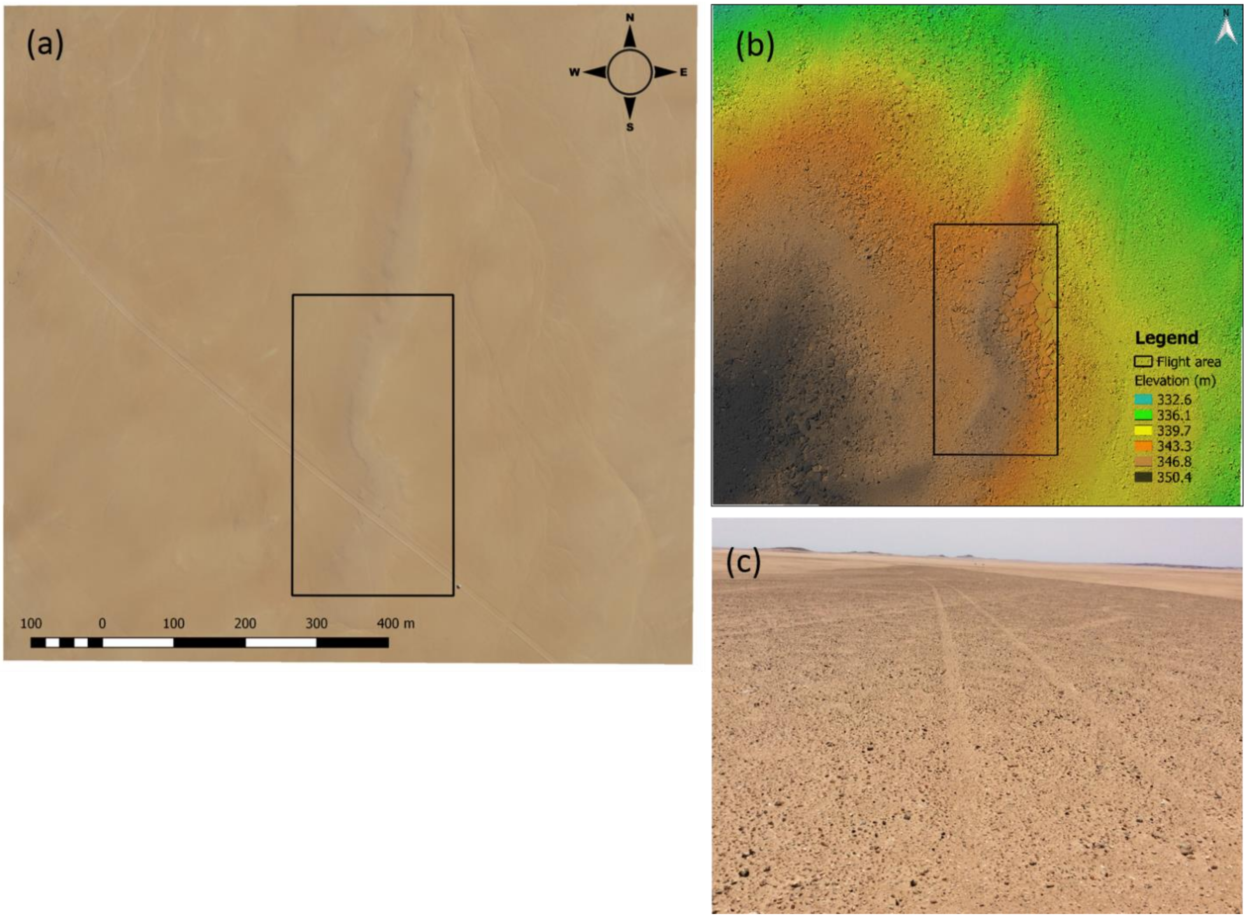

Figure 5. Study site DSM (left) and the scenery (right) with road track with little to no lichen cover.

3.2.2 UAV Aerial Image Data Collection

The study site was firstly surveyed with an eBee Classic (senseFly, Cheseaux-sur-Lausanne, Switzerland) fixed-wing UAV platform, fitted with an S.O.D.A. camera (senseFly) to acquire RGB images under clear sky conditions, on 14 May 2019, to generate a detailed digital surface model (DSM) of the study site (Figure 6). The eBee fixed-wing flights captured RGB images at a much larger spatial extent (500 × 500 m), 120 m flight altitude, and a high spatial resolution of 5.32 cm/pixel.

UAV flight missions were also conducted using a Parrot Sequoia multispectral sensor (Parrot SA, Paris, France) on board of a DJI Phantom 4 Pro V2 quadcopter platform, to collect hourly time-series multispectral image datasets. The Sequoia sensor captures green (G), red (R), red edge (REG), and near infrared (NIR) image bands simultaneously (Parrot Sequoia manual 2022). Some specifications are indicated in Table 1 and Table 2. The camera is also supported by a sunshine sensor that faces the sky and has the same spectral bands. For each image frame, the sensor can measure any incoming irradiance, allowing the irradiance measurement to be used for radiometric correction. This allows for the comparison of images over time despite changes in lighting at the time of image acquisition and registering GPS location of images.

Figure 6. Parrot Sequoia and sunshine sensor mounted on DJI Phantom 4 Professional drone (a) and eBee Classic senseFly drone (b). A standard AIRINOV calibration reflectance target (c), and a Graphic illustrating how to hold the sensor over the calibration target for pre-flight radiometric calibration (d).

Table 1. Spectral information of the Parrot Sequoia multispectral senor

Band Number	**Band Name**	**Center Wavelength (nm)**	**Bandwidth (nm)**	**Spectral Range (nm)**
1	Green	550	40	530 – 570
2	Red	660	40	640 – 680
3	NIR	735	10	730 – 740
4	REG	790	40	770 - 810

Table 2. Specifications of the Parrot Sequoia multispectral senor

Camera type	**Multispectral**
Name	Parrot Sequoia
Focal length (mm)	3.98
HFOV (◦)	61.9
Spectral bands (nm)	4
Spectral range (nm)	530 – 810
Size dimension (mm)	
Image size (pixels)	1280 × 960
Sensor size (mm)	4.8 × 3.6
Bit depth	12-16-bit
Image format	RAW/TIFF
Weight (g)	800

Eight-hourly time-series multispectral imagery was captured under clear sky conditions from 08:00 to 17:00 on fog day of 7 September 2020. Even though we flew every hour from 8am, hours of 12:00 and 14:00 pm were missed out due to high wind speed, this also the time with higher sun glare issues, and considering the available battery for the platforms. This study used time series of this one day for further time series analysis, not only due to time constraints, but also that it experienced early fog lifting, thus it provided full observations. The multispectral time-series flights were done at a constant 80 m flight altitude, with a 9.24 cm/pixel spatial resolution. Images were acquired with an 80% forward and 90% side overlap, flight speed 5 m/s and flight times of 15-23 minutes depending on the wind conditions. According to flight altitude, the size of a single shot footprint image covered a ground with a width of 96 m and length of 72 m. All flight missions were conducted with a single grid flight pattern with flight lines parallel to the ridge and with the cameras in nadir-view position.

The study area is located in the vicinity of the SASSCAL Fognet weather stations transect from the coast (west) to inland (east) direction. Therefore, weather data were retrieved from Coastal Met, Kleinberg, Sophie Hoogte and Gobabeb weather stations located from the west and east of the study plot, respectively. Therefore, this weather stations gave the best indication of the weather conditions during the UAV time series flights. The study used time series analysis of one day only (7 September 2020) with the total fog occurrence was 0.3 mm, 2.5 mm, 0.4 mm and 0.0 mm at Coastal Met, Kleinberg, Sophie Hoogte and Gobabeb weather stations, respectively. The total solar irradiance was 20.68 MJ/m^2, 21.7 MJ/m^2 and 22.45 MJ/m^2 at Coastal Met, Kleinberg, and Sophie Hoogte weather stations, respectively (Figure). There was no record of total solar irradiance at the Gobabeb weather stations. Figure 7 shows the fog occurrence found during the missions. The information of the missions can be found in Table 3.

Table 3. Table the description of the UAV multispectral data and climatic condition.

Site	**Date**	**Time**	**Platform**	**Fog**	**Wind Speed max (m/s) (Coastal Met station)**	**Incoming radiation (W/m^2) (Coastal Met Station)**
Swartbank	**07-09-2020**	**8**	DJI Phantom 4	**Yes**	**6.4**	**3.27.7**
Swartbank	**07-09-2020**	**9**	DJI Phantom 4	**Yes**	**7.7**	**658.2**
Swartbank	**07-09-2020**	**11**	DJI Phantom 4	**Yes**	**8.6**	**877.0**
Swartbank	**07-09-2020**	**13**	DJI Phantom 4	**Yes**	**7.6**	**765.0**
Swartbank	**07-09-2020**	**15**	DJI Phantom 4	**Yes**	**7.1**	**439.1**
Swartbank	**07-09-2020**	**16**	DJI Phantom 4	**Yes**	**7.4**	**222.8**
Swartbank	**07-09-2020**	**17**	DJI Phantom 4	**Yes**	**7.0**	**36.0**

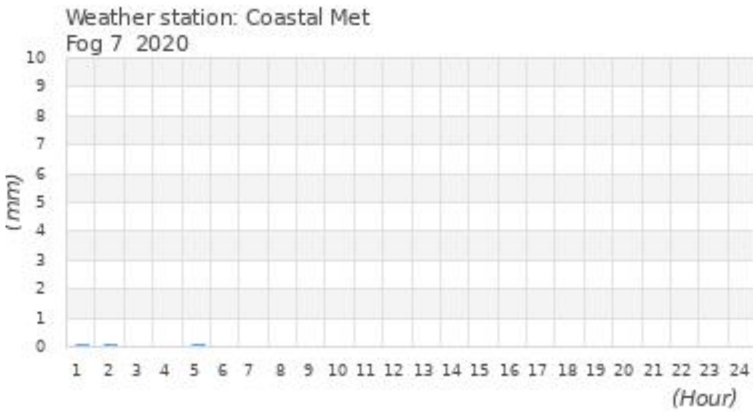
Weather station: Coastal Met
Fog 7 2020
(mm)
0 1 2 3 4 5 6 7 8 9 10
1 2 3 4 5 6 7 8 9 10 11 12 13 14 15 16 17 18 19 20 21 22 23 24
(Hour)

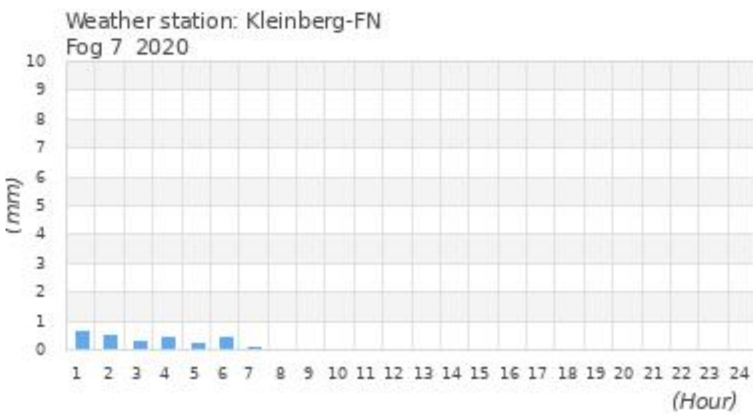
Weather station: Kleinberg-FN
Fog 7 2020
(mm)
0 1 2 3 4 5 6 7 8 9 10
1 2 3 4 5 6 7 8 9 10 11 12 13 14 15 16 17 18 19 20 21 22 23 24
(Hour)

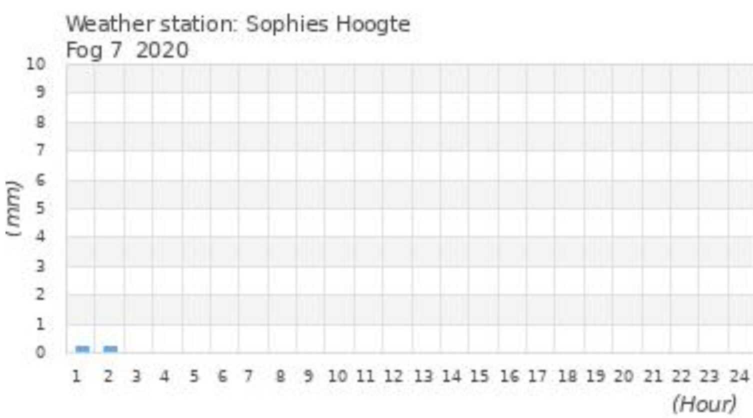
Weather station: Sophies Hoogte
Fog 7 2020
(mm)
0 1 2 3 4 5 6 7 8 9 10
1 2 3 4 5 6 7 8 9 10 11 12 13 14 15 16 17 18 19 20 21 22 23 24
(Hour)

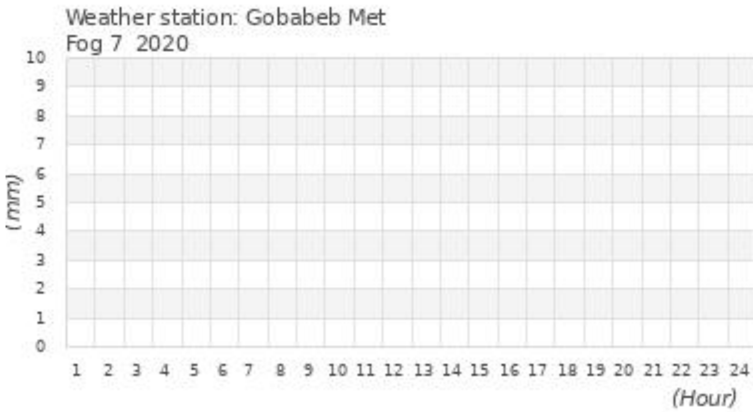

Figure 7. Hourly time series of fog occurrences at Kleinberg, Coastal Met, Sophies Hoogte, and Gobabeb SASSCAL Fognet weather stations, on 7 September 2020, the date of UAV image data collection.

3.2.3 UAV Image Processing

The multispectral images were processed in the photogrammetry software Pix4DMapper 4.0.21 (Pix4D SA, Lausanne, Switzerland) to generate orthomosaics images and the final reflectance for each spectral band (red, green, blue and near-infrared), and NDVI maps from the Sequoia multispectral camera, The multispectral imagery was processed with the Pix4DMapper Ag-Multispectral template with the “merge reflectance map tiles” option set to true. The orthomosaics, reflectance and NDVI images had an average GSD of 9.24 cm/pixel. The pre-and post-flight imagery of a reflectance calibration panel captured during each survey and was used for the radiometric correction in Pix4DMapper. Not all time-series UAV multispectral imageries were processed, due to processing errors caused by images with no geolocation and, those suffering from sun glares at solar noon (10:00 to 15:00).

The RGB images acquired by the eBee SODA RGB camera were processed in the Pix4DMapper 3DMap template, to generate orthomosaics, digital surface model (DSM) and digital terrain model (DTM) with a resolution of 5.32 cm/pixel.

Six ground control points (GCPs) targets of 60 x 60 cm permanently deployed in the mission area prior to UAV flights, their position measured with handheld GPS were used for image geo-referencing in all Pix4DMapper projects.

3.2.4 Image analyses and statistical analyses

Image analyses were performed in QGIS v.3.16.0 software for visualizing, clipping, and extracting data from the multispectral images, VI maps and DSM. Spatial terrain modelling was also carried out to obtain elevation dataset from the DSM of the high spatial resolution RGB ortho-mosaiced imagery.

Prior to data extraction, individual raw multispectral images were also geo-referenced using one of the GPCs and five more other visible and stable features in the raw images and resampled to the same extend and resolution using bilinear interpolation. The orthomosaic multispectral image were subset to the same spatial extent of the study boundary to remove edges errors due to no overlap.

Three vegetation indices (NDVI, NDRE, and SAVI) were derived to test their effectiveness in correcting for factors influencing the multispectral images (Table 4). A radiometrically uncorrected pixel values based NDVI was also calculated to assess how it varies from the radiometrically corrected reflectance value based NDVI. This also enabled us to assess how atmospheric noise influences NDVI.

Table 4. Vegetation indices used for the radiometric correction comparison. The bands are: R (Red), G (Green), Re (Red edge), NIR (Near infrared).

Index	**Description**	**Equation**	**Reference**
NDVI	Normalized Difference Vegetation Index	*NDVI = (NIR – R)/(NIR + R)*	*Rouse et al. (1974)*
SAVI	Soil-Adjusted Vegetation Index	*SAVI = (1 + L)(NIR – R)/(NIR + R + L)*	*Huete (1988)*
NDRE	Normalized Difference Red-Edge Index	*NDRE = (NIR – RE)/(NIR + RE)*	*Barnes et al. (2000)*

To analyze the effects of brightness variation (i.e. due to solar-, surface- and sensor-viewing geometries variation and topography) in UAV multispectral images and VIs, we used 15 10 × 10 m (100 m^2) Areas of interest (AOIs) defined along topographic and brightness gradient (Figure 9). The 15 AOIs were grouped into 3 plot position groups of topography (i.e. west, center of the ridge and east side of the ridge). They represented the brightness variations effects in the images. These AOIs enable the analyzing the effects of sun-sensor-surface viewing angle on raw individual footprint multispectral images, orthomosaics multispectral images and VI.

The 15 delineated ROIs were saved as ESRI polygon shapefiles and used extract key descriptive statistical metrics (cumulative sum, mean, maximum, minimum, coefficient of variation, and standard deviation) from all the time series multispectral images and VI maps. These summary statistics were used for further graphical display and statistical analyses in RStudio (R Core Team 2021). Statistical analysis was undertaken to test the main effect of the plot position groups (i.e. brightness variation) on the reflectance values or pixel values of UAV image dataset (i.e. multispectral images and VI values), and to evaluate the differences between means of plot position groups. The normality assumptions were met, after Shapiro test. Therefore, a one-way ANOVA were performed, followed by **Tukey HSD pot-hoc test for pairwise comparisons**. All tests were considered significant at $p < 0.05$. Bar plots with error-bars were created using the R package "ggplot2". The time series of individual footprint raster images were read and plotted into the local environment using package "raster" in RStudio. While visual time series maps of the orthomosaics reflectance multispectral image and VI were created in QGIS v3.16.0. The Elevation model maps were created in QGIS v3.16.0.

3.3 Results

The presence of environmental and technical factors, such as relief, solar elevation, sun-, sensor- and surface- illumination and viewing angles/geometry are the factors that influence brightness in UAV imagery. In this section, showed the consistency of the lighting variations in UAV image datasets (i.e. multispectral imagery and VI maps) rather than the absolute accuracy of spectral reflectance values.

3.3.1 Brightness variation in individual raw UAV Parrot Sequoia multispectral imagery

The illumination brightness variation due to solar- and sensor-viewing geometries variation had visible effects across the hourly time series of individual raw footprint multispectral images from the 07 September 2020 flight, a fog day (Figure 8). The brightness variation was less pronounced in the morning at 08:00-09:00 and in the late afternoon at 16:00-17:00 than in the midday hours of 10:00-15:00, in all multispectral image bands. The brightness variation was less pronounced in the red edge and NIR bands than the red and green bands, respectively, throughout the day.

The brightness (i.e. sun glare) varies with the position of the sun, with brighter areas in the direction opposite the sun, and darker areas in the direction of the sun (or away from the Sun) (Figure 8). The changing illumination geometry also caused vignetting effects, which were shown as increasing variation in DNs or pixel values across the individual raw footprint multispectral image bands. These effects were more prominent in the green and red bands than in the NIR and red edge bands, respectively (Figure 8 and Figure 9). The result also indicated vignetting effects to be the increase in pixel values in the direction opposite the sun and an increase in a circular manner away from the image centre (Figure 8 and Figure 9). There was the brightness gradient relative to the incident sun which caused brightness inconsistency (i.e. non-uniform illumination) across in the footprint imagery (Figure 8 and Figure 9).

The UAV missions were performed at different times of days to monitor the effects of the variation of solar elevation angle and weather conditions. Table 5 shows the results of sun elevation angle sun azimuth and altitude for the time series pictures in Figure 8, determined using the National Oceanic and Atmospheric Administration (NOAA) sunrise/sunset and solar position calculator (US Department of Commerce, NOAA 2021). These are the angle of the sun at the time and location specified. The brightness images effect in the time series pictures in Figure 8 correspond with the sun angle, altitude and azimuth (Table 5)

Table 5. Information of the 07 September 2020 UAV flights performed and climatic conditions

Flight time (hh:mm)	**Solar azimuth**	**Solar elevation angle (°)**	**Incoming radiation (W/m²) (Coastal Met station)**	**Wind (m/s) (Coastal Met station)**
08:00	78.18	11.83	3.27.7	6.4
09:00	70.96	25.06	658.2	7.7
10:00	61.56	37.65	877.0	8.6
11:00	48.06	48.93	765.0	7.6
13:00	332.71	57.52		
15:00	308.8	46.95	439.1	7.1
16:00	296.27	35.34	222.8	7.4
17:00	287.01	21.93	36.0	7.0

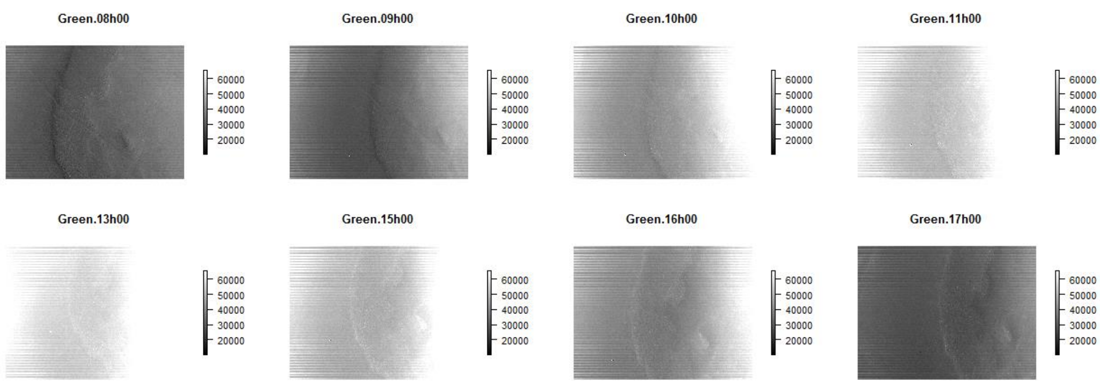

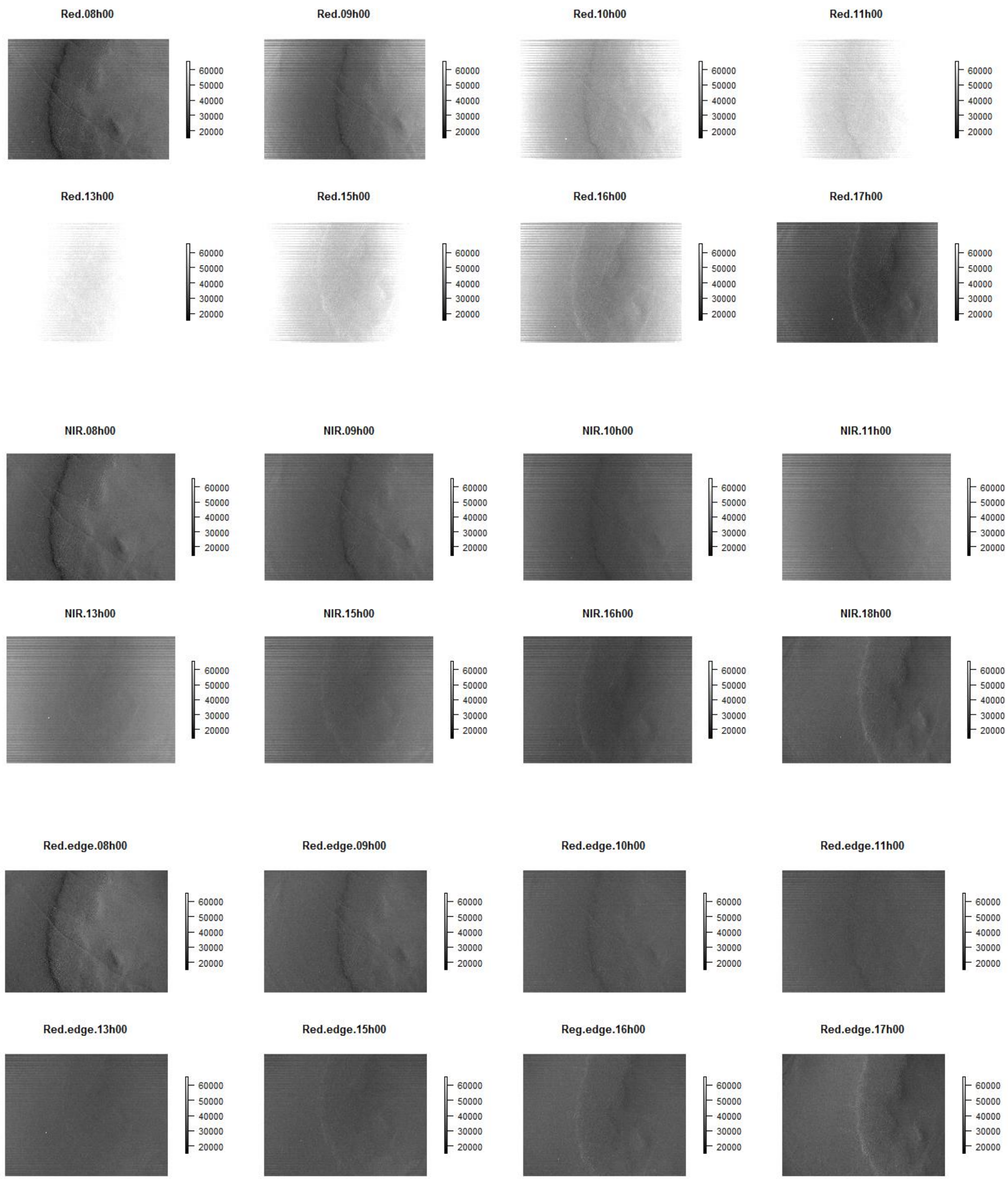

Figure 8. Brightness variation effects in time series of Parrot Sequoia multispectral individual raw bands (i.e. original single footprint images) acquired at 80 m flight altitude on a fog day, 07 September 2020, Swartbank site.

The time series were collected from 08:00 am to 17:00 pm, but 12:00, 14:00 were missed out not only due to less batteries availability, but also because these time of day there was extreme sun intensity.

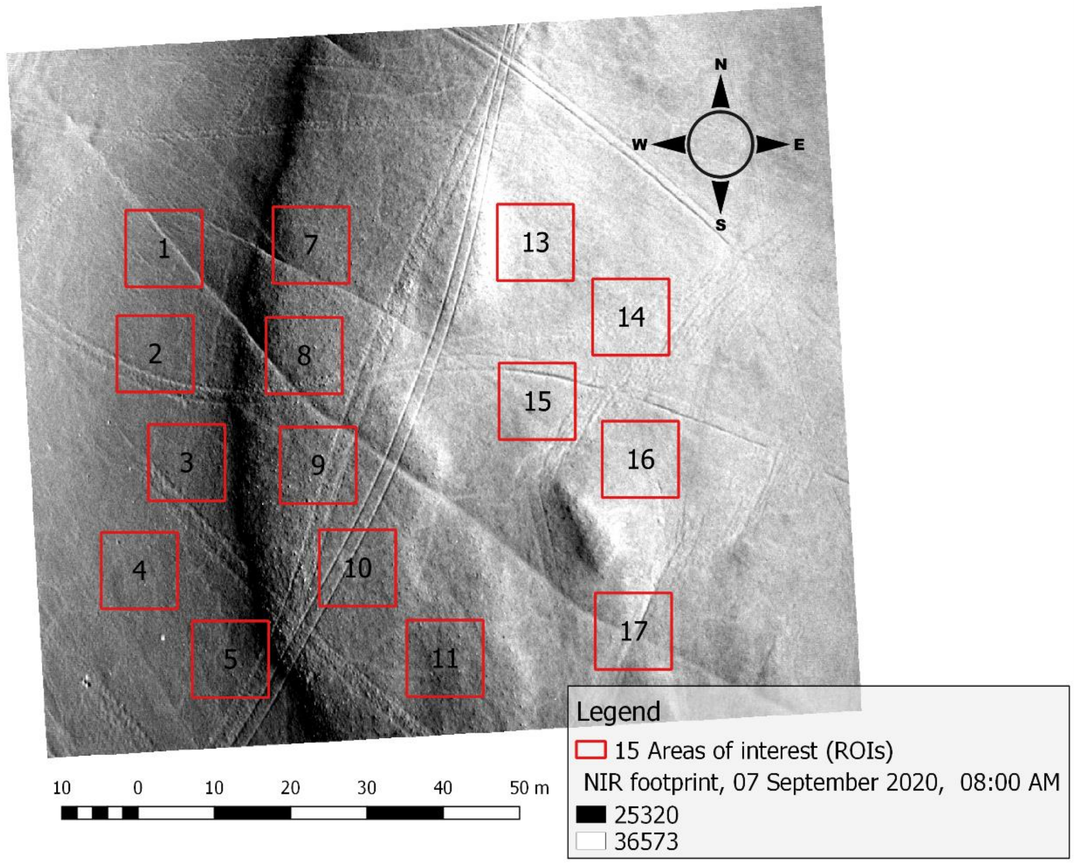

Figure 9: A close visual of a georeferenced NIR individual footprint raw image with brightness variation effects, captured in an 80-m flight altitude at 08:00 am, on 07 September 2020, Swartbank site. The red squares are the 15 ROIs established across three plot positions relative to the brightness gradient, to assess the influence of brightness variation on reflectance in individual footprint raw images, and orthophoto mosaics of reflectance and VIs maps.

The means pixel values of the plot position groups (i.e. west, center, and west side of the ridge) were more consistent for the Red edge than the NIR bands, and for the NIR band more than for the Green and Red bands, respectively (Figures 10 to 13). The variations in mean pixel values were less between the west and centre than in the east plot positions. There was an increase in pixel values at noon and midday than in the morning and late afternoon hours.

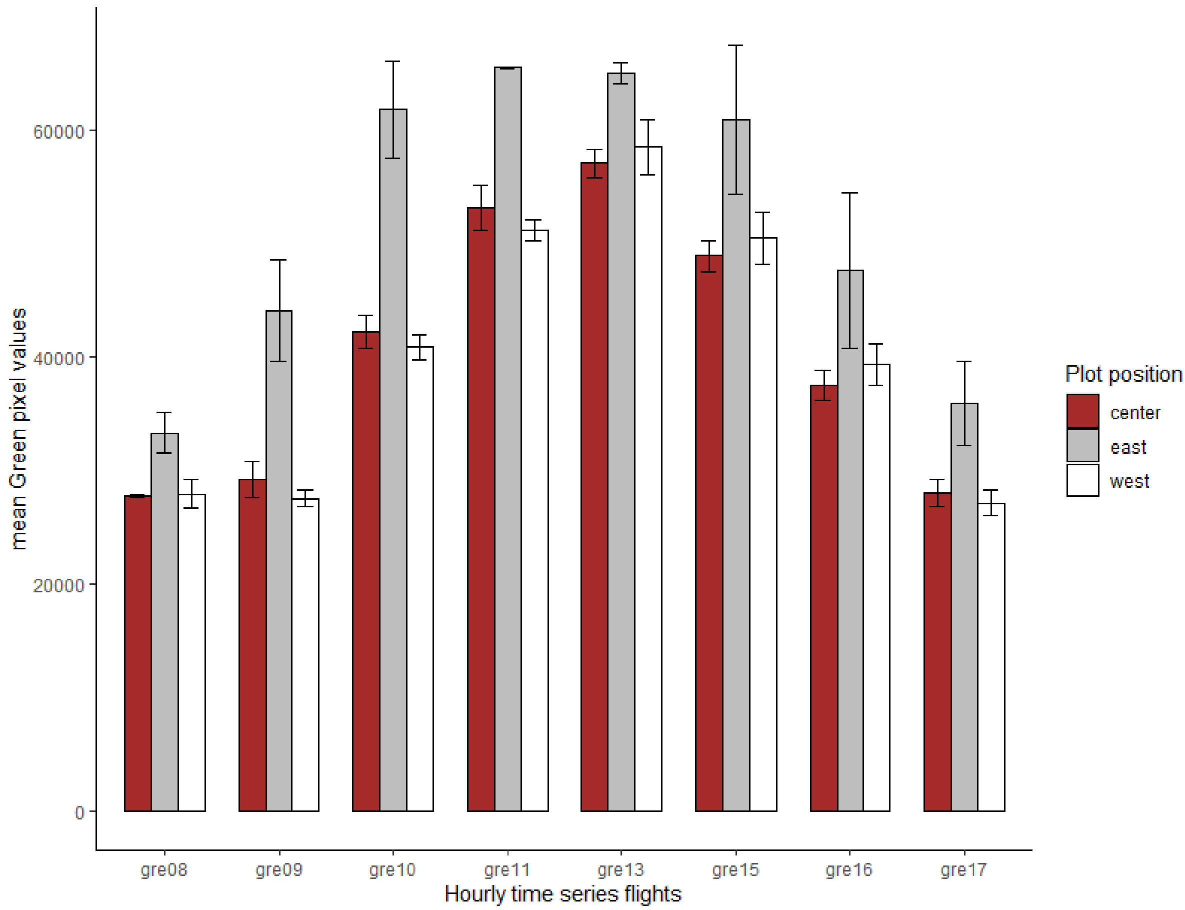

Figure 10: Plot positions representing the west, center, and west side of the ridge, with brightness variation in pixel values across the raw green band (530 – 570 nm), in each time series 80 m flight, 07 September 2020, Swartbank site. The hourly time series images for the green band were gre08 = 08:00, gre09 = 09:00, gre10 = 10:00, gre13 = 13:00, gre15 = 15:00, gre16 = 16:00, gre17 = 17:00.

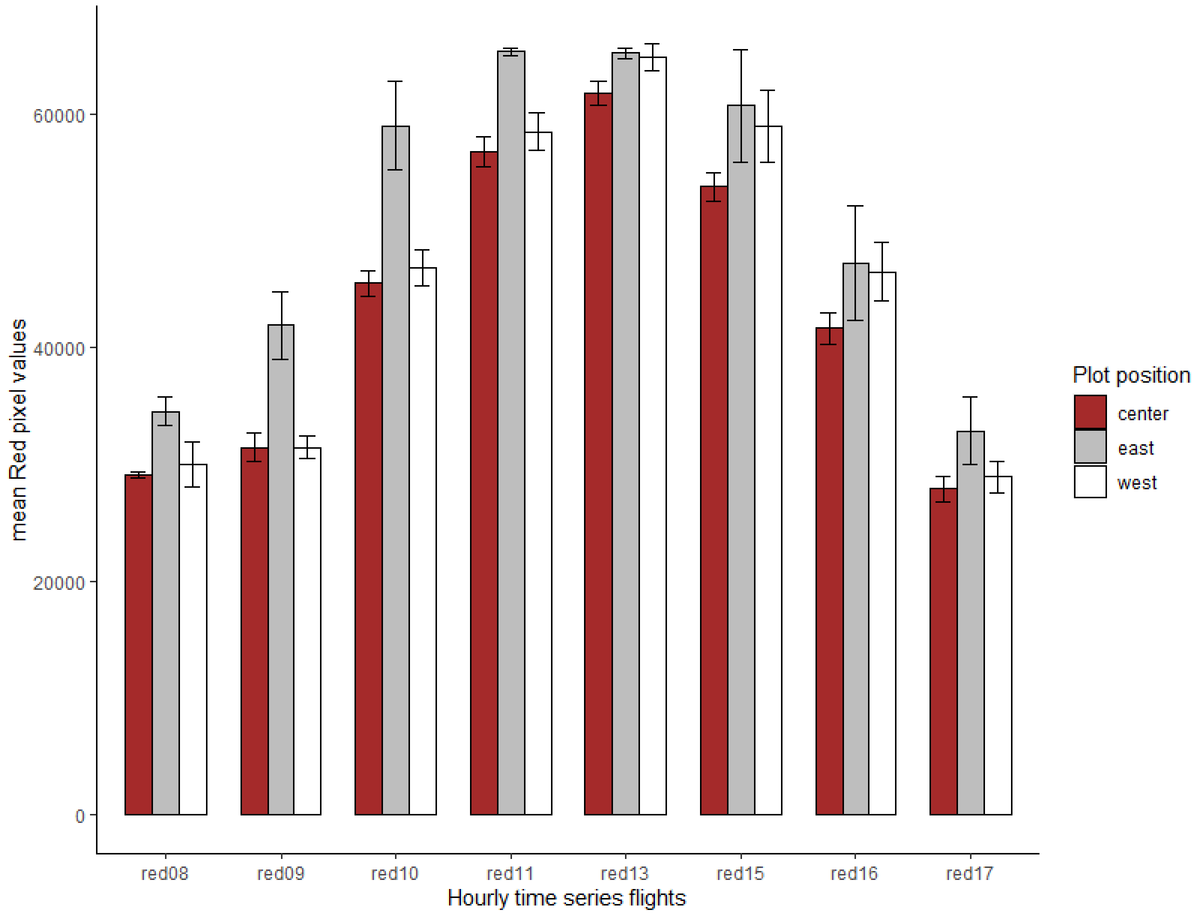

Figure 11: Plot positions representing the west, center, and west side of the ridge, with brightness variation in pixel values across the raw red band (640 – 680 nm), in each time series 80 m flight, 07 September 2020, Swartbank site. The hourly time series images for the green band were red08 = 08:00, red09 = 09:00, red10 = 10:00, red13 = 13:00, red15 = 15:00, red16 = 16:00, red17 = 17:00.

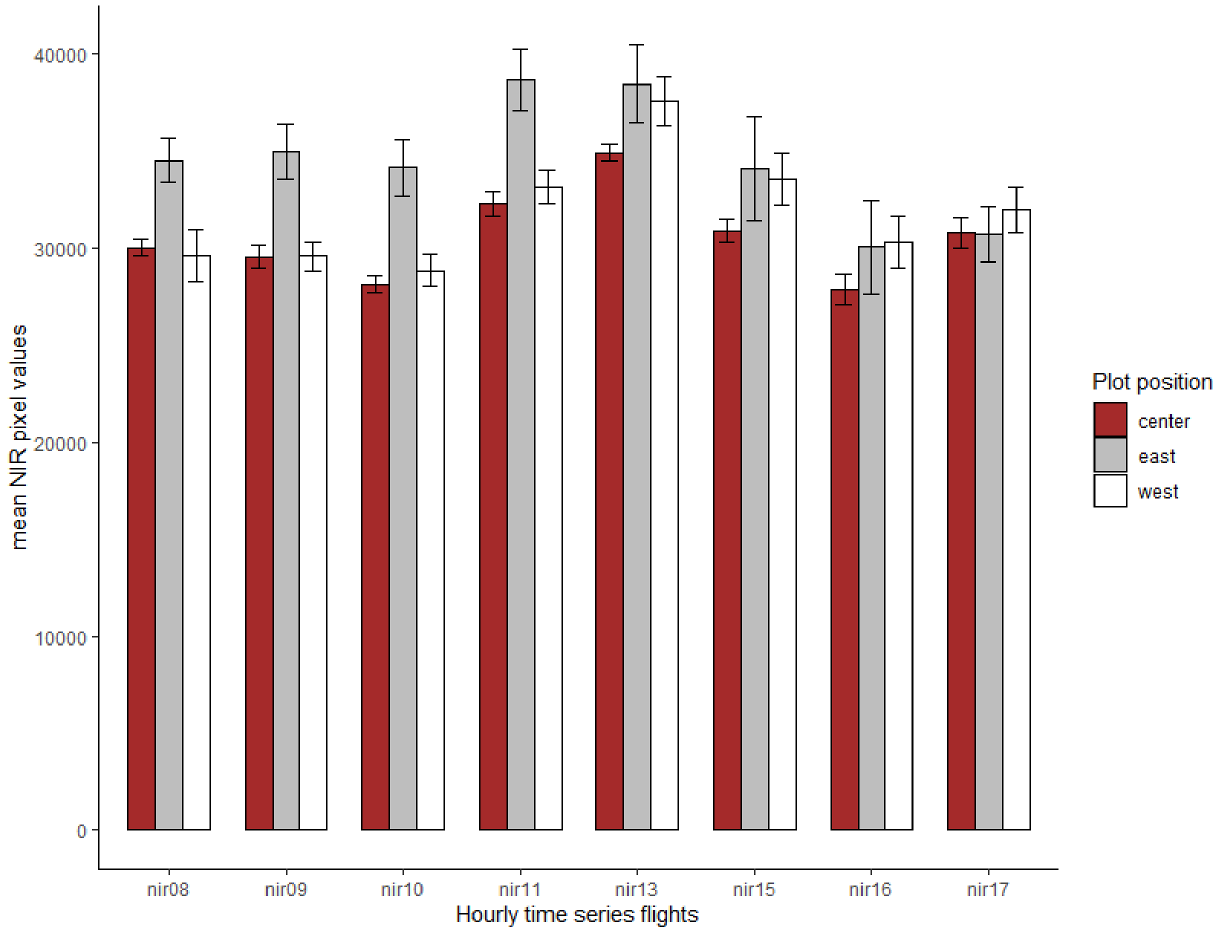

Figure 12: Plot positions representing the west, center, and west side of the ridge, with brightness variation in pixel values across the raw red band (730 – 740 nm), in each time series 80 m flight, 07 September 2020, Swartbank site. The hourly time series images for the NIR band were nir08 = 08:00, nir09 = 09:00, nir10 = 10:00, nir13 = 13:00, nir15 = 15:00, nir16 = 16:00, nir17 = 17:00.

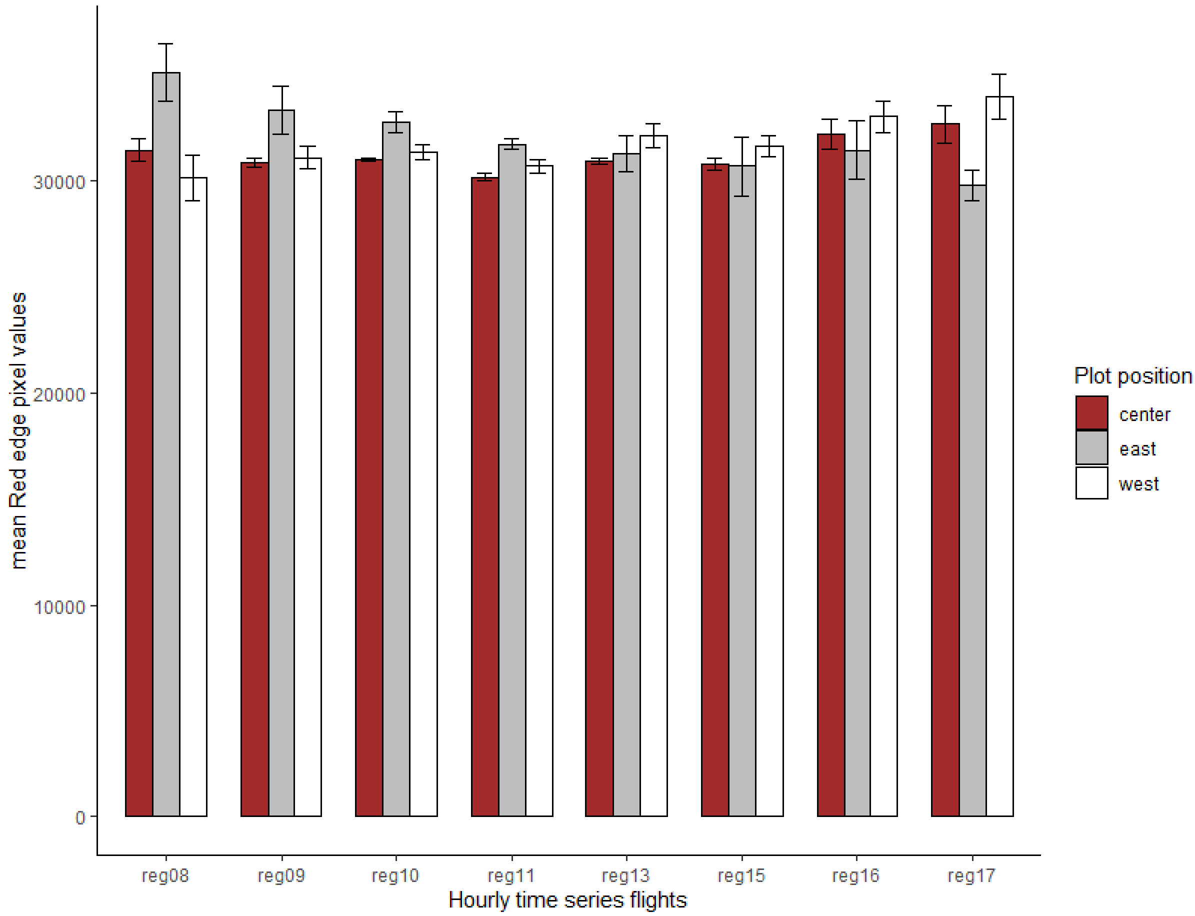

Figure 13: Plot positions representing the west, center, and west side of the ridge, with brightness variation in pixel values across the raw red band (730 – 740 nm), in each time series 80 m flight, 07 September 2020, Swartbank site. The hourly time series images for the red-edge band were reg08 = 08:00, reg09 = 09:00, reg10 = 10:00, reg13 = 13:00, reg15 = 15:00, reg16 = 16:00, reg17 = 17:00.

In raw individual footprint multispectral images, the results of one-way ANOVA tests showed that the main effect of plot position (i.e. brightness variation effects) on pixel values was statistically significant and large for all multispectral bands ($P < 0.05$) (Table 6). Therefore the means of the pixel values of the plot position groups differed significantly at the 95% confidence level, in each time series raw individual multispectral band. The main effect of plot position on pixel values is not statistically significant and large for 17:00 NIR image ($F(2, 12) = 2.70$, $p = 0.108$; Eta2 = 0.31, 95% CI [0.00, 1.00]) and 15:00 red edge image ($F(2, 12) = 2.77$, $p = 0.103$; Eta2 = 0.32, 95% CI [0.00, 1.00]). The means pixel values of 17:00 NIR image and 15:00 red edge image were the only time series bands that did not vary between plot position groups, due to less brightness variation effects.

Post-hoc comparisons using the Tukey HSD test revealed that in the morning hours (08:00 to 10:00) the mean pixel values for west-centre group positions are not significantly different from each other ($P > 0.05$), in all multispectral bands (Table 7). In the late afternoon, there was no significant different in the mean pixel values of all the groups ($P > 0.05$) for the 15:00 red edge, 16:00 red edge, and 17:00 NIR image.

Table 6: One-way ANOVA results for plot position group.

	NIR	**RED EDGE**	**RED**	**GREEN**
08:00	52.79*	0.89*	0.86*	0.89*
09:00	78.39*	0.81*	0.93*	0.93*
10:00	78.39*	0.90*	0.92*	0.96*
11:00	75.01*	0.92*	0.95*	0.98*
13:00	13.55*	0.92*	0.85*	0.89*
15:00	7.28*	**0.32**	0.60*	0.77*
16:00	5.11*	0.45*	0.52*	0.68*
17:00	**2.70**	0.88*	0.70*	0.85*

Note: * indicates a statistically significant difference with p< 0.05.

Table 7: Tukey HSD post-hoc comparisons of means.

Flight time	Comparison groups	NIR	RED EDGE	RED	GREEN
08:00	east-center	4486.0950*	3638.957*	5443.5727*	5555.8983*
	west-center	**-424.5248**	**-1327.466**	**937.5225**	**152.8676**
	west-east	-4910.6198*	-4966.423*	-4506.0502*	-5403.0308*
09:00	east-center	5446.76013*	2495.6175*	10462.37444*	14830.857*
	west-center	**67.19821**	**238.5187**	**19.29937**	**-1664.065**
	west-east	-5379.56192*	-2257.0988*	-10443.07507*	-16494.922*
10:00	east-center	6006.9100*	1796.906*	13478.726*	19512.297*
	west-center	**712.5727**	**335.917**	**1334.089**	**-1372.341**
	west-east	-5294.3373*	-1460.989*	-12144.637*	-20884.639*
11:00	east-center	**6388.0260**	1577.4554*	8580.910*	12325.435*
	west-center	867.7138*	**532.6797**	1694.349*	**-1919.797**
	west-east	-5520.3122*	-1044.7757*	-6886.561*	-14245.232*
13:00	east-center	3535.7401*	**344.1669**	3444.559*	7930.699*
	west-center	2668.6312*	1177.5621*	3102.918*	**1432.330**
	west-east	**-867.1089**	833.3952*	**-341.641**	-6498.370*
15:00	east-center	3204.7227*	**-81.41543**	6956.473*	12003.60*
	west-center	2642.3589*	**857.58944**	5209.733*	**1591.32**
	west-east	**-562.3638**	**939.00486**	**-1746.740**	-10412.28*
16:00	east-center	**2185.2451**	**-750.9823**	5533.9815*	10154.488*
	west-center	2459.5493*	**842.5706**	4840.2231*	**1888.633**
	west-east	**274.3042**	**1593.5529**	**-693.7583**	-8265.854*
17:00	east-center	**-122.6149**	-2899.720*	4963.317*	7913.7240*
	west-center	**1119.1970**	1279.088*	**997.032**	**-866.5976**
	west-east	**1241.8119**	4178.808*	-3966.285*	-8780.3216*

Note: * indicates a statistically significant difference with p< 0.05.

3.3.2 Brightness variation in the orthomosaics UAV multispectral imagery

The brightness variation effects and the vignetting effects across the time series of raw individual footprint images, due to the influence of the solar elevation, anisotropic reflectance, and sun-sensor-surface illumination and viewing angles/geometry, were reintroduced in the orthomosaics multispectral images (Figures 14 to 17). The 11:00 mosaicked image was not a full mission. Although the raw 13:00 footprint image was shown, the 13:00 mosaicked image was left out because it had the most extreme sun glare effects and run into image processing failure.

The vegetation indices maps (e.g. NDVI, SAVI and NDRE) from the orthomosaics of radiometrically corrected reflectance-based images and uncorrected pixel values-based images, still showed the visible sun glares and brightness variation effects corresponding with the effects in raw individual images (Figures 19 to 22). The brightness variation effects across the VIs maps were smaller than across orthomosaics multispectral bands.

The illumination or brightness variations across the orthomosaics images were more consistent for the Red edge than the NIR bands, and the NIR band more than the Green and Red bands, throughout the day. But images closer to midday (especially at 11:00 and 15:00) lost detail features as they were more affected by brightness variation, than the morning (08:00) and late afternoon (17:00) multispectral images.

The reflectance images in the morning (08:00) and late afternoon (17:00), had a difference in brightness between the image section in the direction opposite the sun and those in the direction of the sun, as well as shade effects caused by lower sun elevations and topography (Figures 14 to 17). In the morning, the 08:00 reflectance maps showed an increase in reflectance values on the east side of the map (i.e. brighter section in the direction opposite the sun), than on the west side (i.e. dark shaded section in the direction of the sun). The opposite was true in the late afternoon approaching sunset, whereby the 17:00 reflectance maps showed an increase of reflectance on the west side of the map (i.e. brighter section) than on the east side (i.e. dark section). However, this shading effect gets weaker with the increasing sun elevation angle closer to noon.

There was also an increase in reflectance values in both orthomosaics reflectance images and VI maps, due to the vignetting effects and stripping effects corresponding with the edge effects in raw individual multispectral images (Figures 14 to 17). The reflectance values in the green and red images were noticeably higher and outside of the possible reflectance range with increasing solar elevation in the flights taken closer to solar noon or midday (from 10:00 to 15:00). This influence is more observed in the uncorrected pixel value–based NDVI (Figure 19).

The observed stripping edge effects and brightness variation effects in orthomosaics images are corresponding with the edge effects in the single individual raw images. The extreme brightness and vignetting effects around the edges of the individual images were re-introduced with brighter stripes around the side-overlaps in the mosaicked images. The plots that fall within the brighter sections had a higher reflectance value compared to the dark well-illuminated sections. These striping effects are more pronounced in the green and red bands compared to the NIR and red edge reflectance bands. These effects are less pronounced in the morning (08:00 and 09:00), and late afternoon (16:00 – 17:00), but more during midday (11-15:00) at high solar elevation, in both reflectance images and VIs maps.

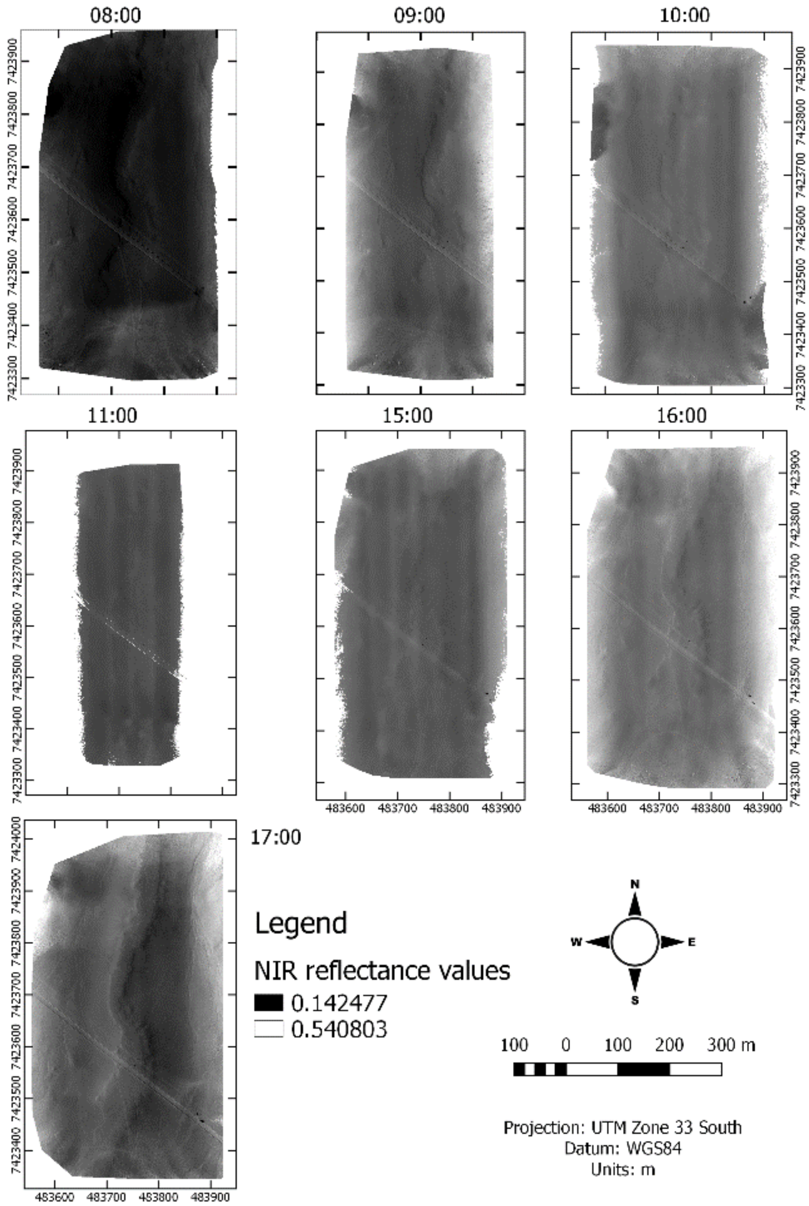

Figure 14. NIR reflectance map time series of 8h, 9h, 10h, 11h, 15h, 16h, and 17h, of the Swartbank experimental lichen field, 7th September 2020. This map illustrates the effects present in the NIR images after radiometric correction. The 11h mosaicked image was not a full mission. The 13h mosaicked image with the most extreme sun glare effects was left out because it run into image processing failure in the Pix4Dmapper.

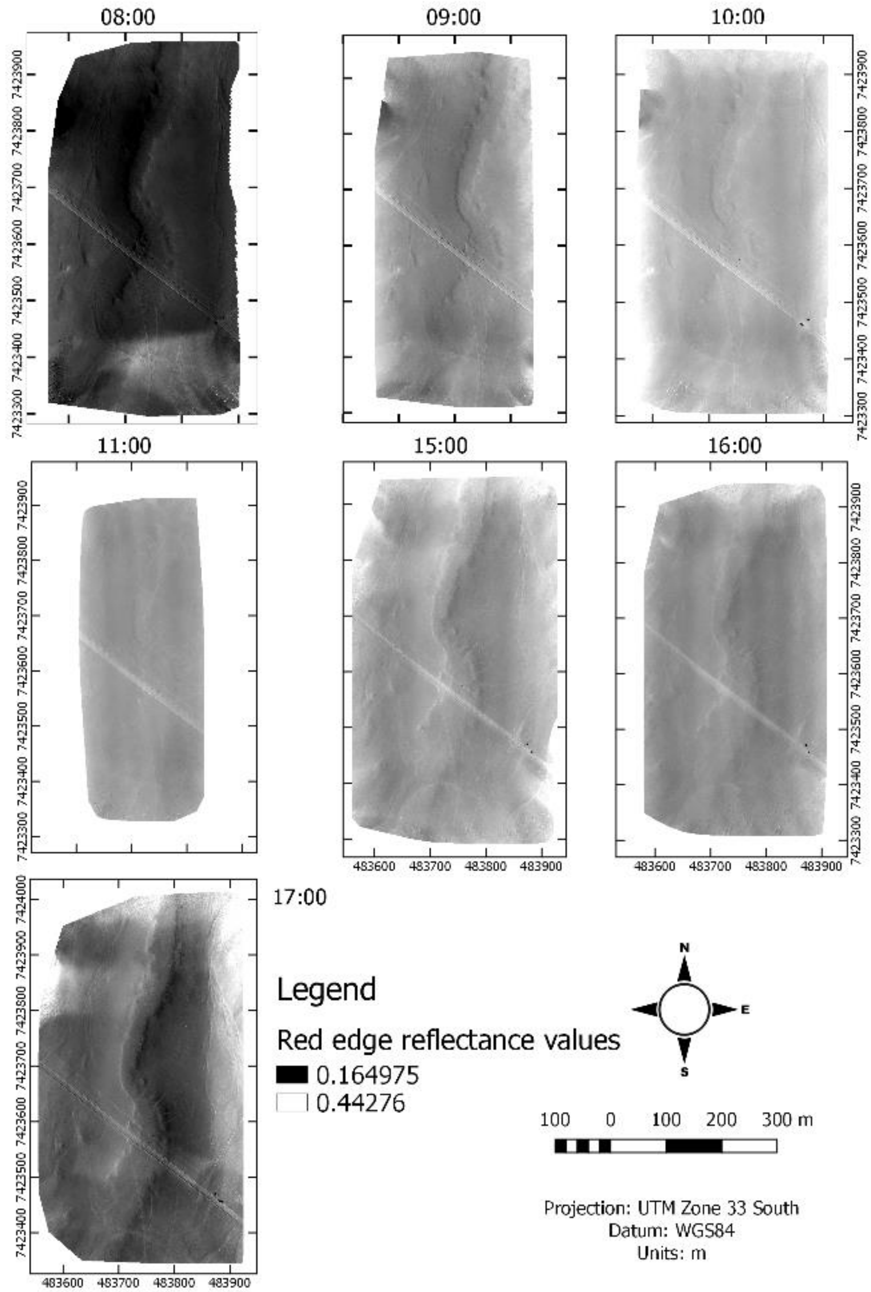

Figure 15: Red-edge reflectance map time series of 8h, 9h, 10h, 11h, 15h, 16h, and 17h, of the Swartbank experimental lichen field, 7th September 2020. This map illustrates the effects present in the Red-edge images after radiometric correction. The 11h mosaicked image was not a full mission. The 13h mosaicked image with the most extreme sun glare effects was left out because it run into image processing failure in the Pix4Dmapper.

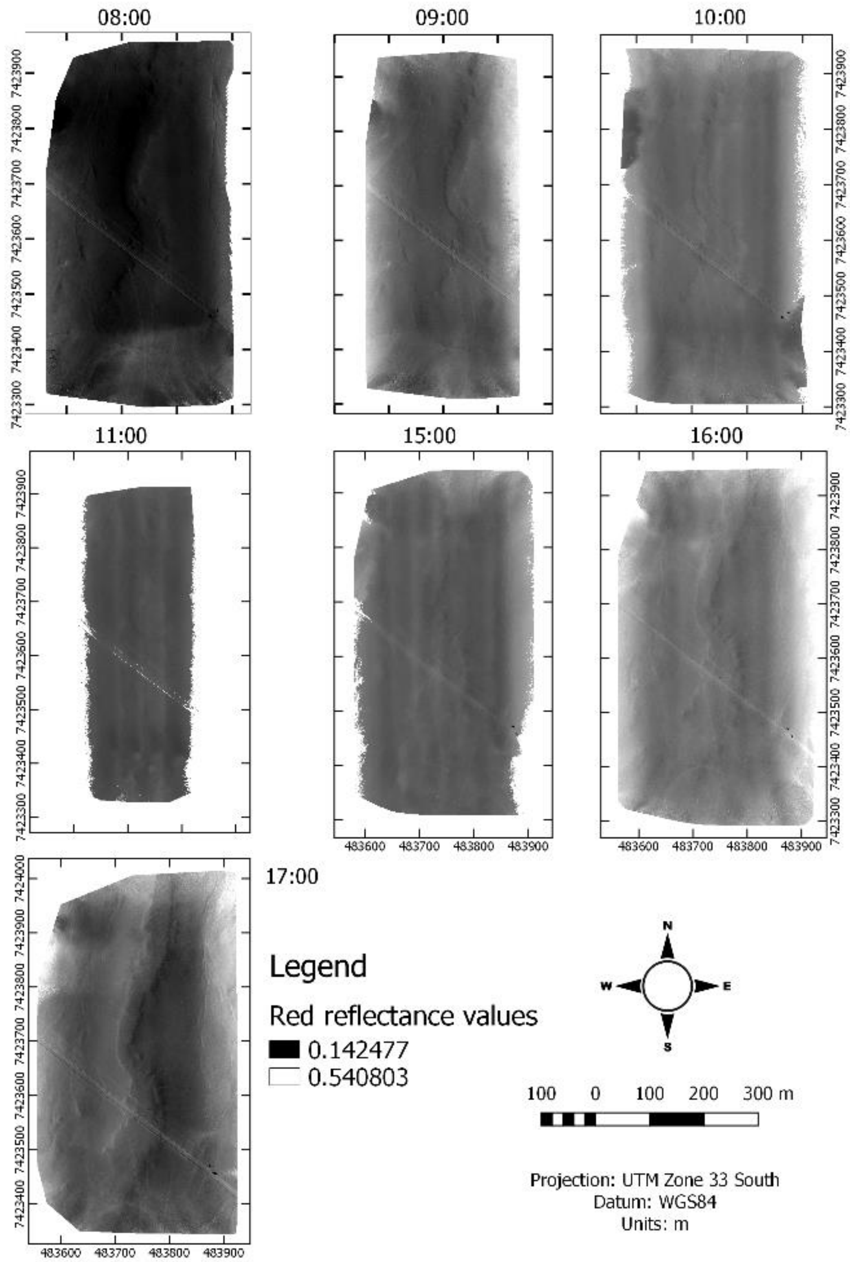

Figure 16: Red reflectance map time series of 8h, 9h, 10h, 11h, 15h, 16h, and 17h, of the Swartbank experimental lichen field, 7th September 2020. This map illustrates the effects present in the Red images after radiometric correction. The 11h mosaicked image was not a full mission. The 13h mosaicked image with the most extreme sun glare effects was left out because it run into image processing failure in the Pix4Dmapper.

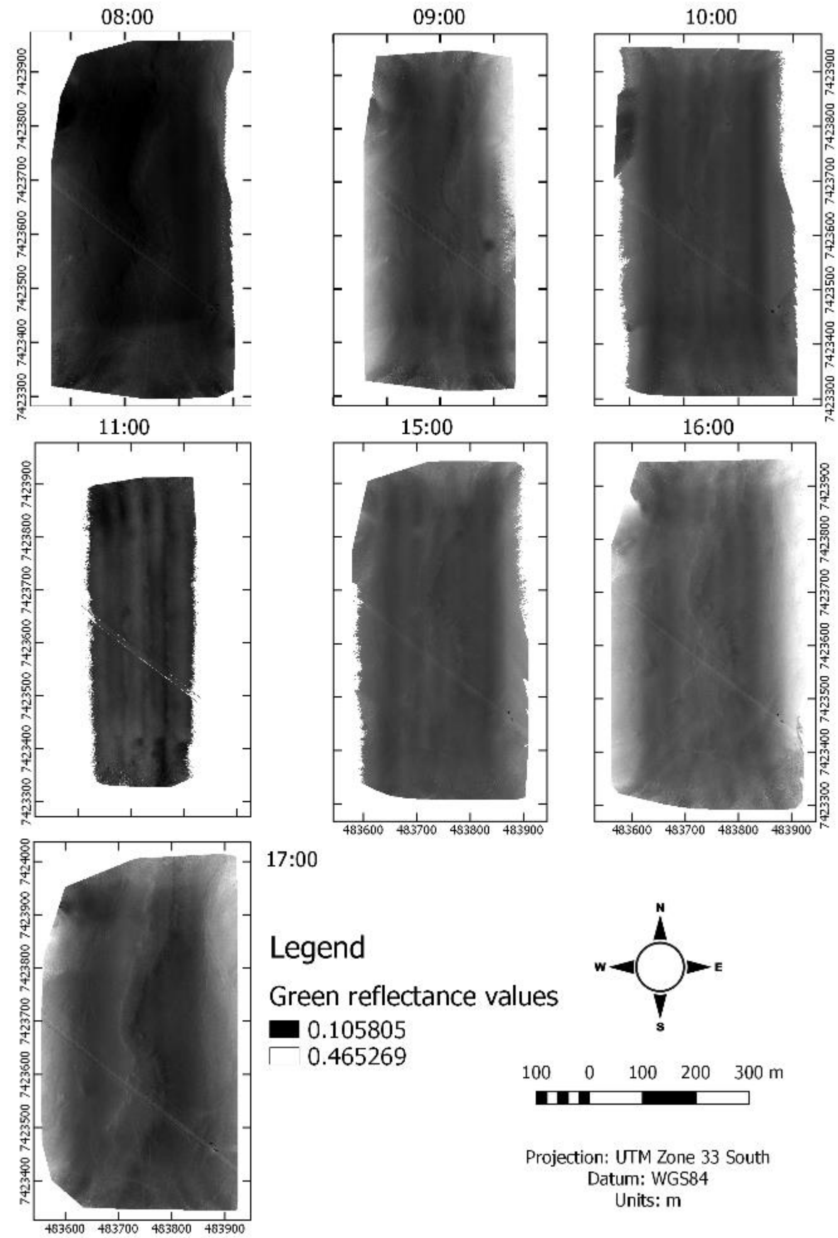

Figure 17: Green reflectance map time series of 8h, 9h, 10h, 11h, 15h, 16h, and 17h, of the Swartbank experimental lichen field, 7th September 2020. This map illustrates the effects present in the Green images after radiometric correction. The 11h mosaicked image was not a full mission. The 13h mosaicked image with the most extreme sun glare effects was left out because it run into image processing failure in the Pix4Dmapper.

3.3.3 Brightness variation in the Vegetation indices (VI)

The radiometrically uncorrected NDVI derived from pixel values-based multispectral bands had lower values throughout the day (Figures 19), compared to the corrected reflectance-based NDVI (Figures 20). The radiometrically corrected images improved the performance of reflectance-based NDVI to estimate lichens' biophysical properties, while minimizing the effects present in the uncorrected multispectral bands (Figure 19).

The radiometrically corrected soil-adjusted vegetation index (SAVI) minimized soil brightness influences using a soil brightness correction factor, which is often used in arid regions where vegetative cover is low (Figure 21). The results of the radiometrically corrected reflectance-based NDRE map did not seem to perform better than the NDVI, by using the 'Red Edge' spectral band instead of the Red bands (Figure 19).

The multispectral bands had a contrast between areas in full sunlight and shadowed areas which appeared to increase at low solar elevation. The NDVI and SAVI maps corrected for shade caused by terrain variation (hills and valleys) so that the colour of features are emphasized rather than the intensity or brightness of the features. However, there were shadows on the road tracks and riverine which resulted in overestimated reflectance values. The NDVI maps in the morning (at 08:00) and late afternoon (17:00) showed fewer shadow effects on the tracks compared to midday flights. In addition, the oversaturation of reflectance were observed around the GCPs plates in both the corrected the NDVI and SAVI maps.

The effects in the orthomosaics multispectral images were corrected to some extent, but the extreme effects showed up in the corresponding time series VI maps. The effect was much less visible in the VI maps in the morning 08:00 and late afternoon 17:00 flights but appeared to be more intense in the midday 11:00 and 15:00 flights (Figure 8). This means that the high-quality image dataset were those taken at 08:00 and 17:00.

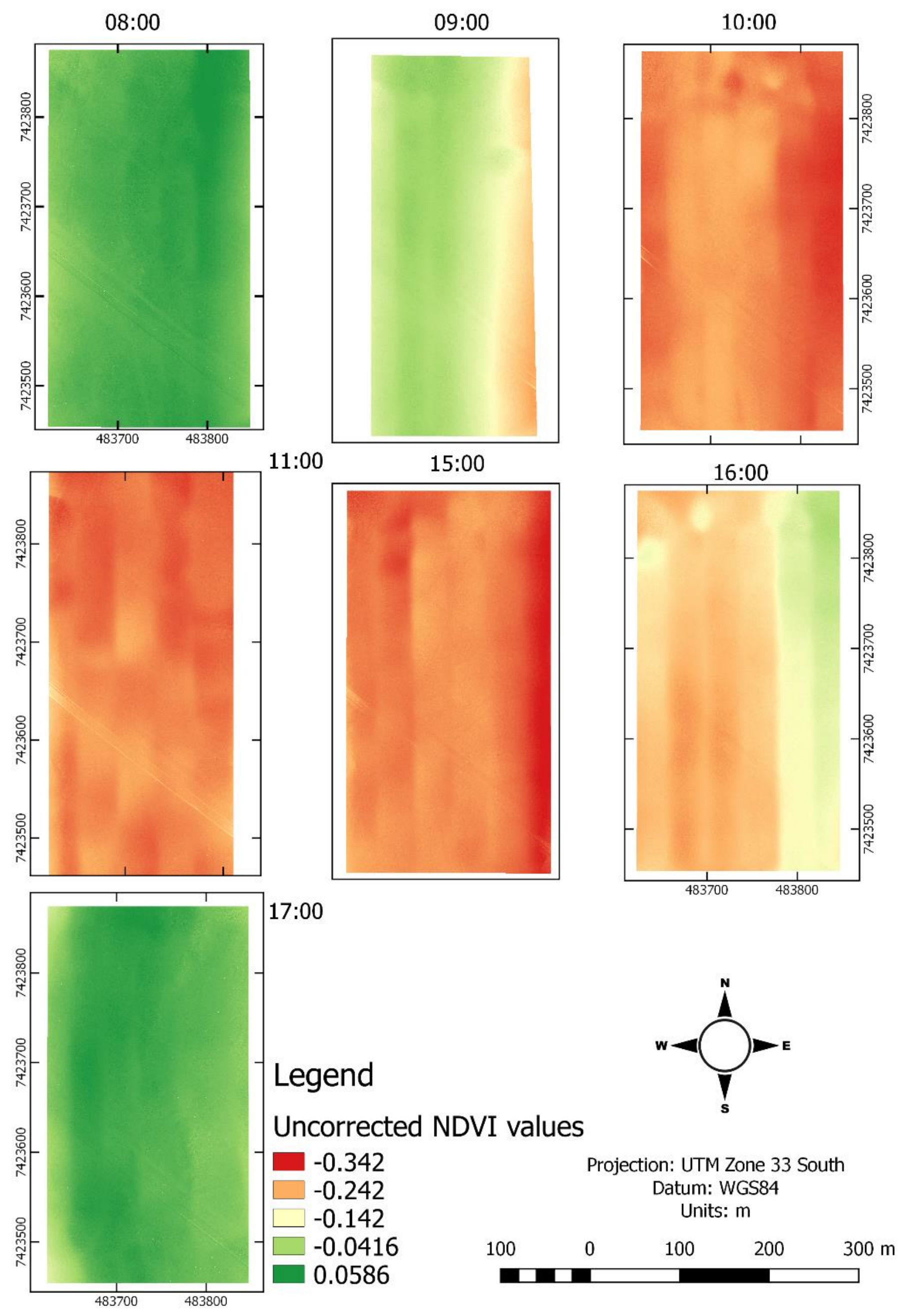

Figure 18: Pixel values based NDVI time series of 8h, 9h, 10h, 11h, 15h, 16h, and 17h, of the Swartbank experimental lichen field, 7th September 2020. This map illustrates the effects present in NDVI maps without radiometric correction.

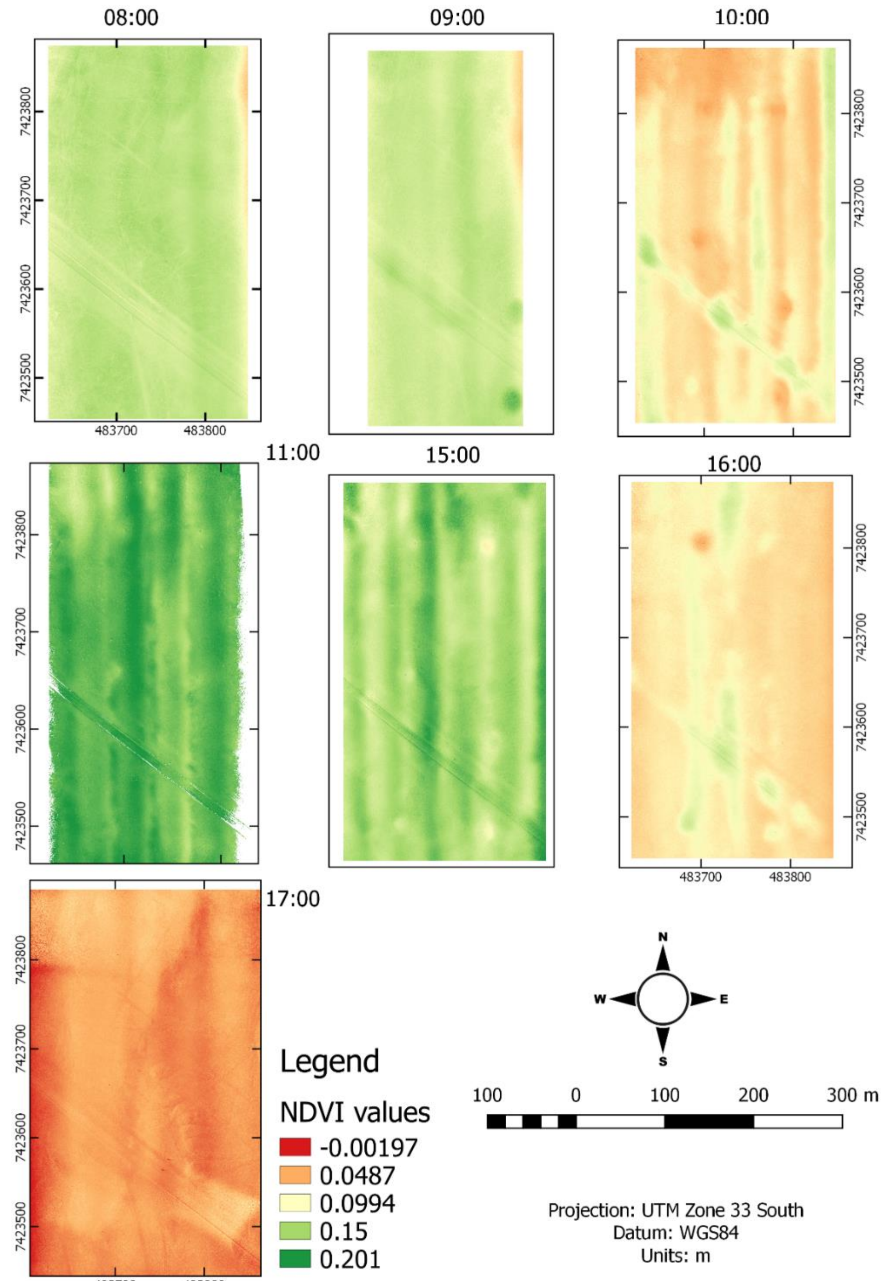

Figure 19: Radiometrically corrected reflectance-based NDVI time series of 8h, 9h, 10h, 11h, 15h, 16h, and 17h, of the Swartbank experimental lichen field, 7th September 2020. This map illustrates the effects present in NDVI maps after radiometric correction.

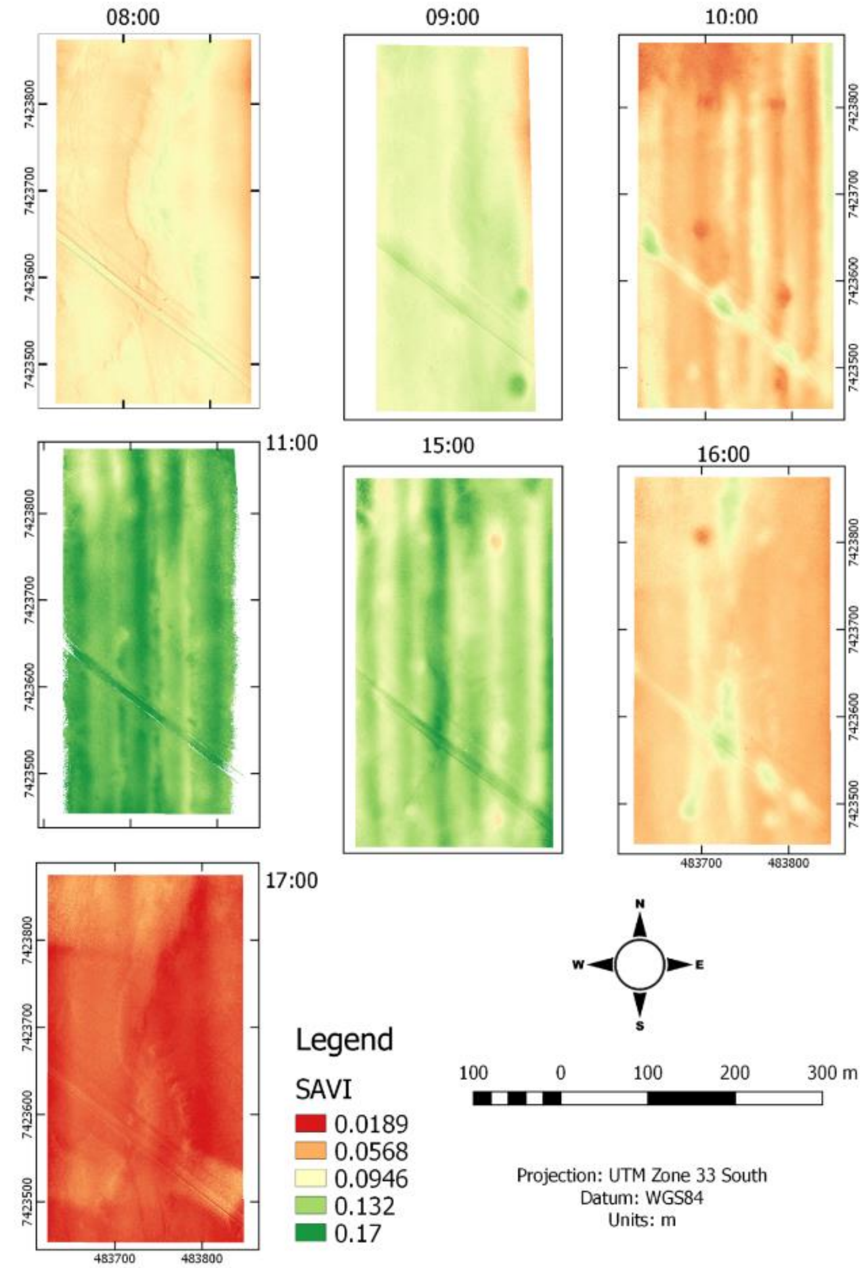

Figure 20: Radiometrically corrected reflectance-based SAVI time series of 8h, 9h, 10h, 11h, 15h, 16h, and 17h, of the Swartbank experimental lichen field, 7th September 2020. This map illustrates the effects present in SAVI maps after radiometric correction.

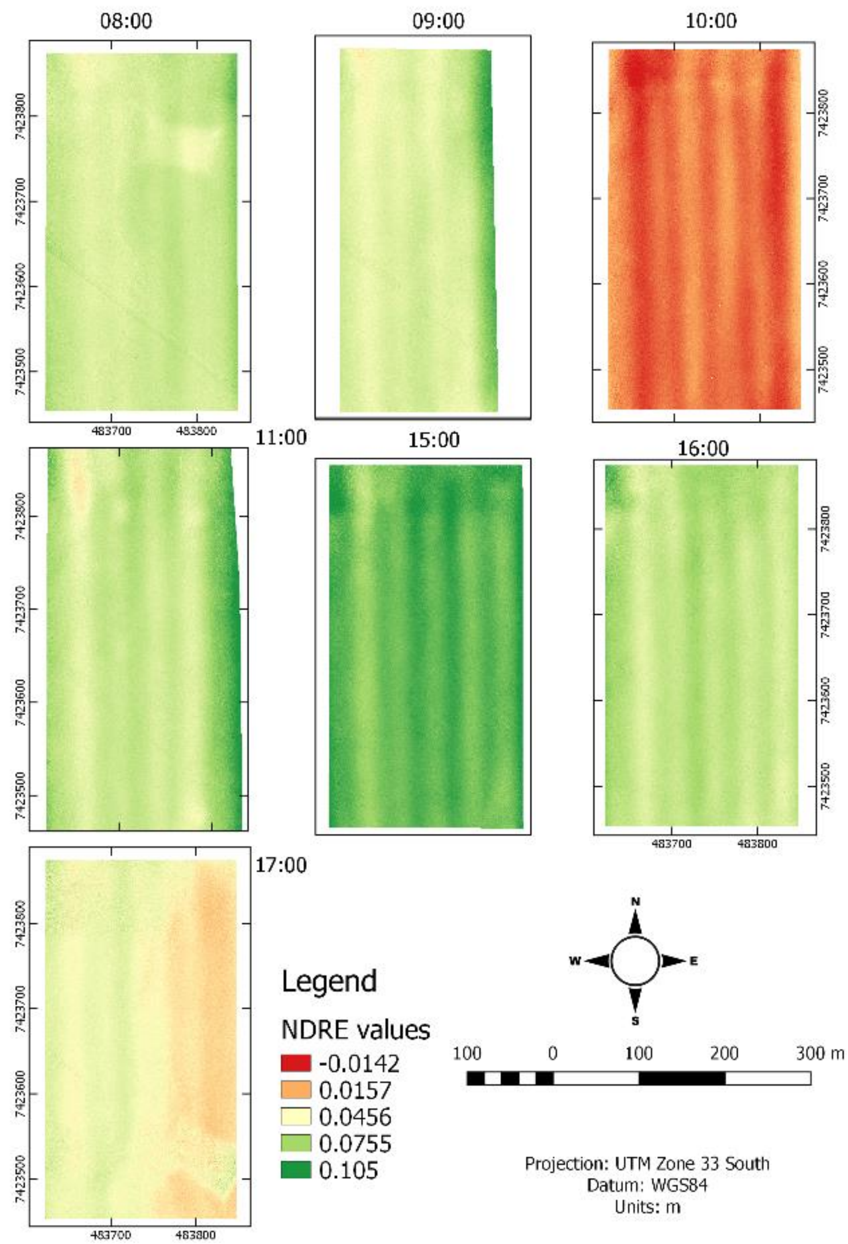

Figure 21: Radiometrically corrected reflectance based NDRE time series of 8h, 9h, 10h, 11h, 15h, 16h, and 17h, of the Swartbank experimental lichen site, 7th September 2020. This map illustrates the effects present in NDRE maps after radiometric correction.

Reflectance inconsistency (i.e. non-uniform illumination) was also present in the VI maps, as shown by image subsets of the SAVI map, including the 15 AOIs in 3 plot position groups (i.e. west, center, and east) along the brightness gradient relative to the incident sun (Figure 23). The 3 plot position groups represented the brightness variations effects in the images and were used to assess the effects of brightness variations on image data.

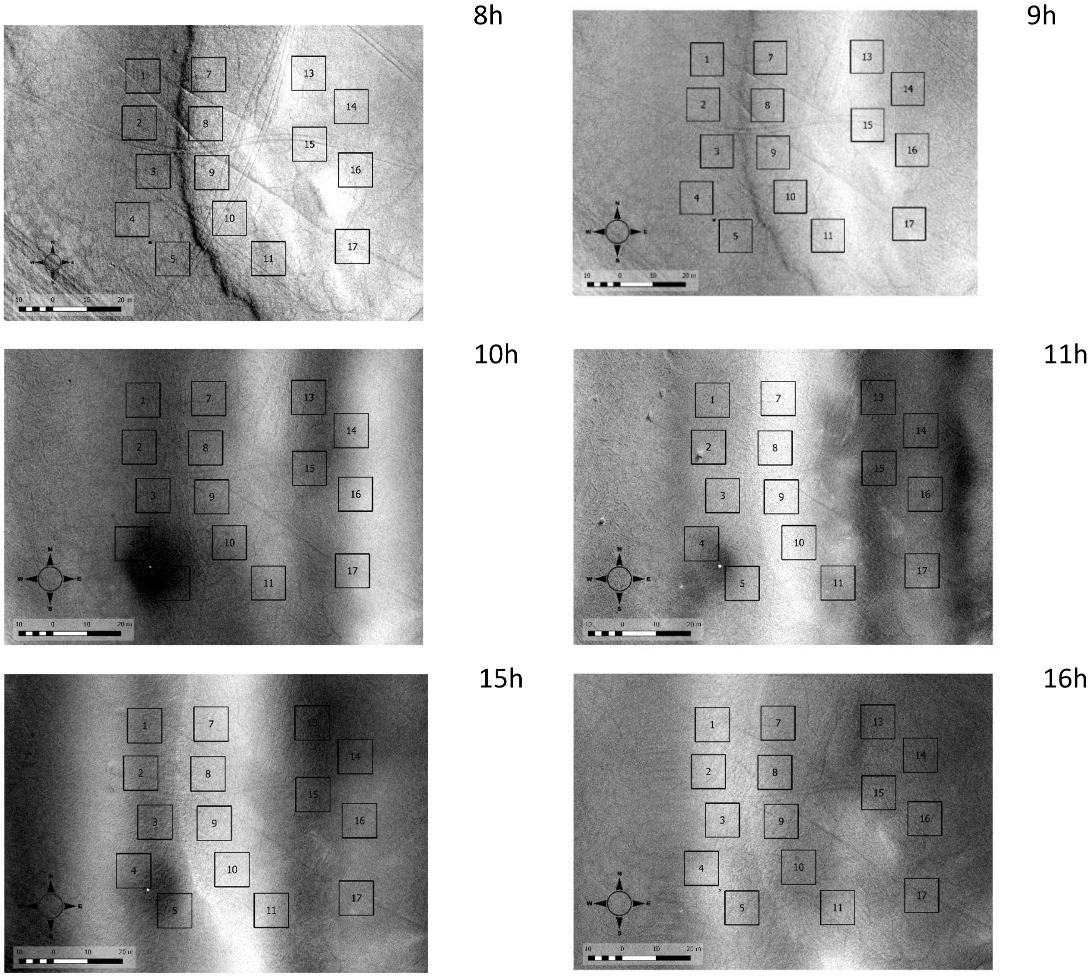

17h

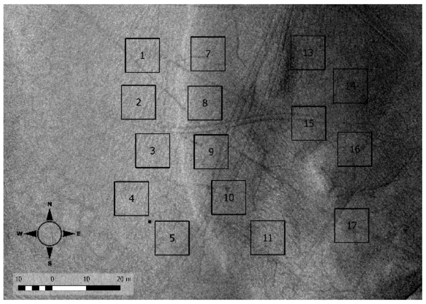

Figure 22: Time series of the radiometrically corrected reflectance-based SAVI for Swatbank experimental lichen field, on the 7th September 2020 flights. This map illustrates brightness gradient and black squares are the ROIs used to analyse differences in brightness in orthophotos mosaics of reflectance and VI in the plot position groups (i.e. west, center, and east).

Table 8 showed results of one-way ANOVA tests of the mean of plot position groups (i.e. west, center, and east). The means of reflectance or pixel values in the plot position groups were statistically significant and large for all VI ($P < 0.05$). Therefore the mean reflectance values of the plot positions differed significantly at the 95% confidence level, for each time series VI. However, there was no significant difference in the means values of plot position ($P > 0.05$), in the 09:00 NDVI ($F (2, 12) = 2.23$, $p = 0.150$; $Eta2 = 0.27$, 95% CI [0.00, 1.00]) and 16:00 NDRE ($F (2, 12) = 1.63$, $p = 0.236$; $Eta2 = 0.21$, 95% CI [0.00, 1.00]).

In Table 9 post-hoc comparisons using the Tukey HSD test revealed that the mean values of the paired plot position groups were mostly significantly different from each other ($P < 0.05$). However, in the morning, the 08:00 NDVI showed, that the mean pixel values of east-center positions are not significantly different from each other ($P > 0.05$). The 09:00 NDVI, the mean pixel values of all plot position groups were not significantly different from each other ($P > 0.05$).

During the late afternoon, only in the 16:00 NDRE, the mean pixel values of all plot positions were not significantly different from each other ($P > 0.05$). While in the 16:00 uncorrected NDVI, only the west-center positions the mean pixel values of all plot positions were not significantly different ($P > 0.05$). In the 17:00 uncorrected NDVI, only the east-center and west-center were not significantly different from each other ($P > 0.05$).

Table 8: One-way ANOVA results for VIs plot position groups and Tukey HSD post-hoc comparisons.

ANOVA	**Signif. codes: 0 '***' 0.001 '**' 0.01 '*' 0.05 '.' 0.1 ' ' 1**		
Data name	**Multiple R-squared**	**Pr(>F)**	**Signif. Codes**
uc_NDVI08	0.77	0.000134	***
uc_NDVI09	0.92	3.63E-07	***
uc_NDVI10	0.71	0.000604	***
uc_NDVI11	0.48	0.0204	*
uc_NDVI15	0.78	0.000125	***
uc_NDVI16	0.84	1.80E-05	***
uc_NDVI17	0.41	0.0438	*
NDVI08	0.75	0.000234	***
NDVI09	0.27	**0.15**	
NDVI10	0.66	0.00159	**
NDVI11	0.83	2.64E-05	***
NDVI15	0.84	1.52E-05	***
NDVI16	0.9	9.49E-07	***
NDVI17	0.9	9.49E-07	***
SAVI8	0.94	3.32E-08	***
SAVI9	0.71	0.000634	***
SAVI10	0.68	0.00103	**
SAVI11	0.84	1.85E-05	***
SAVI15	0.85	1.31E-05	***
SAVI16	0.91	3.87E-07	***
SAVI17	0.91	4.45E-07	***
NDRE08	0.86	7.29E-06	***
NDRE09	0.56	0.00716	**
NDRE10	0.52	0.0122	*

NDRE11	0.46	0.0238	*
NDRE15	0.53	0.0109	*
NDRE16	0.21	**0.236**	
NDRE17	0.84	1.67E-05	***

Table 9: One-way ANOVA results for VIs plot position groups and Tukey HSD post-hoc comparisons.

Tukey multiple comparisons of means - 95% family-wise confidence level									
		uc_NDVI		**NDVI**		**SAVI**		**NDRE**	
Time	**Comparison groups**	**p adj**	**Signif. codes**	**p adj**	**Signif. codes**	**p adj**	**Signif. codes**	**p adj**	**Signif. codes**
8	east-center	0.0122982	*	**0.2490133**		0.0001205	*	0.0007823	*
8	west-center	0.0304734	*	0.0002122	*	0.0000123	*	0.0107021	*
8	west-east	0.0000935	*	0.0034577	*	0	*	0.0000051	*
9	east-center	0.0000078	*	**0.7580205**		**0.0852513**		0.0400775	*
9	west-center	0.0456688	*	**0.3901329**		0.0273738	*	0.0069283	*
9	west-east	0.0000004	*	**0.135945**		0.0004583	*	**0.602566**	
10	east-center	0.0005834	*	**0.3080412**		**0.2599251**		**0.3421491**	
10	**west-center**	**0.386742**		0.0202176	*	0.0154545	*	0.0096656	*
10	west-east	0.0060576	*	0.0013425	*	0.0008549	*	**0.1263924**	
11	east-center	0.026424	*	0.0000179	*	0.0000125	*	0.018964	*
11	west-center	**0.9331892**		0.0092603	*	0.0036318	*	**0.3764012**	
11	west-east	0.0496756	*	0.0048648	*	0.0076491	*	**0.2042631**	
15	east-center	**0.609415**		0.0000284	*	0.0000155	*	**0.9771384**	
15	west-center	0.0001668	*	0.0000695	*	0.0001405	*	0.0168188	*
15	west-east	0.0007758	*	**0.8032745**		**0.2964982**		0.024304	*
16	east-center	0.0000166	*	0.000355	*	0.0000835	*	**0.4039486**	

16	west-center	**0.1231332**		0.0009681	*	0.0011246	*	**0.2375448**	
16	west-east	0.000371	*	0.0000006	*	0.0000003	*	**0.921505**	
17	east-center	**0.6620742**		0.000355	*	0.0000987	*	0.0000129	*
17	west-center	**0.1751619**		0.0009681	*	0.0011717	*	0.0406936	*
17	west-east	0.0394744	*	0.0000006	*	0.0000003	*	0.000771	*
Note: * indicates a statistically significant difference with p< 0.05.									

3.1 Discussion

3.3.1 Brightness variation in UAV multispectral imagery

The results show that brightness variations affect the quality of the UAV images significantly. The Solar elevation and topography are the causes of the brightness variations in the images. This brightness variation affects thee homogeneity of the UAV imagery, making radiometric correction of UAV images harder in time of days with high sun intensity and clear sky conditions.

Data visualization results showed anisotropic reflectance (i.e. sun glare or brightness effects) both in the raw individual footprint images, radiometrically corrected orthomosaics images, and VI maps were stronger at higher solar elevation with direct radiation (Figure 8). The green and red image images showed stronger sun glare effects than the NIR band and red edge images. The higher the solar elevation, the higher the vignetting effects and brightness gradient variation effects across the multispectral images. This is a typical issue for UAV imagery gathered under full-sun conditions as observed by other research studies (Kelcey and Lucieer 2012, Rasmussen *et al.* 2016, Adler 2018, Fernández-Guisuraga *et al.* 2018, Tu *et al.* 2018, Assmann 2019, Stow *et al.* 2019). We also observed bright image sections were in the opposite direction of the sun, while the dark sections were in the direction of the sun, because shade effect caused by lower solar elevation, high topography, for example, the ridge running across the site. These findings agree to with other researchers who investigated the importance of the plot position relative to the incident solar radiation before plots were cropped to assess the impacts of the experimental treatments (Rasmussen *et al.* 2016).

Analysis of the different sun elevation angles per band showed that the orthomosaics from missions with sun elevation angles from 38° to 47° are more homogeneous and have less shadows, since pixels with low DN values are less frequent. The lack of more missions on the same day with different sun elevation angle do not allow to get further conclusions. The images taken at higher solar elevation at midday from 10:00 to 15:00 had greater vignetting effects and brightness variations, compared to those taken at lower solar elevation in the morning from 08:00 to 09:00, and in the late afternoon from 16:00 to 17:00. This suggested morning and late afternoon images at lower solar angle are most suitable. However, this differs from what other researcher who suggested that the general rule is to fly as close to solar noon with a maximum of 2 - 3 hours before or after solar noon, to minimise brightness variations image. Therefore, we recommend that in an area in low altitudes, flight time to be around 08:00 am, when the solar elevation is between 12° and 25° and around 17:00 pm at solar elevation between 35° and 22°.

3.1.1 Brightness variation in Vegetation Indices (VIs)

The radiometrically corrected VIs in Pix4Dmappr can mitigate illumination differences and atmospheric effects, to some degree, but it does not successfully correct for severe distortions present in the associated multispectral images. Time series flights with severe distortions present in both reflectance images and VI maps were captured at midday from 11:00 to 15:00. Uncorrected pixel values-based NDVI showed a lower value of lichen photosynthetic activity than corrected reflectance-based NDVI. Therefore, VIs should be derived from the radiometrically and atmospherically corrected reflectance-based multispectral images.

We observed that plots in the dark sections (i.e. shade) in the direction of the incident solar radiation had significantly greater VIs values than the brighter sections in the opposite direction of the sun. This observation agrees with the trends observed in another study where huge contrasts exist in UAV-derived VI between image parts toward the direction of the sun and those opposite the sun, in images taken in sunny conditions (Rasmussen *et al.* 2016). Brede *et al.* (2015) also observed a similar effect, that NDVI showed a weaker reaction in parts in the opposite direction of the sun, in the tropical rainforest.

Our results also found an increase in the NDVI reflectance values with increasing solar angle. This result coincide with research done in a site in the Canadian Arctic which also found an increase in NDVI with solar elevation (Assmann 2019). On the other hand, other research found that NDVI was lower in the flight nearest solar noon (Brede *et al.* 2015, Stow *et al.* 2019). This suggests that the responses of UAV-derived VI to solar elevation are be site-explicit, thus flight planning should consider varying solar elevation effects (Assmann *et al.* 2019).

The VIs images emphasize a specific phenomenon that is present while mitigating other factors that degrade the effects in the image. Therefore, the results from the SAVI corrected for shading problems due to high topography and lower solar elevation (Figure 21). However the SAVI had lower values of lichen photosynthetic activity than the NDVI. This makes it difficult to compare the SAVI values to other research studies that have used NDVI to determine the actual threshold value of lichen's photosynthetic response. Moreover, the sample plots in different brightness image section should be compared separately measurements because the illumination conditions of the paired plot position groups were not all similar. Therefore measurements must be derived from plots that are under the same brightness conditions for further analysis.

3.1.2 Suggested ways to improve the quality of UAV images

Radiometric and atmospheric correction had been for the most part disregarded because of the low UAV flight altitude. This contextual analysis showed the differences between radiometric corrected NDVI versus uncorrected NDVI, and confirmed that atmospheric and other distortions negatively influences the spectral data collected by UAVs sensors at different times of the day. The effects of atmospheric noise, soil brightness, solar- surface-viewing geometry variation, on reflectance present in the uncorrected pixel values based NDVI underestimates the estimation of lichen photosynthetic activity. This is similar to a study which that showed that without radiometric correction the NDVI created was lower contrasted with the handheld spectrometer (Adler 2018). The atmospheric noise in images rule the performances of VI at different flights time of day, thus radiometric and atmospheric correction is fundamental in working on the appraisal precision of UAVs-based images.

It was required to test how well radiometric correction would have impacted another reflectance-based VI that doesn't depend on the red and NIR band. Therefore, the differences between radiometric corrected NDVI and NDRE were an indication of the strong effects present in the red band compared to the red edge band, rather than the fact that the two VI are proxies for different biophysical parameters of plants.

The outcomes show that the red edge and NIR band had the least errors in measured reflectance, but the red band had the most errors in measured reflectance. Even though the red edge band performed best, combining it with the red band in a VI would dramatically reduce the quality and information value of such a VI. In addition, further investigation on error propagation in the NDVI was required to decide whether an advanced radiometric correction specifically for desert regions is appropriate for reflectance-based VI. As a result, the differences between radiometric corrected NDVI and SAVI, allowed us to see the effects of soil brightness and shade on NDVI The shade effects were more shown as darker sections in the image, due to lower sun angle, thus a variation in sunlight distribution. After correction of shadow and soil brightness effects, we can see that the reflectance variation is due to the presence of lichen response to the different distribution of sunlight in opposition directions (west and east of the ridge). The variation is not due to sun angle shade or soil effects but rather a response of lichen to variations in sunlight and moisture distributed in micro-habitats.

3.2 Conclusion

The main objective was to test the performance of the UAV multispectral Parrot Sequoia sensor, in a low vegetation-covered desert area. From the visual inspection, captured multispectral individual footprint images, orthomosaics multispectral reflectance images and VIs maps showed the presence of bidirectional reflectance (BRDF) emerging in images as a brightness gradients due to of solar elevation solar- surface-viewing geometry variation, soil brightness, and topography.

The time of day and coupled solar elevation is other important factor to consider for the long-term application of this system for monitory lichen biocrust. Thus we suggested that images should be captured in the morning at 08:00, before 09:00, and again in the late afternoon hours from 17:00 when there is less impact from sun brightness. Combined with known lichen photosynthetic activity (Lange *et al.* 1994b, 2007, 2008, Karnieli *et al.* 1999), the optimal survey time will be the early morning hours.

UAV image spectral data should be extracted from areas of interest (ROIs) taking into consideration variation in illumination (Rasmussen *et al.* 2016). This means that just few plots from each image should be cropped for further analysis (e.g. from the central part of the image), which require careful image acquisition with overlapping images (Rasmussen *et al.* 2016). We also suggest that when comparing reflectance values between images, if the values are different, it must provide indications of change that are not due to image distortions.

The focus of this study was not to resolve the extreme errors associated with the Parrot Sequoia after radiometric calibration in Pix4Dmapper, but rather to identify them. A potential solution will be the application of the Walthal BRDF model (Honkavaara et al., 2013). Also to be considered is the topography, to resolve the solar-surface viewing geometry (Gu and Gillespie, 1998). The soil brightness, sun intensity and brightness effects should be considered to resolve brightness variation (i.e. BRDF) and vignetting effects. Furthermore, as a long-term solution, we recommend that future research should create radiometric correction algorithms that filter out all the factors we observed to influence the quality of UAV imageries in this low altitude and hyper-arid region.

We visually assessed the effects of high terrain on the flight altitude as well as its effects on the GSD (i.e. pixel size), but we did not observe many variations in both raw footprint images and ortho-rectified images. The flight mission planning applications used for this UAV survey do not allow terrain-following function. Therefore we also assume that the elevation of the area of interest (i.e. Swartbank site) does not change significantly to influence the flight altitude as well as the GSD. However, the raw footprint image was resampled and aggregated to the same extent and spatial resolution, to ensure accuracy in image matching. The digital photogrammetry Pix4Dmapper program aggregates the orthomasiac images to the same average resolution. When the terrain is less pronounced, the results relating to flying height are often inconclusive, and no consistent effect of flying height on vegetation reflectance in UAV image age datasets (Stow *et al.* 2019). Various previous studies used hand-held spectrometers to calibrate the remote sensing imagery (Schultz 2006, Hinchcliffe *et al.* 2017, Adler 2018, Román *et al.* 2019, Chen *et al.* 2020). This is to be considered in further studies to improve the on the performance of similar UAV-based multispectral sensors.

Chapter 4: The application of UAV multispectral imagery to assess the coverage, disturbance, and fog response of lichen-dominated Biological Soil Crusts in the Central Namib

Manuscript of paper to be submitted to:

International Journal of Remote Sensing (ISSN: 1366-5901)

Remote Sensing of Environment (ISSN: 0034-4257)

Remote Sensing (ISSN: 2072-4292)

4.1 Introduction

Lichen and other biological soil crusts (BSCs or biocrusts) are a major part of biodiversity providing vital ecosystem services in semi-arid, arid and hyper-arid environments (Karnieli *et al.* 2003, Belnap *et al.* 2016). An essential, but less understood ecosystem service of lichens is carbon sequestration which affects the climate and food security, and the lichens' role within the Central Namib (Schultz 2006, Lange *et al.* 2008, Wirth *et al.* 2010b). The growth of lichen fields in the hyper-arid coastal Central Namib Desert is fed by weather conditions fluctuating from hyper-aridity to high relative air humidity and frequent fog precipitation (Daneel 1992). Lichens are however very fragile organisms with slow recovery, easily destroyed by reoccurring bergwind conditions during the winter months, as well as trampling actions, particularly from vehicle off-road driving (Daneel 1992, Schultz 2006, Lalley and Viles 2008). Therefore, management of these natural ecosystems requires regular monitoring of disturbance and fog effects on the health and stability of lichen communities.

One of the major challenges concerning monitoring of lichen biodiversity is that field- and lab-based techniques are destructive to the lichens themselves as well as time-consuming. This has hindered long-term monitoring programmes regarding the seasonal dynamics and growth rates of these communities.
Therefore, earlier studies have turned to indirect and non-intrusive remotely sensed data, and it has been proven possible to map lichen biocrust (Wessels and van Vuuren 1986a)**.** Remote sensing of biocrusts has traditionally been dependent on platforms, such as airborne and satellite sensors (Wessels and van Vuuren 1986b, Knox *et al.* 2004, Schultz 2006, Casanovas *et al.* 2015, Rodríguez-Caballero *et al.* 2017, Chen *et al.* 2019, 2020, Román *et al.* 2019, Rieser *et al.* 2021). Although most researchers still rely on satellite-based remote sensing for mapping and monitoring lichens and other BSCs, their studies present several drawbacks, as satellite images are limited by the low spatial and temporal resolutions (often co-siding with cloud cover, thus obstructing the view). Satellite images requires extensive fieldwork to collect reference data for accuracy assessments, thus causing minor environmental impacts (Knox *et al.* 2004, Chen *et al.* 2005, Schultz 2006, Rodríguez-Caballero *et al.* 2017, Rieser *et al.* 2021). Despite their high

spectral resolution, the coarse spatial and temporal resolutions of satellite imagery often provides insufficient detail to monitor lichen cover and to extract detailed biophysical and topographic information. Therefore, these authors recommended the adoption of more advanced remote sensing technological solutions for research, such as unmanned aerial vehicles (UAVs) platforms and associated sensors (Reiter *et al.* 2008, Hinchcliffe *et al.* 2017).

Previous studies have used UAVs for BSCs (Román *et al.* 2019, Havrilla *et al.* 2020), proving that this is an achievable task. Only recently the potential of RGB imagery acquired from UAVs to identify biocrusts in drylands has been explored (Macander *et al.* 2018, Collier 2019, Havrilla *et al.* 2020). Therefore, UAVs integrated with multispectral sensors could greatly improve monitoring of lichen (Blanco-Sacristán *et al.* 2021). The unique spectral properties of lichens can be utilized via the calculation of spectral indices (Wessels and van Vuuren 1986b, Karnieli *et al.* 1999, 2003, Casanovas *et al.* 2015, Rieser *et al.* 2021). Previous studies have found the Normalised Difference Vegetation Index (NDVI) to be the most crucial predictor in estimating BSCs cover (Reiter *et al.* 2008, Chen *et al.* 2019) and for assessing the change in metabolic activity of BSCs after precipitation events, as wet biocrusts are reported to show a significantly higher NDVI than dry biocrusts (Karnieli *et al.* 1999, Rodríguez-Caballero *et al.* 2015, 2017, Chen *et al.* 2020).

The climate conditions control the distribution of lichen biocrusts in drylands at a landscape extent, but topography and soil attributes can influence micro-climatic conditions together with lichen biocrusts distribution at a community scale. Therefore studies have used environmental parameters such as topographic attributes (e.g. slope angle, elevation, and wetness index), meteorological conditions (e.g. fog moisture, soil moisture content, and solar irradiation), and disturbances action, as important auxiliary information in supporting remote sensing data (Loris *et al.* 2009, Blanco-Sacristán *et al.* 2021, Rieser *et al.* 2021). The lichen fields of the Central Namib are not only heavily impacted by changing climatic patterns, but also by the expansion of off-road use activities (Daneel 1992, Lalley and Viles 2006, 2008). Moreover, remote sensing studies have provided valuable information about lichen conditions in degraded areas, prominently damaged by off-road vehicle tracks disturbances (Schultz 2006). However, the large pixel size of the satellite makes it difficult to interpret these changes, when the detail information of the spatial heterogeneity in biocrust condition and topography is lost.

This study assessed the spatio-temporal patterns of lichen photosynthetic activity in response to wet and dry conditions, using time series curves of lichen UAV-based NDVI, as a proxy for quantifying lichen photosynthesis activity. Even though the Soil-Adjusted Vegetation Index (SAVI) was considered best in our previous work, NDVI applied because it enabled comparing our results to similar studies that have used NDVI response of lichens in desert environments. We also assessed the influence of micro-topography and disturbance in off-road tracks on lichen coverage, to explain variations in lichen distribution across space and time and identify signs of lichen recovery in off-road tracks.

4.2 Materials and Methods

4.2.1 Study sites

The Central Namib Desert region experiences a coastal subtropical climate, characterized by the coastal fog belt, reaching further inland at about 50 km from the coast, with average annual fog precipitation estimated at 37 mm per annum, occurring on an average of 146 days a year at the coast (Lalley & Viles, 2006) (Figure 23). Fog events occur during any month of the year, but the heaviest in the winter months of May to September, thus a reliable source of moisture for lichen flora (Daneel, 1992; Lalley, et al., 2006). Rainfall is experienced during the summer months of January to March in short duration and decreases with distance from inland to coastal areas. Gobabeb receives on average less than 20 mm rainfall per annum. Conditions of extremely low humidity are fairly uncommon and are normally associated with winter berg winds. The strong easterly "berg" winds are experienced during the winter months and characteristically result in hot, dry conditions. Temperature extremes are moderated in Namib by the presence of the cold current off-shore. Maximum temperatures in the region of 40°C are mainly experienced during February and March. Evaporation is high in the Namib Desert despite the temperate conditions (Walter, 1986), and it exceeds precipitation in all regions of the Namib.

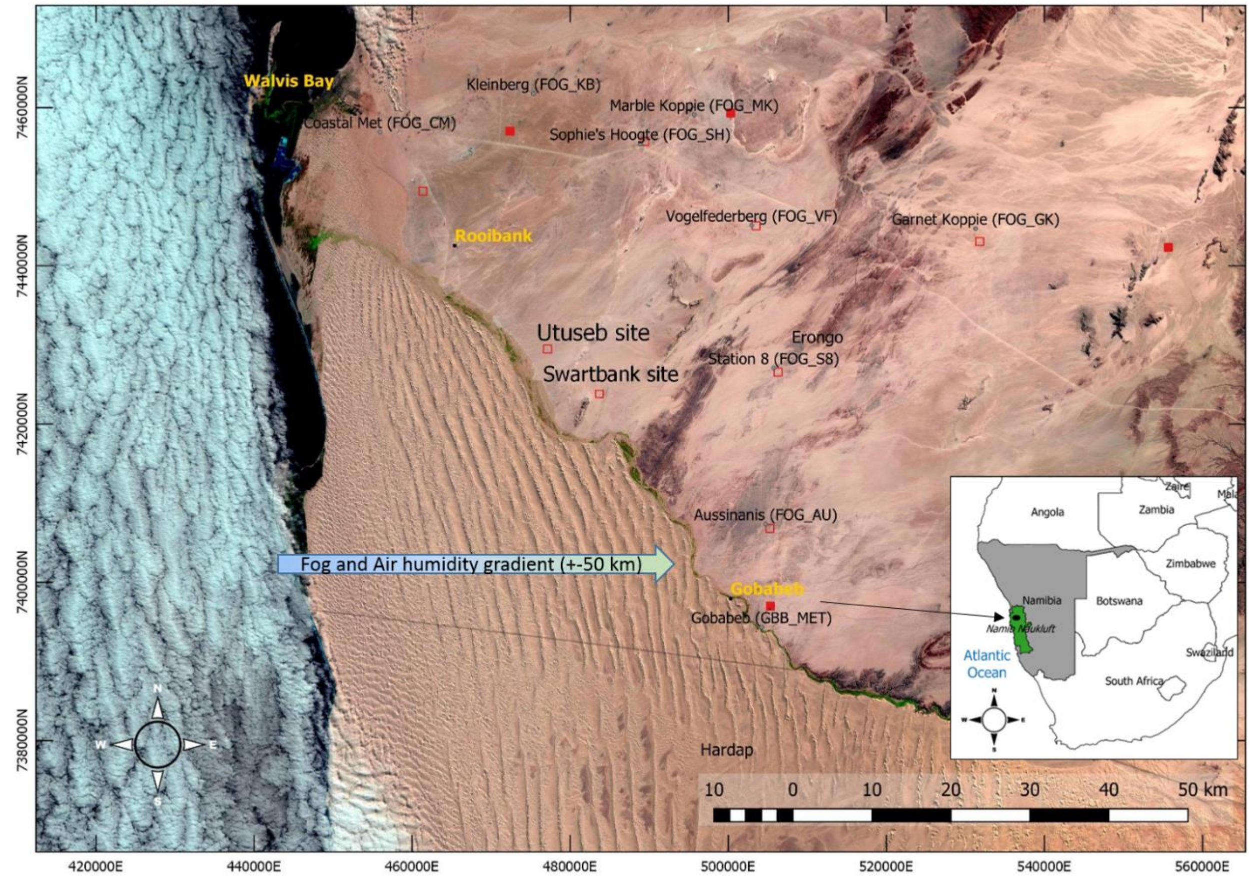

Figure 23. Location of the study area in Central Namib include the Utuseb and Swartbank study sites. Red squares represent the Namibian BIOTA observatories transects, in the Namib Desert Biome (Biodiversity Monitoring Transect Analysis in Africa). The two photos show that lichen density cover is much higher at the coast, for example at the Kleinberg observatory site, compared to be Swartbank site further inland. The base image is a Sentinal-2 image downloaded from the USGS-Earthexplorer, it shows how fog clouds travel from coast to inland, as indicated by the arrow.

The two study sites were located in the Central Namib Desert, Namib Naukluft Park. The Utuseb lichen experimental sites (23°14'51.66"S, 14°46'30.50"E) were located west of the Swartbank mount, which is 30 km inland from the Atlantic Ocean coast and is located in an easterly direction 5km of the Utuseb Topnaar community (Figure 23 and Figure 24). While the Swartbank experimental site (23°17'53.15"S, 14°50'32.11"E) was located leeward (east) side of the Swartbank mount, which is 35km inland from the Atlantic Ocean coast, and 5 km north of the Swartbank settlement. The maximum distance between the two sites was 7.5 km. The UAV-based multispectral aerial surveys focus areas covered mission plots of 500m x 200m and 400m x 250m for the Utuseb and Swartbank sites, respectively (Figure 23 and Figure 24). The elevation of the Utuseb site was ca 229 m above sea level, relatively flat terrain, but located on a shallow west slope (Figure 4.1). Whereas, the Swartbank site was located on a ridge top including the west and east slopes, at a high elevation of approximately 323 m above sea level (Figure 23 and Figure 24). The study sites are dominated by fairly dense lichens on exposed soil and quarzitic rock surfaces of gravel plains. Lichen-dominated biological soil crusts, decrease in density with the fog climatic gradient from coast to inland. In these two experimental sites there are also drainage channels (i.e. washes) but without recent dynamics or changing aspects, and gypsum crusts are visible at the soil surface. These experimental sites are situated in close proximity to about 35 to 40 km from the Gobabeb-Namib Research Institute (Figure 23). and form part of the Namibian BIOTA observatories west-east Transect located in the Namib Desert Biome, which was primarily formed to monitor and chose to observe the dynamics of the extraordinary lichen fields of the Namib in terms of the effects of human land use (for example off-road tracks) and the effects of climatic events as long-term climatic changes.

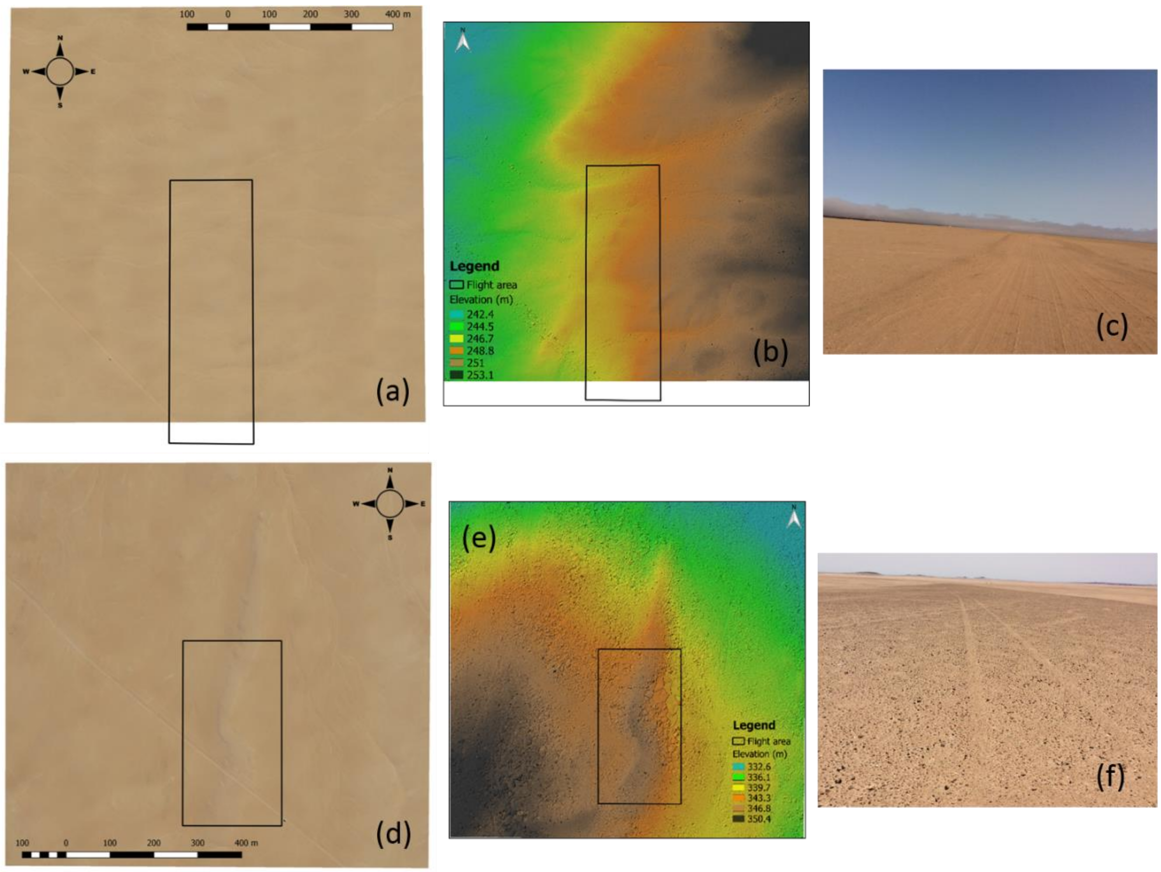

Figure 24. RGB image (a), DSM (b) and the scenery with the main accessible track (i.e. old Swartbank road where rehabilitation done since the filming of the 2012 action thriller (c) for Utuseb study site. RGB image (d), DSM (e) and the scenery (f) for Swartbank study site with road track with little to no lichen cover.

Moreover, study sites are extensively crisscrossed by off-road vehicle tracks, which have heavily damaged the lichen cover within those tracks (Figure 24). These tracks become erosion channels which, whenever rains occur, carry off humus and lead to decline of the seedbanks. Seeds would normally (after rain) germinate into the protection of the lichens to grow into lush, albeit short-lived plant cover. This indicates that land use is of high intensity due to filming, mining, tourism and recreational use, constructions, and maintenance of utilities. A major action scene for the thriller was filmed along the main old Swartbank road in 2012, there is still little to no sign of lichen recovery in the tracks, after rehabilitation was done by the filming company (Figure 24 and Figure 2). The fact that lichens are endangered by off-road vehicle driving and their recovery is very slowly indicates the need for additional conservation (Wessels and van Vuuren 1986a, Lalley and Viles 2008).

Figure 25. This is the type of disturbance which happened on sections of that road! (Source of photo: https://gagadget.com/en/war/145234-the-afu-is-increasingly-using-buggies-at-the-front-same-like-in-mad-max/)

4.2.2 UAV aerial imagery collection and image processing

Time series UAV aerial surveys were obtained using Parrot Sequoia multispectral sensor (Parrot Drone SAS, Paris, France), using two different platforms (Figure 26). Repeated flight surveys were carried out with a DJI Phantom 4 Pro V2 from August- to September 2020 and a follow up survey using a Parrot Disco Pro AG fixed-wing platform during September 2021 (Figure 26). The detailed information on the actual dates of flying are in Appendix 2. The weather condition for the day of UAV flights are found in Table 10 and Appendix 3 show fog occurrence of the flying days.

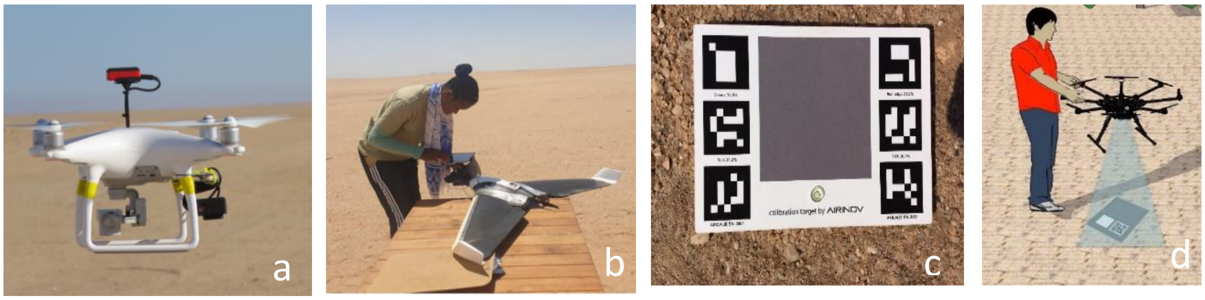

Figure 26. Parrot Sequoia and sunshine sensor mounted on DJI Phantom 4 Professional drone (a) and Parrot Disco Pro AG drone (b). A standard AIRINOV calibration reflectance target (c), and a Graphic illustrating how to hold the sensor over the calibration target for pre-flight radiometric calibration (d).

Table 10. Weather conditions at Coastal Met, Sophies Hoogte, and Gobabeb SASSCAL Fognet weather stations, for the date of UAV image data collection

Flight date	**Weather station**	**Total precipitation (mm)**	**Total fog (mm)**	**Total Solar irradiance MJ/m^2**
August 2020	Coastal Met	0.2	9.5	588.80
August 2020	Sophie Hoogte	4.9	19.4	706.71
August 2020	Gobabeb	0	21.6	
September 2020	Coastal Met	0.3	20.9	660.54
September 2020	Sophie Hoogte	4.9	19.4	706.71
September 2020	Gobabeb	0	2.3	
September 2021	Coastal Met	0.3	39.4	629.43
September 2021	Sophie Hoogte	0.4	32.0	702.36
September 2021	Gobabeb	0	7.0	

The time series UAV aerial surveys were conducted using the Pix4DCapture mission planner app with a grid pattern flight mission, set to 80m flight altitude, resulting in Parrot Sequoia multispectral images with an average ground sampling distances (GSD) of 9.24 cm/pixel. Images were acquired across the track, with an 80% forward and 90% side overlap and flight times ranged between 15-23 minutes depending on the platform, and weather conditions.

Even though UAV flights are recommended to be conducted 2-3 hours before and after solar noon as possible, problems were experienced with image brightness effects due to high solar intensity (see Chapter 3). Nonetheless, all times series flights were conducted from morning 08:00 to 17:00 in the late afternoon, to enable full observations of lichen-dominated BSCs' photosynthetic response to wet and dry conditions, on fog and non-fog days.

The multispectral image data was processed in the digital photogrammetry software Pix4DMapper Pro Desktop 4.0.21 (Pix4D SA, Lausanne, Switzerland) to generate orthomosaics reflectance images (red, green, blue, and near-infrared), radiometrically and atmospherically corrected NDVI images, and digital surface model (DSM) (Figure 24 and Figure 27). The multispectral imageries were processed with the Pix4D Desktop Ag-Multispectral template with the “merge reflectance map tiles” option set to true. Pre- and post-flight imagery of a reflectance calibration panel captured during each survey and was used during the radiometric correction. In addition, six ground control points (GCPs) targets (60 x 60 cm) which were permanently deployed in the flight mission areas prior to UAV flights, were used for geolocation subsequent images exactly in relation to previous images. Their position were measured with a handheld GPS, meaning that no absolute precise location was achieved.

Not all multispectral images were collections from particular time series flights could be processed successfully, due to images suffering from sun glare when taken close to solar noon (10:00 to 15:00) (see Chapter 3), or with incomplete geolocation or image overlap errors within such mission sets. Although from a scientific perspective it may be interesting to assess the lichens in the berg wind (“eastwind”) conditions from May to July, due to the practicality of flying the UAV in such conditions this was not done.”

4.2.3 Meteorological data

Determining lichen photosynthetic response to fog input required meteorological data as auxiliary data to support UAV multispectral observations, and to explain how meteorological conditions and major micro-topographical habitats (i.e. ridges, quarzitic gravel plains, river wash/channel) influence lichen cover and metabolic activity. Therefore important weather dataset included in this research for understanding the fog extent was accessed from the SASSCAL Weathernet(SASSCAL WeatherNet - Weather stations in Namibia 2022). It was particularly retrieved from the Kleinberg-FN Station, Coastal Met, Sophies Hoogte and Gobabeb station because it shares the same fog climatic zones are the study sites. Therefore, weather data were retrieved this SASSCAL Fognet weather stations t because they in a west to east direction of the study sites.

4.2.4 Ground Data Collection

All the ground observations of lichen coverage were done in December 2021, after the UAV observations were completed. The ground observations of lichen coverage was estimated as described by Daneel (1992), using a 1 x 1 m (1 m^2) quadrat with 100 subdivisions of 10 x 10 cm.

At the Swartbank site, 24 1 x 1 m (1 m^2) quadrats frames of PVC pipes were deployed at 5 m intervals along a topographic transect that is across the ridge which was selected away from the heavy disturbed main old Swartbank track areas, in January 2021, prior to UAV flight observations **(Figure 27).** This ensures assessing the influence of micro-topography (i.e. slopes and elevation) on lichen-biocrust coverage and fog distribution, to supports UAV observations. This topographic transect was only done at Swartbank site, because of the ridge that run along the mission plot.

In both study sites, a linear disturbance transect of 150 m long was selected perpendicular from the main old Swartbank track, to assess the impact of disturbance by off-road track with different intensities, and identify signs of lichen recovery from disturbance and after rehabilitation (and comparing disturbed versus intact areas).

The quadrats were placed every 5 m intervals to accommodate for the resolution of the pixel size, generating 30 sampling points for disturbance transects. The recording information included the number of lichens, lichen coverage, dominant lichen species per quadrat, type of substrates (i.e. soil or rock), and micro-habitats (i.e. tracks, plains and river washes). Lichen cover was measured by estimating the percentage area covered by each lichen within the 10 x 10 cm subdivisions, and adding all the 100 subdivisions to get the total or accumulation sum of lichen percentage cover per quadrats.

Photographs of each quadrats were taken at Nadir at shoulder height, using a digital camera, Nikon. This allowed further validation of the lichen coverage and identification of lichen species names. The quadrats sampling point's locations were recorded with a handheld GPS the location of the samples were plotted in QGIS V3.16.0. The GPS location was done because the quadrats of the disturbance transect was not permanently placed in the field during the UAV flight, like at the topographic transect for Swartbank site. This enable us to use sampled plots for data extraction from the NDVI images.

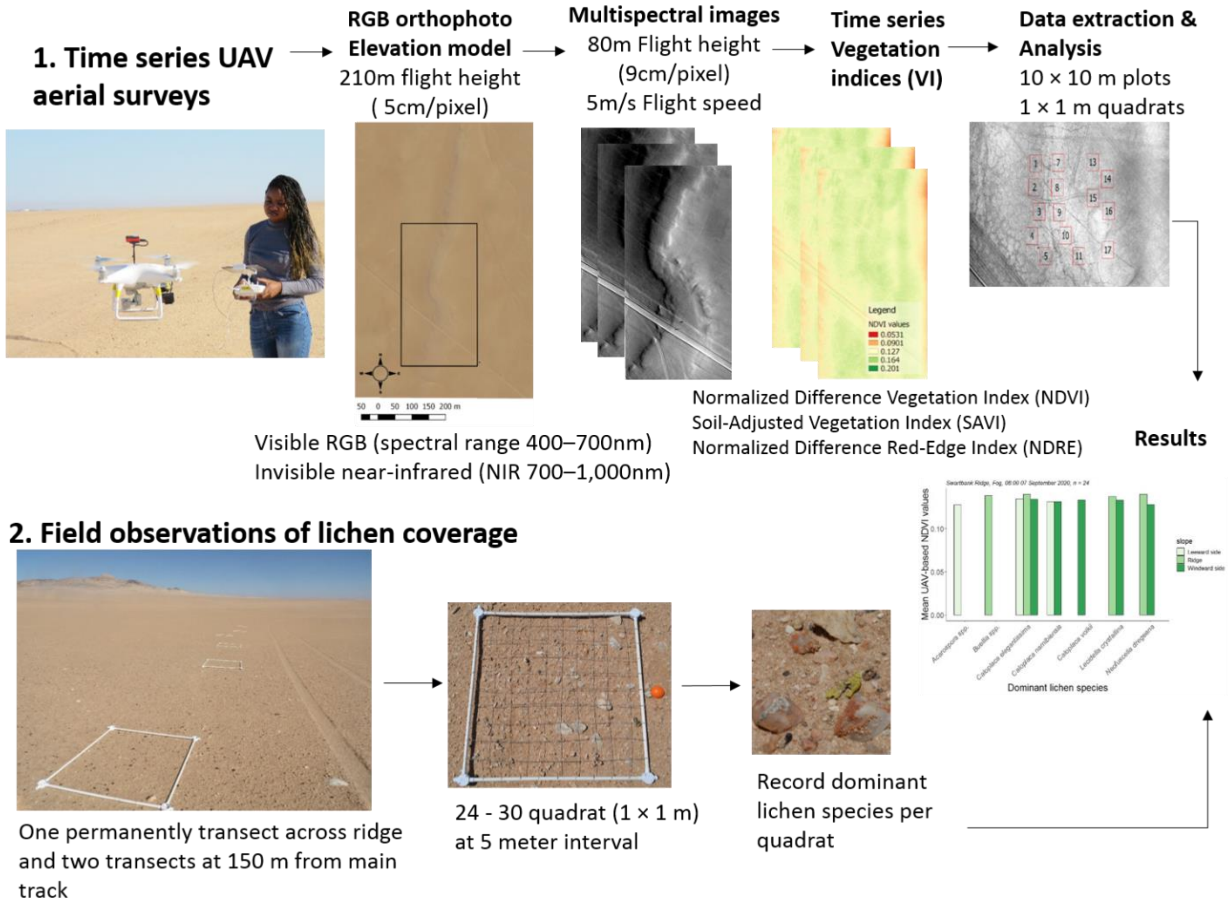

Figure 27. Illustration of undertaking ground observations and time series unmanned aerial vehicle (UAV) imagery, at Swartbank Ridge, Central Namib. The time series UAV aerial surveys are described in Sections 4.2.2, and the ground observations in Sections.

4.2.5 Image Data Extraction and Statistical Analysis

To extract the temporal profiles of lichen NDVI response to wet and dry conditions three 10 × 10 m (100 m^2) areas of interest (AOIs) defined on different elevation taking into account the variations in illumination conditions (i.e. bright and dark image sections) in the time series reflectance-based NDVI images. The three sample plots were selected on the different altitudes (i.e. west side, ridge top and east side) only for Swartbank site. In both study sites, times series curves of UAV-based NDVI (presenting lichen photosynthetic activity) for fog and no-fog days, were extracted from these three sample plots 10 × 10 m created in QGIS 3.16.0. Initially, to be able to achieve full analysis and comparing of the variability in different micro-topographic habitats, 15 plots were created for both study sites. However only three plots in both sites were used to extract the time series profiles of lichens' NDVI response overtime, due to time constraints on data analyses. Nonetheless, these three plots were able to it gives an indication of how lichen photosynthetic response to wet and dry condition varies overtime.

In addition, to assess the influence of micro-topography (elevation) and off-road tracks disturbance on lichen coverage, and compare UAV-based NDVI data to ground cover, the 1 m^2 quadrat plots from topographic and disturbance transects were used for extracting data.

All the defined sample plots were used to calculate descriptive statistical summaries (e.g. mean, standard deviation, maximum and minimum) from the NDVI reflectance maps and elevation model created in QGIS 3.16.0. The attribute data such as micro-habitats (tracks, plains, river washes), disturbance fields, as well as all the ground recorded data were joined. In the Swartbank Ridge transect, plots were categorized as the ridge top, windward side and the leeward side of the ridge. This in relation to the influence of fog moisture distribution travelling from the west to the east, and deposited from high altitude to low altitude areas. Therefore, this allowed for the evaluating the influence of topography on the fog moisture availability, as well as on lichen density cover.

To assess the changes between the wet and dry lichen NDVI, change detection analysis was performed in QGIS 3.16.0, whereby matching pixels of the different NDVI images were compared and subtracted from each other. The differences were calculated by subtracting the 09:00 and the 17:00 NDVI form the 08:00 NDVI, all from the same fog day of 07 September 2020. All image dataset was georeferenced to reduce geolocation error during this image pixel comparisons.

Statistical analysis was performed in the R statistical environment, version 3.4.2 (R Core Team 2021). Line plot, bar plot and scatterplots are created using the R package "ggplot2". Time series anlysis was performed using line plots with error-bars to create temporal curves of lichen NDVI for both fog and non-fog days. Time series UAV-based NDVI values from both fog and non-fog days were used include in the analyses to assess how wet and dry condition influences the estimation of lichen photosynthetic activity. As well as to illustrate the temporal changing patterns of lichen photosynthetic response overtime. The time series profiles of the mean NDVI values representing the photosynthetic activity of lichen biocrusts, were compared to time-series weather plots of fog and relative air humidity.

The influence of micro-topography on lichen abundance cover, lichen species diversity and was examined by comparing total lichen ground-observed cover and lichen mean UAV-based NDVI values from the 24 observations across the Swartbank ridge on different on top of the ridge, wind- and lee-ward side of the ridge, which receive a varying distribution of fog moisture. The bar plots of total lichen ground-observed cover and lichen mean UAV-based NDVI values were further grouped as by the dominant lichen species to further understanding how different lichen species photosynthetically respond to moisture availability on different micro-topographical habitats.

To determine whether lichen cover and lichen NDVI response depend on elevation (m), as the study area fog moisture availability is controlled by the topographic attributes, elevation values from the 24 sample pot across the Swartbank ridge were used for creating scatterplot and a fit polynomial regression model to the dataset. In addition to that, polynomial regression analyses of the time series NDVI in wet and dry conditions were generated to see how well it corresponds with a trend from ground observations and how it varies due to difference of wet and dry lichens.

The influence of off-road tracks on lichen coverage was evaluated by comparing lichen cover and lichen NDVI in damaged and intact areas. Bar plots of the total lichen ground-observed cover and lichen mean UAV-based NDVI values linked to the 30 observations along the disturbance transects for both sites, were created and further grouped by disturbed (i.e. tracks and washes) versus undisturbed areas (i.e. plains). The ground cover and the lichen NDVI were grouped by the dominant lichen species from the sampled plot by coming the two dataset into a table. This gave an insight of how lichens respond differently to disturbance.

Statistical analysis was unperformed to determine presence of significant differences between habitat with one-way ANOVA and Student-test (t-tests), after the non-normal distribution of the data was met using Shapiro-Wilk test. The Kruskal-Wallis tests were undertaken, where normality assumptions were not achieved. All tests were considered significant at $p < 0.05$.

4.3 Results

4.3.1 Spatio-temporal patterns of lichen-dominated BSCs response to wet and dry conditions

The time series curves of lichen NDVI reflectance values in response to moisture availability were observed taking into consideration the variation in illumination conditions of the sampled plots between hourly time series flights. The well-illuminated images were taken in low solar elevation at 08:00 in the morning and later afternoon at 17:00, which was 3 hours before and after noon (Figure 28).

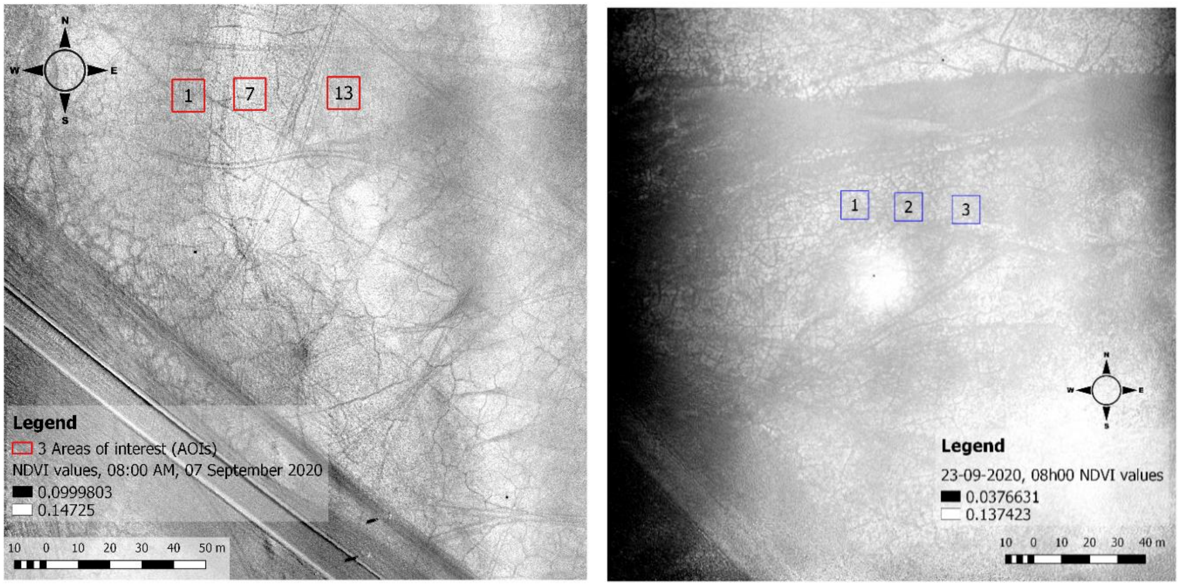

Figure 28. The 10 × 10 m² area of interest (AOIs) was used for temporal profiles of lichens' NDVI reflectance response to moisture between the time series flights, for the Swartbank site (left) and Utuseb site (right). Only 3 AOIs were sampled at each site for temporal curves, plots 1, 7, and 13 on the west, ridge, and east of the slope of the Swartbank Ridge, respectively.

The temporal curves showed a clear pattern of lichens' photosynthetic activity response to moisture variability overtime. The days with fog days had higher mean NDVI values than non-fog days (See Figure 29, Appendix 6, Appendix 7 and Appendix 8). In the morning at 08:00 with high fog moisture input or high relative air humidity, there was a high mean NDVI compared to 09:00. The morning hours also had higher NDVI than the late afternoon hours from 16:00 to 17:00 because of low moisture availability as temperature increases on a no-fog day. However, on a fog day followed by night fog, there was an interesting rise in NDVI in the late afternoon at 17:00 with mean NDVI values of 0.3 (Figure 29 and Figure 30).

There were overestimated higher mean NDVI values in the midday flights (10:00-15:00) at high solar elevation than in the morning and late afternoon with lower solar elevation (Figure 29 and Figure 30). This showed rather a direct relationship with solar elevation than what we expected. This also indicated the influence of sun, sensor, and soil brightness effects on NDVI values causes high NDVI values.

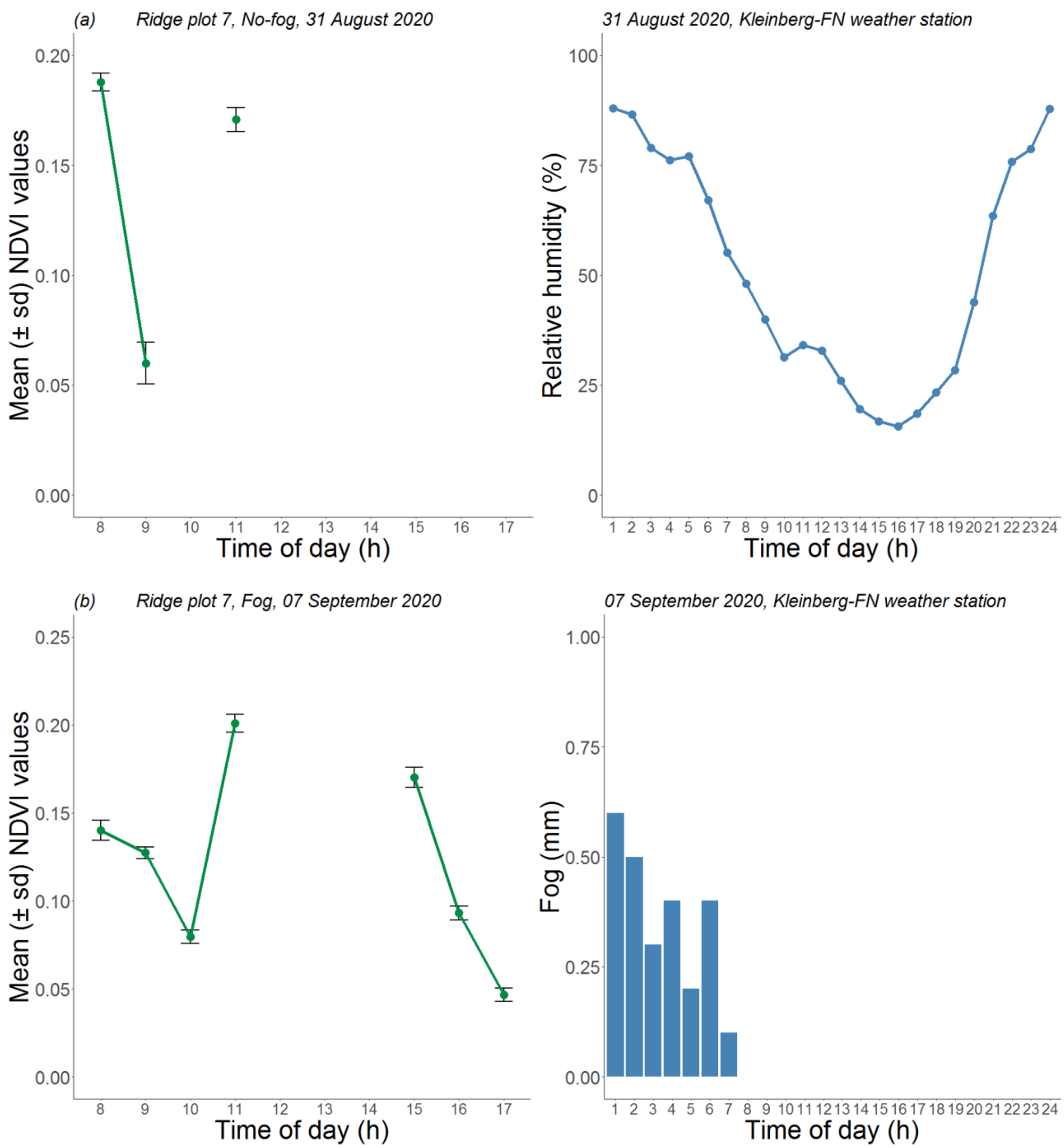
(a)
Ridge plot 7, No-fog, 31 August 2020
Mean (± sd) NDVI values
0.00
0.05
0.10
0.15
0.20
8 9 10 11 12 13 14 15 16 17
Time of day (h)
31 August 2020, Kleinberg-FN weather station
Relative humidity (%)
0
25
50
75
100
1 2 3 4 5 6 7 8 9 10 11 12 13 14 15 16 17 18 19 20 21 22 23 24
Time of day (h)
(b)
Ridge plot 7, Fog, 07 September 2020
Mean (± sd) NDVI values
0.00
0.05
0.10
0.15
0.20
0.25
8 9 10 11 12 13 14 15 16 17
Time of day (h)
07 September 2020, Kleinberg-FN weather station
Fog (mm)
0.00
0.25
0.50
0.75
1.00
1 2 3 4 5 6 7 8 9 10 11 12 13 14 15 16 17 18 19 20 21 22 23 24
Time of day (h)

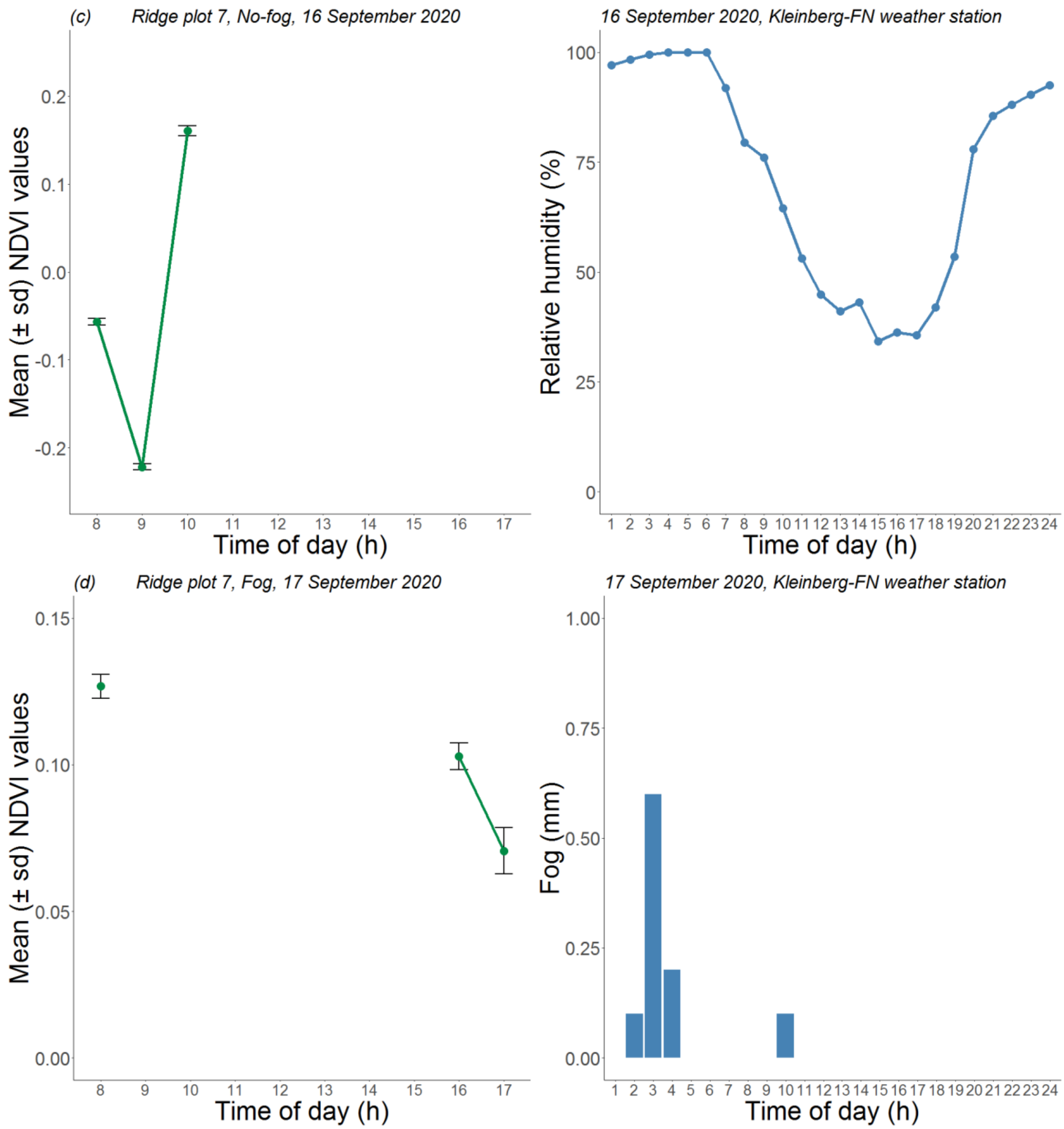

Figure 29. Unevenly spaced time series of mean UAV-based NDVI reflectance values for lichen response to fog and non-fog events in the AOI 7 on the ridge slope, Swartbank experimental site. Time series of fog and relative air humidity data measured at the Kleinberg-FN weather station, which shares the same fog climatic zones as the study sites.

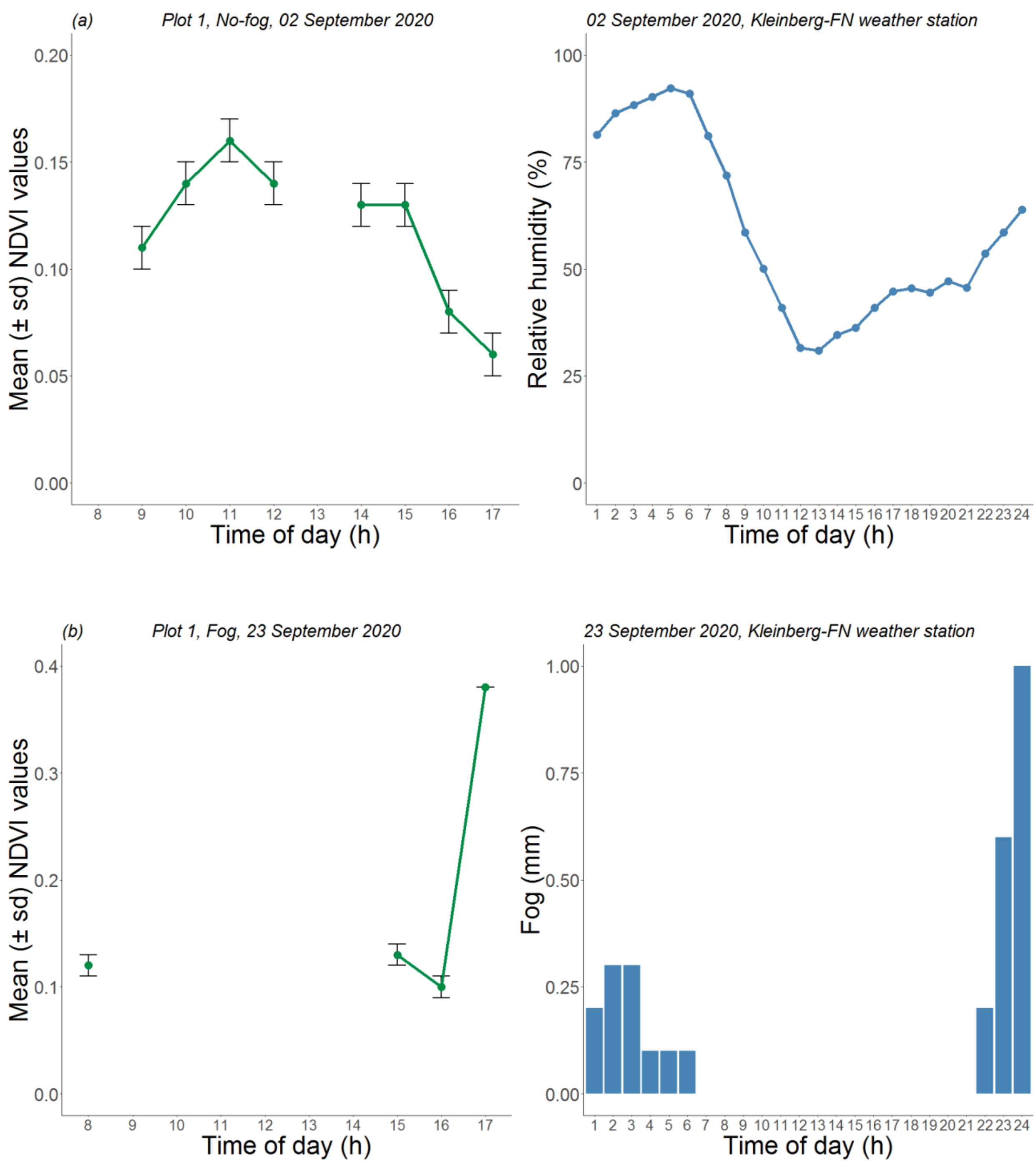
(a)
Plot 1, No-fog, 02 September 2020
Mean (± sd) NDVI values
Time of day (h)
02 September 2020, Kleinberg-FN weather station
Relative humidity (%)
Time of day (h)
(b)
Plot 1, Fog, 23 September 2020
Mean (± sd) NDVI values
Time of day (h)
23 September 2020, Kleinberg-FN weather station
Fog (mm)
Time of day (h)

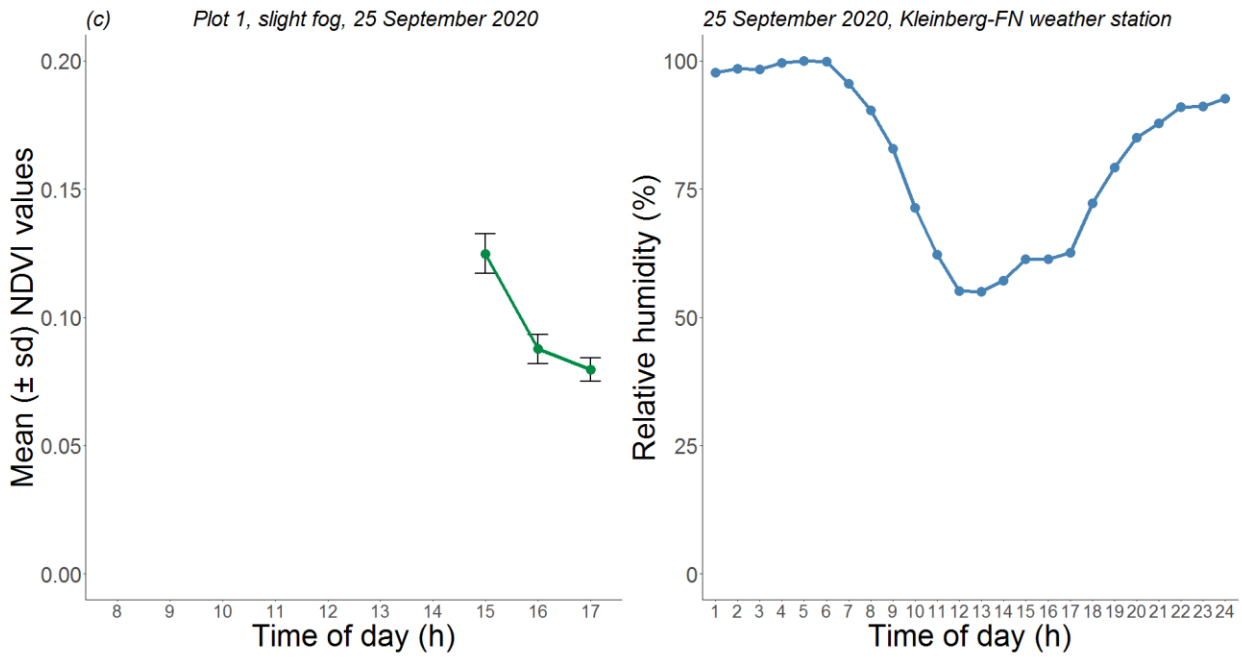

Figure 30Unevenly spaced time series of NDVI mean reflectance values for lichen response to fog and non-fog events in the AOI 1 on the ridge slope, Utuseb experimental site. Time series of fog and relative air humidity data measured at the Kleinberg-FN weather station, which shares the same fog climatic zones as the study sites.

Temporal analysis lichens' activity in wet and dry time of day

Image per-pixel differences results indicated that on the day of fog, lichens are more active in the morning at 08:00 - 09:00 (when wet), compared to late afternoon at 17:00 (when dry) (Figure 31). Per-pixel differences in NDVI between 08:00 and 09:00 showed low difference or change. But there was a high positive change between 08:00 and 17:00, as lichens were more active and wet in the morning than in the late afternoon.

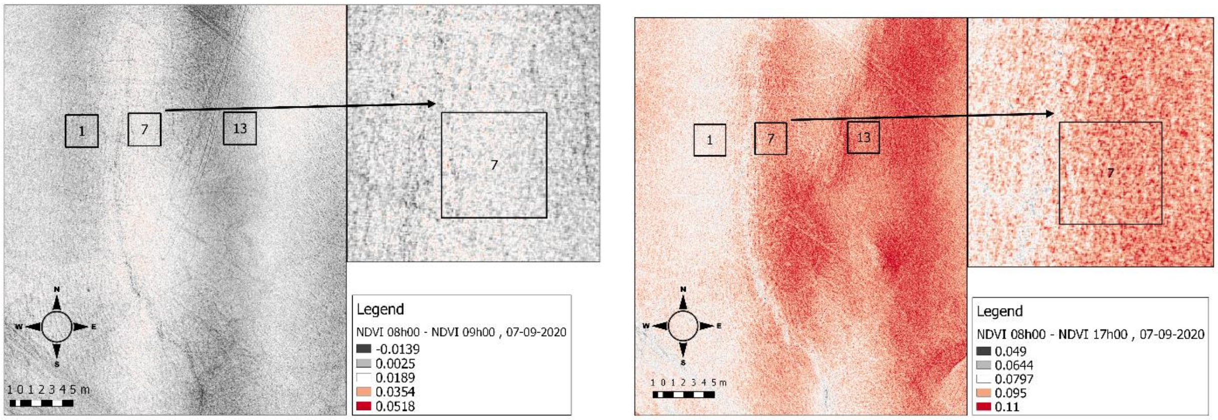

Figure 31. Per-pixel differences between 08h00 NDVI and 09h00, as well as 17h00, indicating the magnitude of change between the wet and dry time of day from a fog day of 07 September 2022, at Swartbank site. The values 0 indicates no change, positive values indicate increased activity, while low negative values indicate decreased activity. The areas outlined in black squares (10 x 10 m), were the areas of interest (AOIs), but only 3 AOIs were used for time series profiles, for example, AOI 7 was used for time series curves of the Swartbank site in Figure 4. 4.

4.3.2 Influence of micro-topography (elevation) on lichen coverage in wet and dry conditions

Crustose lichens species, colonizing rocks and soil substrates were the morphological type observed in both study sites (Figure 32). A total of 11 lichen species were observed, including one observation of a foliose lichen species, at Swartbank. The most dominant lichen species have varying morphological characteristics (Figure 33). There was greater lichen species diversity and density coverage in the Swartbank site compared to the Utuseb site.

Caloplaca elegantissima

Caloplaca namibiensis

Caloplaca volkii

Caloplaca sp.

Neofuscelia dregeana

Buellia sp.

Lecidella sp.

Lecidella crystalline

Acarospora sp.

Acoraspora gypsi-deserti

Xanthoparmelia walteri

Figure 32. Ground observations of *c*olonies of the 11 lichen species found in the study area.

Ground observations of total lichen cover and species diversity were found to be higher on the ridge than on the windward and leeward sides (Figure 33). It also showed that lichen species richness and abundance cover was more on the windward compared to the leeward side (Figure 33).

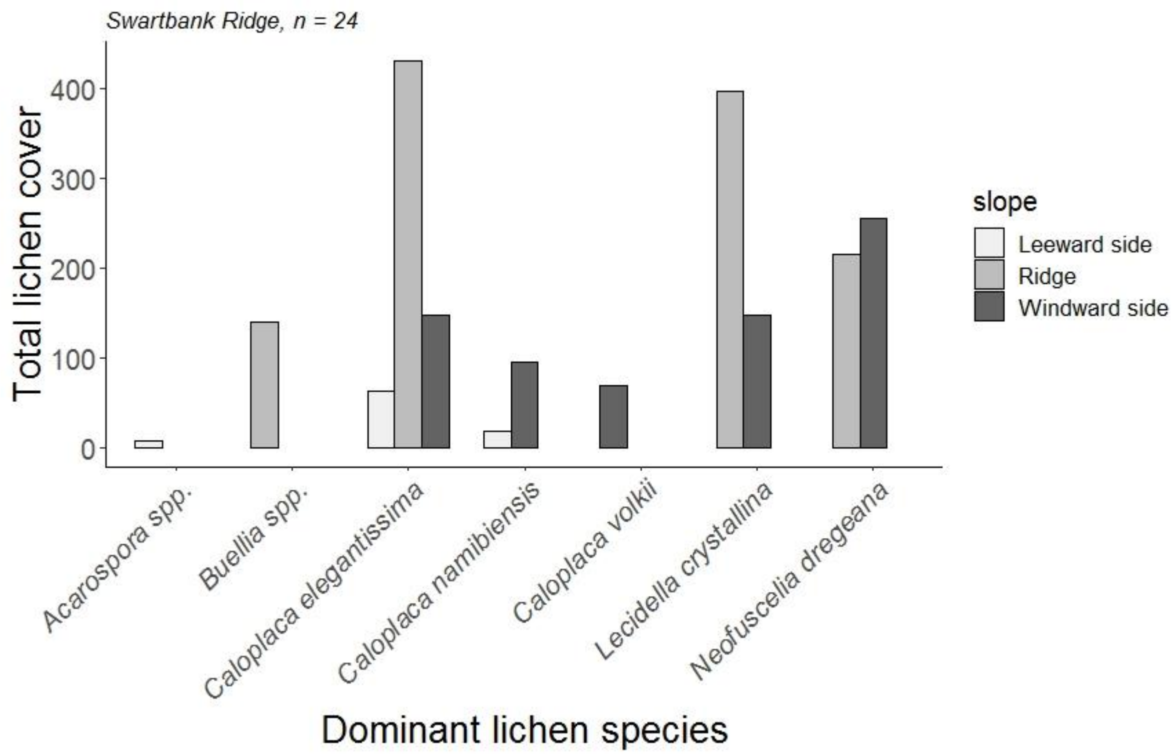

Figure 33. Ground observation of lichen species diversity and total cover collected along a 100 m topographical transect across a ridge, and measured using the 24 sample plots of permanently place 1 m^2 quadrats on different slopes (i.e. ridge, windward, and leeward side) representing micro-habitats, the n = 24 is the total observations in the quadrats or sampled plots, Swartbank study site

The UAV-based NDVI values of lichen photosynthesis activity correlate with ground-observed lichen coverage (Figure 34, Figure 35, Figure 36, and Figure 37). The different lichen species have different NDVI responses to moisture availability on different sides of the ridge (Figure 34, Figure 35, Figure 36, and Figure 37). The mean NDVI values were higher on the ridge than on the windward and leeward sides. At 08:00 the ridge showed high NDVI, but lee- and wind-ward sides showed to be less different in mean NDVI value (Figure 34). At 09:00 the ridge had high NDVI values than the windward side followed by the leeward side

(Figure 35). In the late afternoon (17:00), NDVI response is higher on the windward side of the slope, than on the leeward side (Figure 36 and Figure 37).

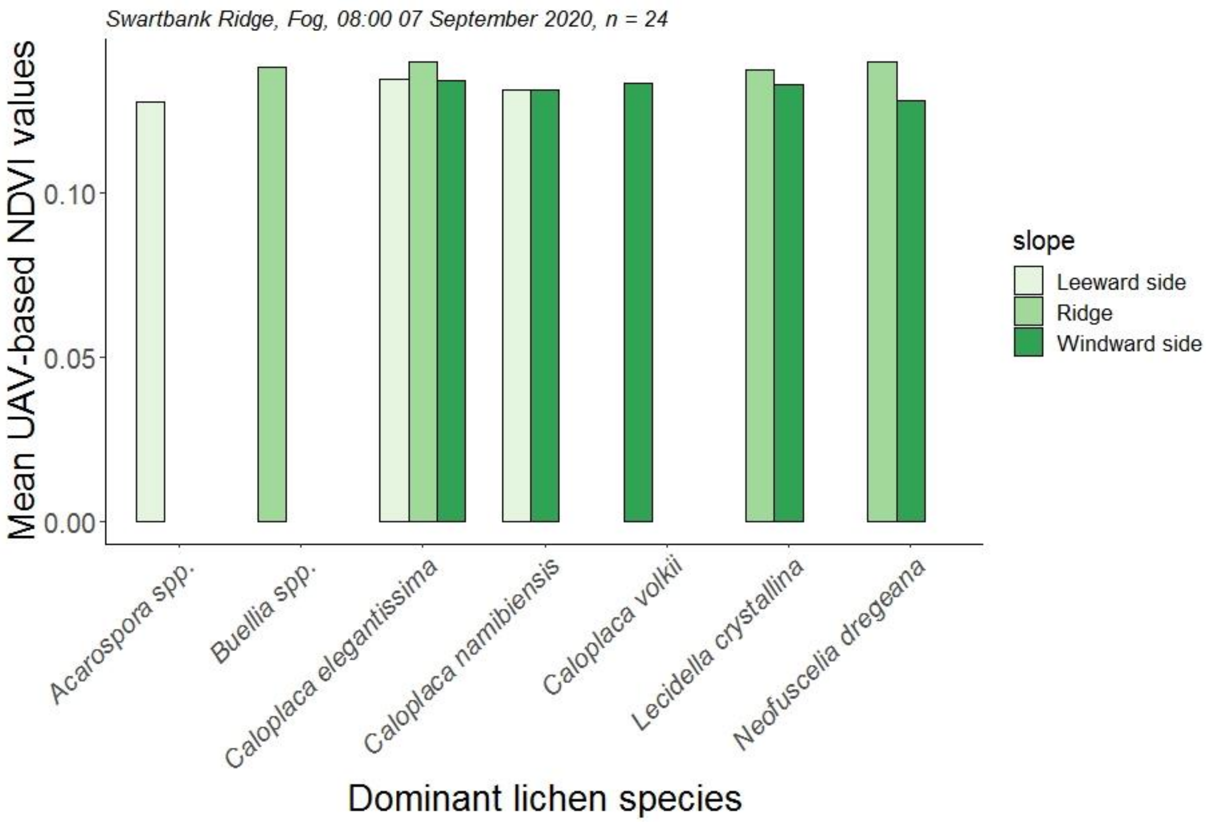

Figure 34. Mean UAV-based NDVI values representing different photosynthetic activity of dominant lichen species extracted from the 24 sample plots of permanently place 1 m^2 quadrats on different slopes (i.e. ridge, windward, and leeward side) representing micro-habitats, along a 100 m topographical transect across a ridge, the n = 24 is the total observations in the quadrats or sampled plots, a fog day 08h00, 7 September 2020, Swartbank site.

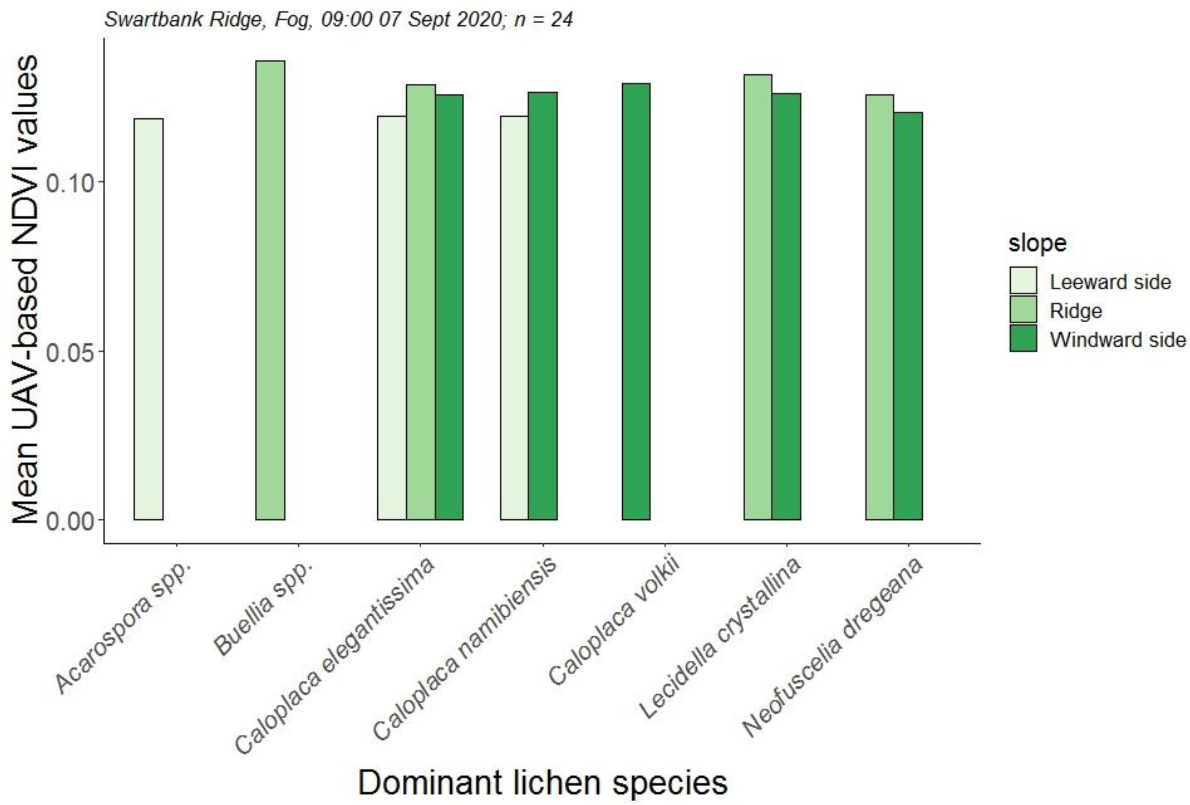

Figure 35. Mean UAV-based NDVI values representing different photosynthetic activity of dominant lichen species extracted from the 24 sample plots of permanently place 1 m2 quadrats on different slopes (i.e. ridge, windward, and leeward side) representing micro-habitats, along a 100 m topographical transect across a ridge, the n = 24 is the total observations in the quadrats or sampled plots, a fog day 09h00, 7 September 2020, Swartbank site.

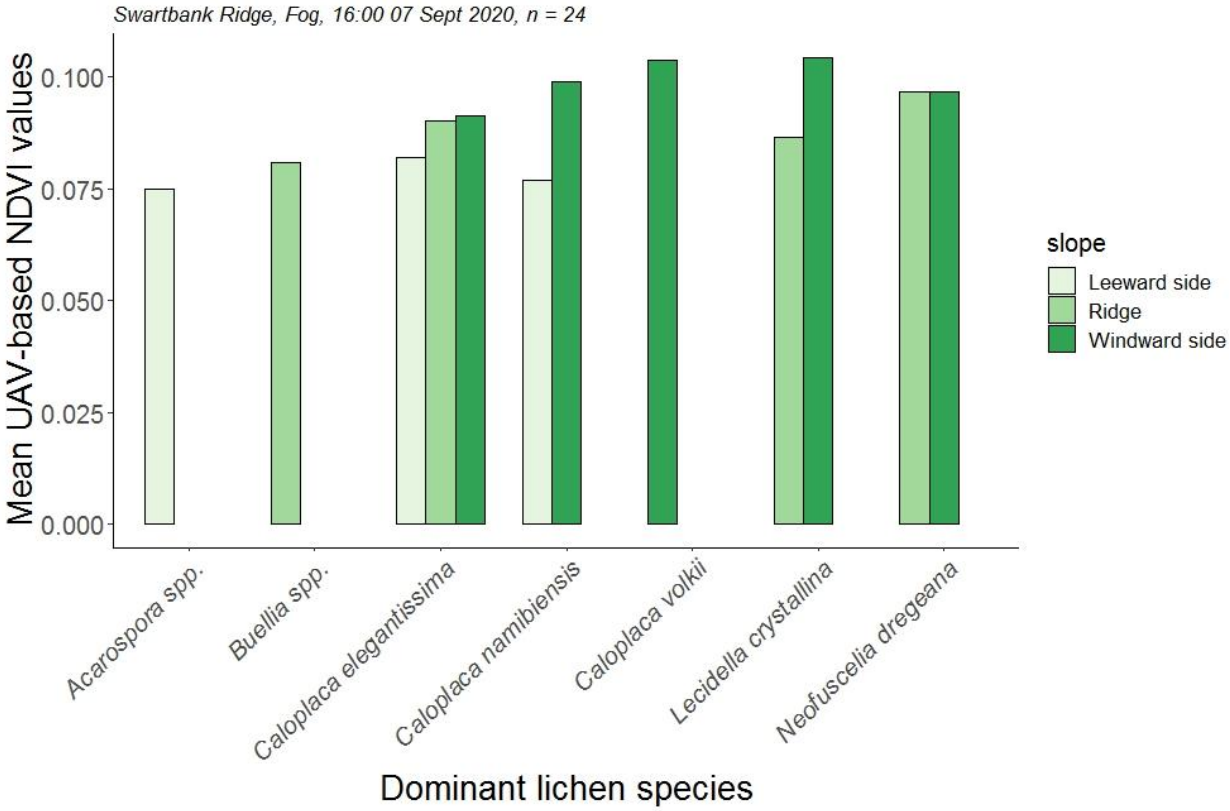

Figure 36. Mean UAV-based NDVI values representing different photosynthetic activity of dominant lichen species extracted from the 24 sample plots of permanently place 1 m2 quadrats on different slopes (i.e. ridge, windward, and leeward side) representing micro-habitats, along a 100 m topographical transect across a ridge, the n = 24 is the total observations in the quadrats or sampled plots, a fog day 16h00, 7 September 2020, Swartbank site.

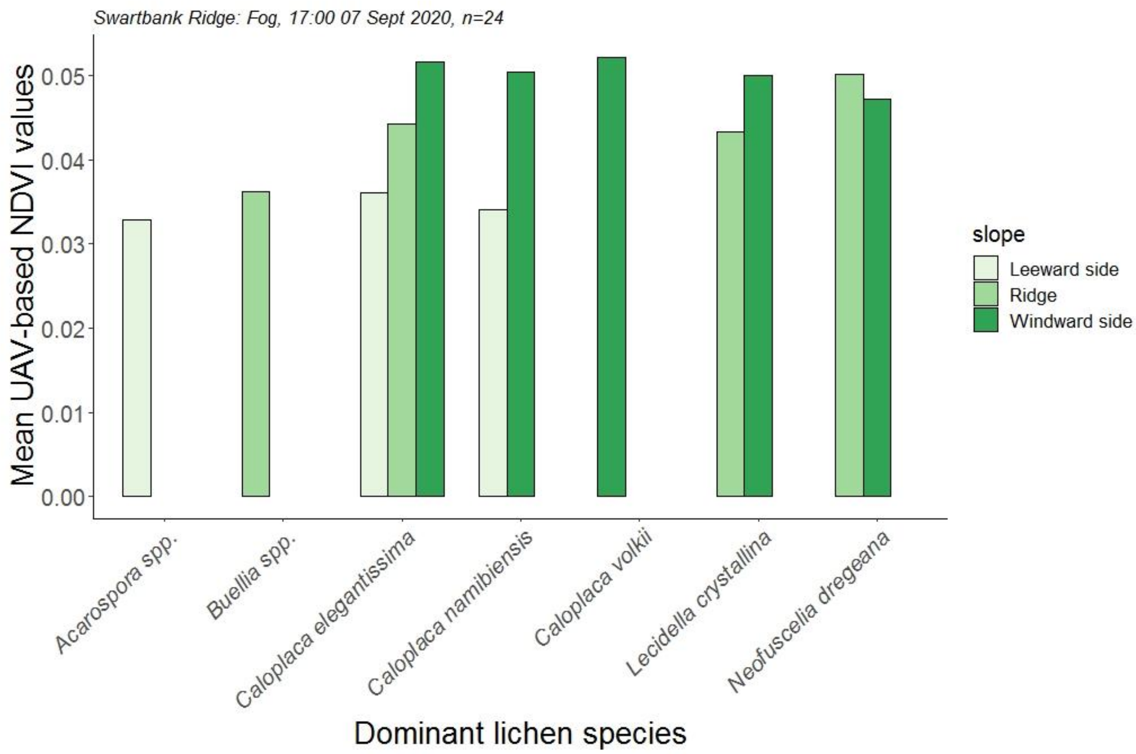

Figure 37. Mean UAV-based NDVI values representing different photosynthetic activity of dominant lichen species extracted from the 24 sample plots of permanently place 1 m2 quadrats on different slopes (i.e. ridge, windward, and leeward side) representing micro-habitats, along a 100 m topographical transect across a ridge, the n = 24 is the total observations in the quadrats or sampled plots, a fog day 17h00, 7 September 2020, Swartbank site.

Ground-observed lichen cover has a positive relationship and significant trend with elevation data, with p-values of < 0.05 (Figure 38). In wet conditions at 08:00, there was also a positive trend between UAV-observed NDVI values and elevation data, with p-values of < 0.05 (Figure 39). But in dry conditions at 17:00, the association between UAV-observed NDVI values and elevation data, was not significant (Figure 40). This shows that dry conditions negatively influence the accurate estimation of lichen NDVI response. The elevation parameter showed to be a good predictor of ground lichen coverage and lichen NDV response. The polynomial trend of UAV-based NDV values shows to be corresponding with ground-observed lichen coverage.

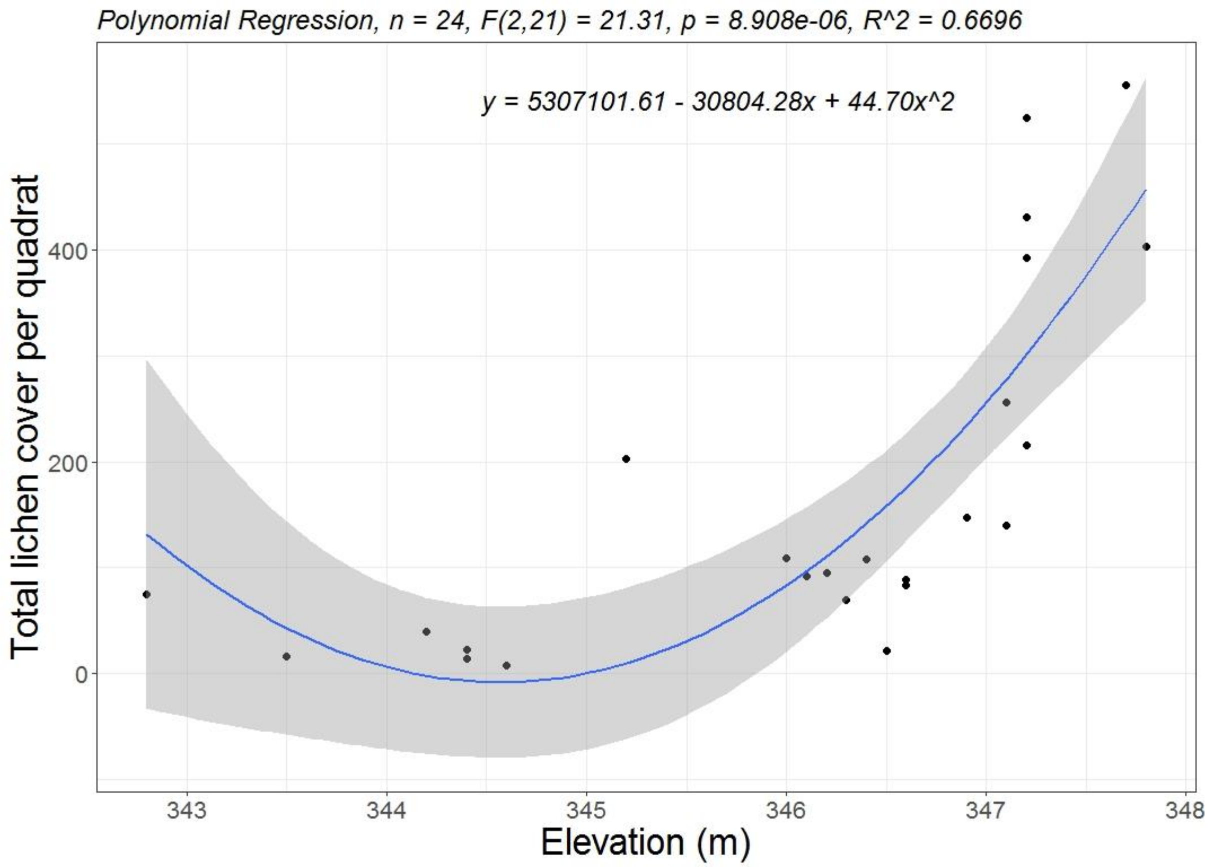

Figure 38. A polynomial regression showing a relationship between elevation (m) and ground observations of total lichen cover, measured from the 24 sample plots of permanently place 1 m^2 quadrats on different elevation and slopes (i.e. ridge, windward, and leeward side) representing micro-habitats, along a 100 m topographical transect across a ridge, the n = 24 is the total observations in the quadrats or sampled plots, Swartbank site. The polynomial trend-line is shown with 95 percent confidence intervals (shaded), along with r^2 and p-values.

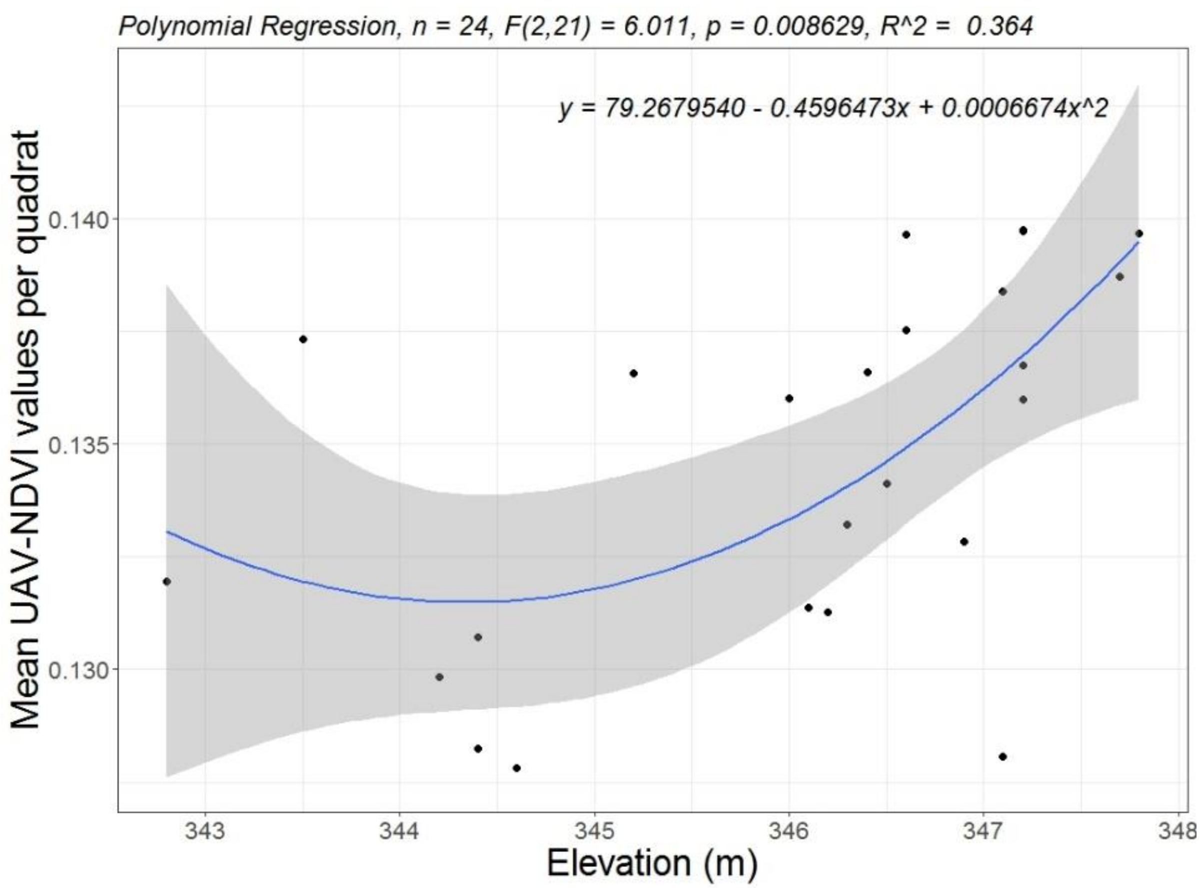

Figure 39. A polynomial regression showing a relationship between elevation (m) and mean UAV-based NDVI, referring to the metabolic activity of lichen, extracted using the 24 sample plots of permanently place 1 m2 quadrats on different elevation and slopes (i.e. ridge, windward, and leeward side) representing micro-habitats, along a 100 m topographical transect across a ridge, the n = 24 is the total observations in the quadrats or sampled plots, on a wet time of day 08h00, 7 September 2020, Swartbank site. The polynomial trend-line is shown with 95 percent confidence intervals (shaded), along with r^2 and p-values.

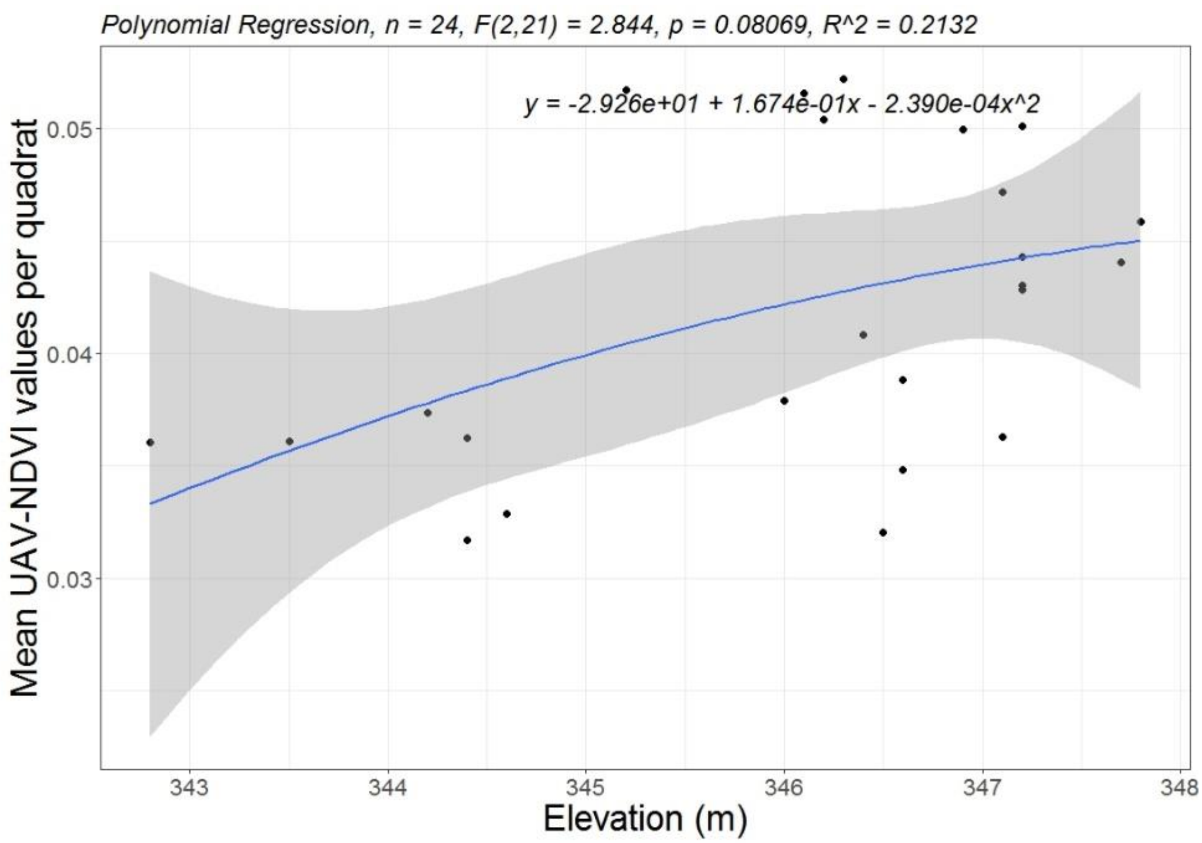

Figure 40. A polynomial regression showing a relationship between elevation (m) and mean UAV-based NDVI, referring to the metabolic activity of lichen, extracted using the 24 sample plots of permanently place 1 m2 quadrats on different elevation and slopes (i.e. ridge, windward, and leeward side) representing micro-habitats, along a 100 m topographical transect across a ridge, the n = 24 is the total observations in the quadrats or sampled plots, on a dry time of day 17h00, 7 September 2020, Swartbank site. The polynomial trend-line is shown with 95 percent confidence intervals (shaded), along with r^2 and p-values.

4.3.3 Influence of off-road tracks disturbance on lichen coverage

There was a significant difference in ground-observed lichen cover between the habitats such as plains, tracks, and washes (p-value < 0.05). Lichen cover is higher in undisturbed plains than in disturbed areas of tracks, in both sites (Figure 41a). Even though there was no statistically significant difference in mean UAV-NDVI between undisturbed plains and disturbed areas of tracks (p-value > 0.05), there are ecological differences (Figure 41b).

In the sampled locations there was lower lichen cover at Utuseb than at Swartbank, this is because Utuseb observations were sampled on lower-lying plains close to washes, while Swarbank had a samples were on the ridge. Areas with high topography received more water, thus higher lichen cover at high elevation plains than lower-lying plains. Nevertheless, at a large extent the Utuseb site had more lichen density than the Swartbank site, because it has a short distance to fog than Swartbank.

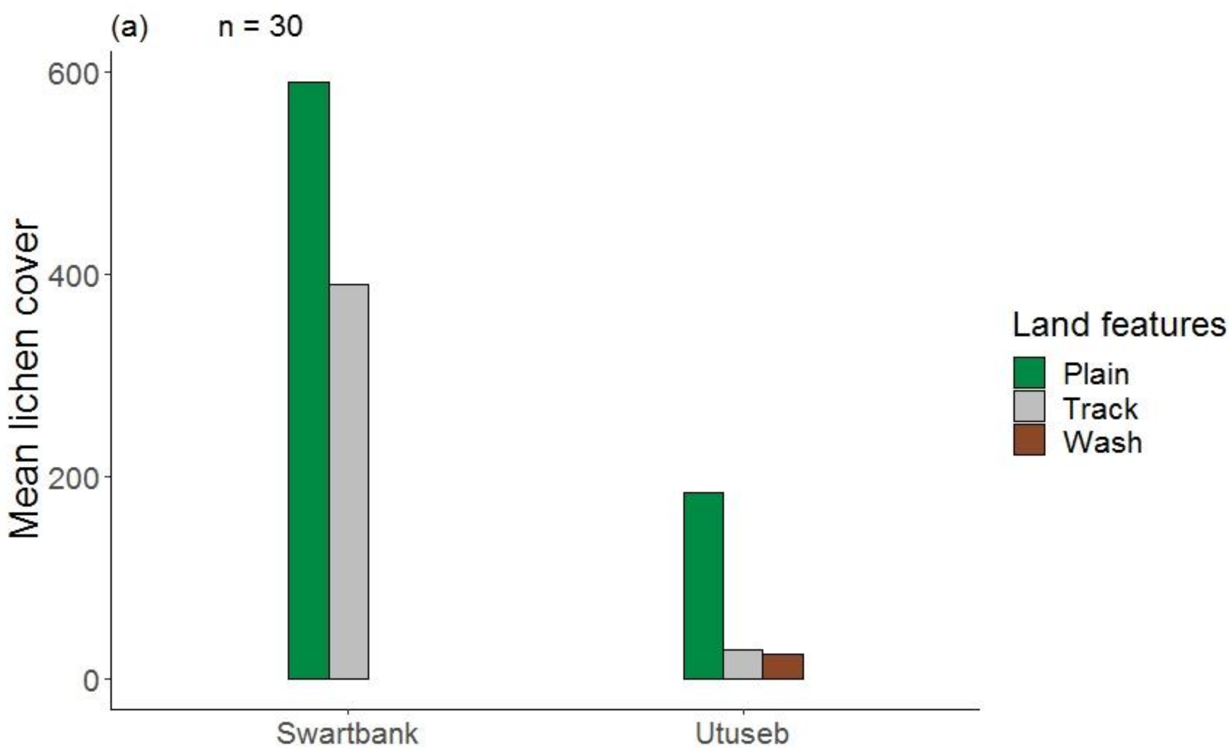

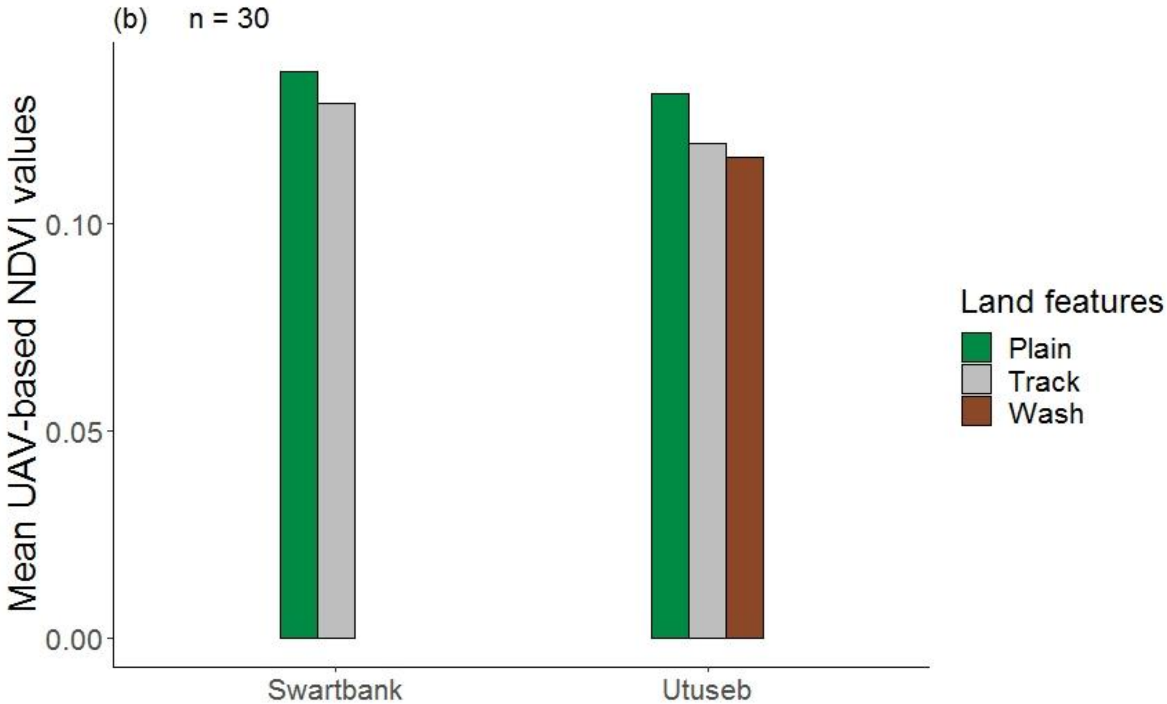

Figure 41. The influence of plains, off-road tracks, and river washes on ground-observed lichen cover (a) and mean UAV-based NDVI, represent lichen photosynthetic activity (b). These 30 samples were measured along a disturbance transect from the main road to 100 m inland, using the 1 m^2 quadrants, in both sites.

The total lichen cover was found to be less in the tracks than on the plains (Figure 42a). All lichen species reacted to disturbances differently. The two species only found in high intensity tracks and reduced in cover were only *Buellia sp.* and *Acarospora sp*. The *C. elegentissima* and *C. volkii* were only found on the plains areas where there was no evidence of tracks and other visible disturbances. Lichen NDVI reflectance values are related to ground cover (Figure 42b).

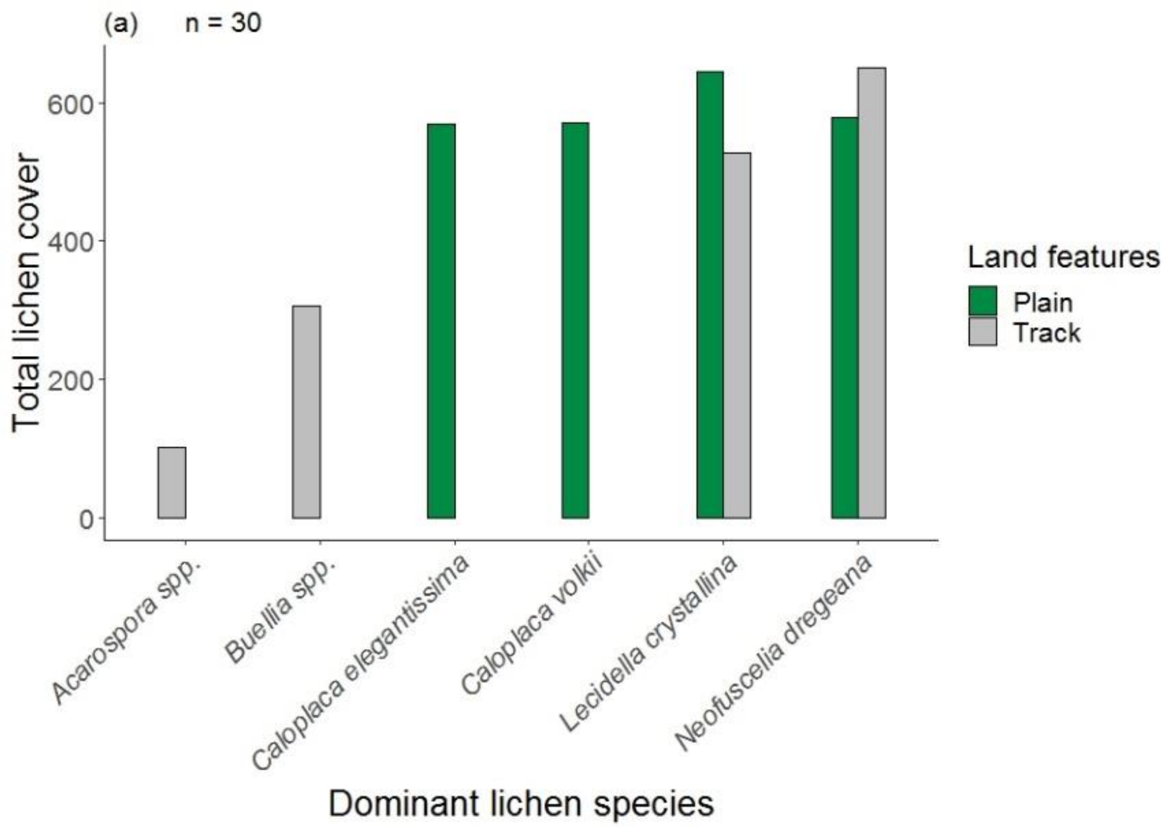
(a)
n = 30
Total lichen cover
600
400
200
0
Land features
Plain
Track
Acarospora spp.
Buellia spp.
Caloplaca elegantissima
Caloplaca volkii
Lecidella crystallina
Neofuscelia dregeana
Dominant lichen species

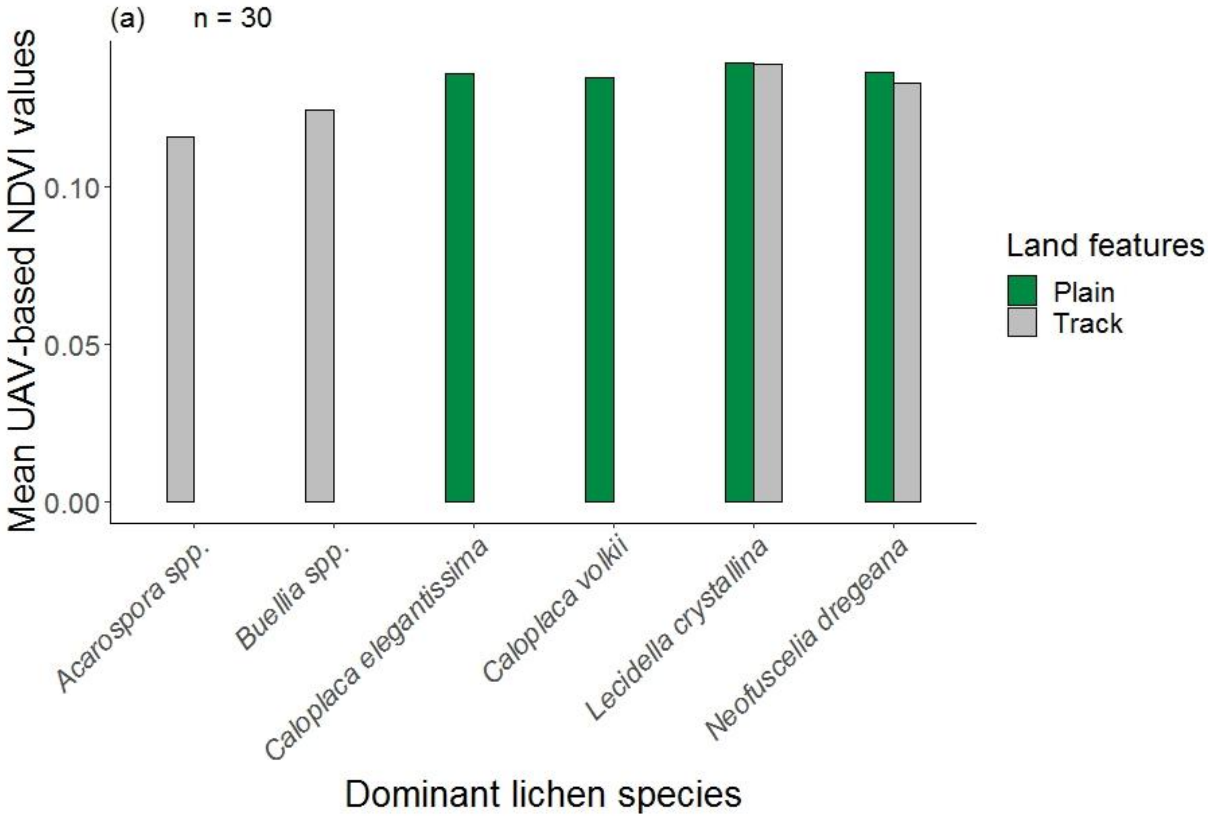

Figure 42. Ground observation of lichen species diversity and abundance cover (a), and mean UAV-based NDVI of lichen photosynthetic activity (b) in undisturbed plains and disturb areas of road track, in the Swartbank study site. These 30 samples were measured along a disturbance transect from the main road to 100 further inland, using the 1 m² quadrants.

4.4 Discussion

This study demonstrated that the application of UAV-based NDVIs provides valuable information about the photosynthetic activity response of lichen-dominated biocrusts to moisture availability, and disturbance response to off-road vehicle tracks, in a hyper arid environment. Our outcomes proved that with high-spatial resolution UAV image datasets, we were able to effectively monitor lichen-dominated biocrusts activity in response to fog by utilizing NDVI alone without biocrust-specific indices recently created for dry and semi-dry drylands.

4.4.1 Temporal curves of lichen photosynthetic activity response to wet and dry conditions

Time series curves of UAV-based NDVI showed higher lichen photosynthetic activity response in wet conditions than in dry conditions, because of varying fog events and air humidity. This agrees with previous studies, that lichen BSCs are considered poikilohydric, i.e., being only active when sufficient water is available (Lange *et al.* 1994b, 2008, Karnieli *et al.* 1999, Burgheimer *et al.* 2006, Casanovas *et al.* 2015). On a fog day, we observed a high mean NDVI in the morning directly after fog lifts at 08:00, which highlights that lichens become active under these conditions (Figure 29 and Figure 30). However, as fog moisture starts to decrease at 09:00 after fog there was a drop in NDVI mean values (Figure 4.4 and Figure 4.5).

Late afternoon (16-17:00) hours showed less NDVI than morning hours when there is low air humidity. These similar patterns were observed by Lange *et al.* (2008) field- and laboratory-based observations of lichens in the Namib Desert with extensive rates of positive net photosynthesis only immediately after sunrise from 07:30 to 10:30; and then the lichens dried and were almost completely inactive until sunset. We also found an interesting pattern of high NDVI values maximum value of 0.30, in the late afternoon (17:00), when there is high air humidity due to proceeding night fog (Figure 30). This suggests that lichens not only depend on fog moisture input but also on high air humidity. These similar results were also identified by (Karnieli *et al.* 1999, 2003) when they found that the high NDVI values may be caused by the photosynthetic activity of non-vascular lower plants, consisting of mosses, lichens, algae, and cyanobacteria, which cover most of the rock and soil surfaces in semi-arid regions. They found that the spectral reflectance curves of lower plants can be similar to those of the higher plants and their NDVI values can be as high as 0.30 units (Karnieli *et al.* 1999, 2003, Casanovas *et al.* 2015). This also confirms results by Lange *et al.* (2008), who also found that lichen were hydrated later in the afternoon due to water vapour uptake at higher air humidity, this increased hydration allows a short period of very low rates of photosynthesis just before sunset.

UAV-based NDVI was lower on a non-fog day compared to a fog day, suggesting that lichens were in an inactive state. However, lichens are shown to be active in the early morning with high humidity, which again agrees with the trend observed by Lange et al. (2008) that lichens do not only depend on fog moisture alone but also absorb the moisture within the air. Our observations also showed similar observations to other studies done in the desert (Karnieli *et al.* 1999), temperate (Reiter *et al.* 2008), and Antarctic Peninsula (Casanovas *et al.* 2015) regions, that activity of BSCs is also known to continue for up to five days after rainfall events of 0.4 mm when the conditions are moderate when the evaporation rates are low due to moderate solar irradiation and temperatures.

The performance of the UAV-fitted Sequoia multispectral sensor is highly influenced by sun intensity and soil brightness effects, at higher solar elevations, than compared to low solar elevations in the morning and later afternoon. This is a known challenge when sampling primarily in hot dryland areas with higher sun intensity, where bare soil and rocks are the immediate background substrates (Chapter 3). Therefore, we were no able to sample during the midday timeframe on either fog or non-fog days (10:00 and 15:00). In addition, this study was unable to show any support from the UAV based results that link to these findings of Lange et al. (2008). Furthermore, it would be of interest to see if there is any way to do observation during midday with remote sensing data, because our method experienced a drawback in this environment at midday.

4.4.2 Influence of micro-topography (elevation) on lichen coverage

The results from a topographic cross-section transect across the Swartbank ridge, showed a high significant difference in lichen species richness and lichen abundance cover on different slopes (i.e. windward side, ridge, and leeward side), as areas with high elevation have more lichen abundance cover and diversity than areas with low elevation (Figure 33). This suggests that the ridge receives more fog moisture distribution and has more substrates to support an increase in lichen growth. All the different slopes differ in lichen coverage and species diversity because they receive different amounts of fog moisture, in relation to the direction of incoming (i.e., from west to east) and retreating (i.e., east to west) of fog precipitation. For example, at Swartbank site, sampled the plots on the ridge and windward side had higher NDVI values than the plot on the leeward side, because the ridge and windward side receives high moisture distribution than the leeward side **(**Figure 34, Figure 35, Figure 36, and Figure 37). Therefore, this supports the hypothesis that the windward side had more lichen cover than the Lee side of the ridge. This is based on the fact that, in areas with a high relief landscape, moisture-laden fog clouds or air may not be able to carry fog if it is in a fog shadow created by a mountain ridge or rocks. As moist air travels, the windward side of a ridge/rock receives more fog moisture than the Lee side. Also, as fog distance reduces or retreats from the lee- side to the windward side, the windward side holds moisture longer than the leeward side. These results were similar to other studies which indicated that as fog travels at high altitude and from a west to east direction (i.e. coast to inland), the top of the ridge and windward side (west) of the ridge would have more lichen cover than the leeward side (east) (Schieferstein and Loris 1992). Additionally, during the morning, the NDVI values were higher on the windward side (on the west) than on the lee-ward side (on the east) as conditions are more moderate on the windward side. As the position of the sun was more to the east lee-ward side during sunrise, thus the east lee-ward side received more sunshine intensity less fog distribution and drier, than the west windward side.

Specific types of lichen species also prefer to grow in specific micro-topography, and on different substrates (i.e. soil and rock types), which shapes their morphological structures and their resilience to micro-climatic conditions (Blanco-Sacristán *et al.* 2021). This also supports that lichens follow a fog climatic gradient because areas with more fog to the coast receiving fog have more lichen cover than areas further inland (Daneel 1992, Lange *et al.* 2008). Lichen density and diversity decrease with distance from the coast (moist air) to inland (dry air). Fog distance decreases with increasing distance from coast to inland. The fog banks along the coast travel inland (from westwards to east), and as daytime temperature increases, its moisture carrying capacity reduces (or retreats) from east to west direction.

Therefore, easterly areas close to the coast receive fog earlier and longer, than easterly areas further inland. As a result, lichen cover and morphology vary following a fog gradient.

The relationship between elevation and UAV-derived NDVI (Figure 38) shows similarities to the relationship between elevation and ground observations of Lichen abundance cover (Figure 39). Our study found that elevation is a good predictor of lichen ground cover and NDVI response to moisture input.
Lalley *et al.* (2006), (Reiter *et al.* 2008, Blanco-Sacristán *et al.* 2021) all showed elevation to be an important indicator driver of lichen abundance. Lalley *et al.* (2006) further indicated the proximity to river channels as important. Without results supporting these findings we believe that a valuable data layer on elevation and aspect is crucial to understanding lichen distribution and cover. Therefore, with detailed elevation dataset generated using UAV-based data, validates the hypothesis that higher biocrust cover leads to higher moisture response, as the areas at high elevation receive more fog distribution thus high lichen cover. Furthermore, UAV-NDVI derived in dry conditions has no significant correlation to elevation, compared to wet conditions. This also indicated that moisture conditions influence UAV-based NDVI's ability to detect lichen photosynthetic activity.

4.4.3 Influence of off-road vehicle tracks on lichen coverage

Lichen species diversity and abundance were evaluated on different landforms which were plains, washes, and tracks. The results indicate that there is high lichen cover in plains than in tracks and washes (Figure 41a). Similar results in other study also found that a higher lichen cover in the control areas which provide more material for colonization (Lalley and Viles 2008). As expected, all the plains areas had a higher lichen cover than those of the track areas. Lichen species such as *Caloplaca elegantissima* and *Caloplaca volkii* were barely found in tracks, as they are less resistant to disturbance and may take longer to re-establish.

Lichen species *Buellia sp.* and the *Acarospora sp.* were only found on tracks but not on undisturbed plains, this may be explained by substrates found in tracks to support their regrowth or their resilience to dryness. Other studies found that, the temperature and fog deposits in the tracks versus the control area vary greatly (Lalley *et al.* 2006, Lalley and Viles 2008). Fewer fog deposits and higher temperatures mean a lower recovery rate for lichens in the tracks, as the photosynthetic efficiency of the lichens is reduced and the conditions are not ideal for re-colonization and establishment (Daneel 1992, Schultz 2006).

The present study demonstrates a high statistically significant difference between undisturbed and disturbed areas in ground-cover observations (Figure 42a). Although there was no statistically significant difference between undisturbed and disturbed areas in UAV-NDVI observations, there was ecologically differences. Thus, UAV-NDVI observations are an alternative that is non-destructive and reliable to quickly quantify lichen biocrust metabolic activity and development (Figure 42b). Moreover, we also identified signs of lichen recovery in the road track depending on their longevity, as new tracks showed less lichen coverage than old tracks. NDVI response was also high with increasing distance from the old Swartbank main road, as lichen communities were degraded alongside the access routes. However, considering the size of the lichen field and the actual areas affected the effect seems negligible if disturbance remains confined to these designated access routes.

4.4.4 Implications for Future Research and Conservation Policy Making

Dry and wet conditions showed to influence estimation of lichen photosynthetic responses using UAV-based NDVI, as results are taken from fog days during wet conditions had high NDVI compared to non-fog in dry conditions with suspended lichen metabolic activity. Therefore, minoring of lichens' photosynthetic activity should be taken in wet conditions when lichens are active. Moreover, with global warming, the temperature around the study area is expected to rise in the future, leading to less precipitation in the form of fog and rainfall, which may decrease BSCs growth (Schultz 2006, Lange *et al.* 2008, Michael *et al.*

2010). On the other hand, BSCs are expected to show fewer and shorter periods of metabolic activity during the summer as they become exposed to higher evaporative stress due to lower precipitation rates and higher temperatures.

Complete phenology of when lichen photosynthetic activities could not be evenly evaluated, because of the lack of good quality images taken closer to solar noon (10:00 and 15:00), which caused poor image overlaps or image processing errors. Under uniform cloud conditions and low solar angle, UAV-based observations are less affected by the sunshine intensity and soil brightness.

Therefore, it possible to obtain good quality UAV-based NDVI datasets during the low solar angle, with constant illumination in the morning a 08:00 and late afternoon at 17:00. In addition to that, missing hours were also due to high wind interrupted flights and running out of UAV battery power, thus reducing the chance of obtaining full and even timeseries of lichen NDVIs showing the interesting information of declining patterns of lichen metabolic activity, especially during midday. In this study, there were no results acquired consistently on consecutive days before and after fog events. Therefore, we recommended taking note of high winds during winter in the Central Namib Desert, for continual long-term research of lichens, using UAV platforms. Alternatively, it would be possible to have permanent fixed camera's that have a NIR band and red band as a minimum in place to resolve issues such as wind impact. However, sensors might still be impacted by solar noon, but they can be set to takes images of the same spot repeatedly at higher frequency, because lichens' photosynthetic response varies rapidly. In addition, meteorological data (e.g., precipitation, temperature, and insolation) and surface soil moisture content information recorded by an observational network within or in the immediate surrounding of the study area can increase the significance of the estimation of BSCs' metabolic activity and biomass.

The outcomes may be of specific importance for partners in the nature conservation field and inform the public about the importance of unique areas such as the Namib lichen fields. This research also served as a useful baseline study for follow on long-term drone monitoring of lichens productivity for land management practices in the uranium-rich Central Namib Desert, and as a disturbance response model to improve the protection of fragile lichen communities. Furthermore, biological soil crusts are important indicators of ecological conditions because they are sensitive to disturbances. Monitoring of lichen fields is not only important for assessing lichen and bio-crust coverage and recovery, as well as restoration of degraded areas, but also for hot topics in climate change such as carbon sequestration, changes in land cover, and indicators of spatial fog events in arid zones.

This research study has provided insights into a means to monitor these sensitive environments. This means of monitoring might prove to be a valuable tool to support the Convention on Biological Diversity (CBD), by providing evidence of health and stability of lichen ecosystem and fog dynamics. It also enables informed decision making to manage natural resource and regulate socio-economic land-use

4.5 Conclusion

It is feasible to use UAV-based NDVIs, as a proxy for lichen photosynthetic activity, to measure how different lichen species respond to moisture availability. The results also showed that UAV-derived NDVI (i.e., photosynthetic activity) differs for lichens under wet and dry conditions, and they depend on not only on moisture availability from fog events but also on higher air humidity.

Based on our UAV-derived NDVI temporal curve results, we concluded that lichen photosynthetic activity changes rapidly once the fog is lifting and as sunshine increases. In the morning at 08:00 immediately right after fog has lifted, lichens actively photosynthesize and restart their metabolism again in the later afternoon when there is higher air humidity. Therefore, the best time of day to use UAV-NDVI to detect lichen photosynthetic activity is during the morning at 08:00, and in the later afternoon at 17:00, under wet conditions moderated by adequate fog moisture of high relative air humidity. We also suggest regular monitoring of weather forecasts because lichen activity also occurs hours just before sunset when there is higher air humidity followed by night fog. Unfortunately, the Sequoia sensor performs poorly under high sun intensity and solar elevation, during midday hours (10:00-15:00).

Changes in soil moisture have a great impact on the UAV-NDVI estimation of lichen-dominated biological soil crusts (BSCs). Thus, fog days had higher lichen NDVI response than non-fog days. However, higher NDVI of wet lichens was more obvious than those of dry lichens, on both fog and non-fog days. As a result, UAV-NDVI observed low signs of lichen activity under dry conditions. Dry NDVI do not show clear trends of lichen presences and do not match ground-observed patterns better than wet NDVI. Therefore, we conclude that when using a UAV-based reflectance dataset (i.e. multispectral bands and NDVIs) to estimate lichen biocrusts, observations must be done during the wet condition, particularly the winter season or days with high fog events and humidity.

We also concluded that lichen communities are highly controlled by relief (ridges or rocks) which causes fog moisture to prevail on the windward side but reduces it on the lee-ward side in a fog shadow. As a result, lichen cover and diversity are more on the ridges and windward side compared to the lee-ward side. Moreover, the fine spatial resolution (<10 cm/pixel) of UAV-based elevation data have a direct relationship with lichen coverage and lichen NDVI response, hence it is crucial predictor of lichen biocrusts cover and photosynthesis activity. Elevation provided more insight into the relationship between lichen biocrusts and spatial fog distribution, to explain how lichen species in different micro-topographic habitats may respond differently to fog inputs.

UAV-based NDVI data are supportive in quantifying not only the response of BSCs to fog events but also their response to disturbances caused by off-road track, as well as identifying signs of lichen recovery in off-road track. Undisturbed plains have high lichen cover and lichen NDVIs response to moisture, than in off-road tracks and river washes. But there are signs of lichen recovery on off-road tracks because some lichen species are more resilient to disturbance than others.

In wet conditions, UAV-based observations of lichen NDVI reflectance activity correspond well to ground observations of lichen cover. This indicated that the use of the UAV-derived NDVIs approach is meaningful, and it corresponds well to reality, and hence we considered it successful in estimating the photosynthetic activity of lichen-dominated biocrusts in our study area. This study marks the first time a high-resolution UAV multispectral sensor is utilized as a valuable non-destructive option for reliable retrieval of lichen biocrust photosynthesis activity and lichen health cover that could be incorporated into long-term monitoring programs. Hence, our applied workflow can be transferred to comparable locales in Central Namib and elsewhere, for assessing BSCs coverage. Additionally, our study emphasizes the potential for future research that aims at improving the understanding of the spatiotemporal dynamic of lichens, not only in the Namib dryland but also beyond.

References

Adler, K., 2018. Radiometric correction of multispectral images collected by a UAV for phenology studies. *Student thesis series INES*.

Assmann, J.J., 2019. Arctic tundra plant phenology and greenness across space and time.

Assmann, J.J., Kerby, J.T., Cunliffe, A.M., and Myers-Smith, I.H., 2019. Vegetation monitoring using multispectral sensors — best practices and lessons learned from high latitudes. *Journal of Unmanned Vehicle Systems*, 7 (1), 54–75.

Barnes, E., Clarke, T., Richards, S.E., Colaizzi, P., Haberland, J., Kostrzewski, M., Waller, P., Choi, C., Riley, E., Thompson, T., Lascano, R., Li, H., Moran, M.S., Robert, P., Rust, R., and Larson, W.E., 2000. Coincident detection of crop water stress, nitrogen status and canopy density using ground-based multispectral data. *undefined*.

Belnap, J., Weber, B., and Büdel, B., 2016. *Biological soil crusts as an organizing principle in drylands*.

Blanco-Sacristán, J., Panigada, C., Gentili, R., Tagliabue, G., Garzonio, R., Martín, M.P., Ladrón de Guevara, M., Colombo, R., Dowling, T.P.F., and Rossini, M., 2021. UAV RGB, thermal infrared and multispectral imagery used to investigate the control of terrain on the spatial distribution of dryland biocrust. *Earth Surface Processes and Landforms*, 46 (12), 2466–2484.

Brede, B., Suomalainen, J., Bartholomeus, H., and Herold, M., 2015. Influence of solar zenith angle on the enhanced vegetation index of a Guyanese rainforest. *Remote Sensing Letters*, 6 (12), 972–981.

Burgheimer, J., Wilske, B., Maseyk, K., Karnieli, A., Zaady, E., Yakir, D., and Kesselmeier, J., 2006. Relationships between Normalized Difference Vegetation Index (NDVI) and carbon fluxes of biologic soil crusts assessed by ground measurements. *Journal of Arid Environments*, 64 (4), 651–669.

Canata, T.F., 2021. High-resolution data for mapping the spatio-temporal variability of sugarcane fields. text. Universidade de São Paulo.

Casanovas, P., Black, M., Fretwell, P., and Convey, P., 2015. Mapping lichen distribution on the Antarctic Peninsula using remote sensing, lichen spectra and photographic documentation by citizen scientists. *Polar Research*, 34.

Chen, J., Yuan Zhang, M., Wang, L., Shimazaki, H., and Tamura, M., 2005. A new index for mapping lichen-dominated biological soil crusts in desert areas. *Remote Sensing of Environment*, 96 (2), 165–175.

Chen, X., Wang, T., Liu, S., Peng, F., Kang, W., Guo, Z., Feng, K., Liu, J., and Tsunekawa, A., 2020. Spectral Response Assessment of Moss-Dominated Biological Soil Crust Coverage Under Dry and Wet Conditions. *Remote Sensing*, 12 (7), 1158.

Chen, X., Wang, T., Liu, S., Peng, F., Tsunekawa, A., Kang, W., Guo, Z., and Feng, K., 2019. A New Application of Random Forest Algorithm to Estimate Coverage of Moss-Dominated Biological Soil Crusts in Semi-Arid Mu Us Sandy Land, China. *Remote Sensing*, 11 (11), 1286.

Collier, E.A., 2019. Mapping Biological Soil Crust Cover in the Kawaihae Watershed.

Daneel, J.L., 1992. The Impact of Off-Road Vehicle Traffic on the Gravel Plains of the Central Namib Desert, Namibia. Master of Science in Agriculture. University of Natal, Pietermaritzburg.

Elseroad, A., Peter, J.S., and Uchida, M., 2009. Biological soil crust distribution on the Boardman Conservation Area: Results from 2009 monitoring, 14.

Fernández-Guisuraga, J.M., Sanz-Ablanedo, E., Suárez-Seoane, S., and Calvo, L., 2018. Using Unmanned Aerial Vehicles in Postfire Vegetation Survey Campaigns through Large and Heterogeneous Areas: Opportunities and Challenges. *Sensors*, 18 (2), 586.

Gray, P., Ridge, J., Poulin, S., Seymour, A., Schwantes, A., Swenson, J., and Johnston, D., 2018. Integrating Drone Imagery into High Resolution Satellite Remote Sensing Assessments of Estuarine Environments. *Remote Sensing*, 10, 1257.

Havrilla, C.A., Villarreal, M.L., DiBiase, J.L., Duniway, M.C., and Barger, N.N., 2020. Ultra-high-resolution mapping of biocrusts with Unmanned Aerial Systems. *Remote Sensing in Ecology and Conservation*, 6 (4), 441–456.

Hinchcliffe, G., Bollard-Breen, B., Cowan, D.A., Ashray, D., Gillman, L.N., Maggs-Kolling, G., de Los Rios, A., and Pointing, S.B., 2017. Advanced Photogrammetry to Assess Lichen Colonization in the Hyper-Arid Namib Desert. *Frontiers in Microbiology*, 8, 2083.

Huete, A.R., 1988. A soil-adjusted vegetation index (SAVI). *Remote Sensing of Environment*, 25 (3), 295–309.

Indices gallery-ArcGIS Pro Documentation [online], 2022. Available from: https://pro.arcgis.com/en/pro-app/latest/help/data/imagery/indices-gallery.htm [Accessed 26 Jul 2022].

Karnieli, A., Kidron, G., Glaesser, C., and Ben-Dor, E., 1999. Spectral Characteristics of Cyanobacteria Soil Crust in Semiarid Environments.

Karnieli, A., Kokaly, R.F., West, N.E., and Clark, R.N., 2003. Remote Sensing of Biological Soil Crusts. *In*: J. Belnap and O.L. Lange, eds. *Biological Soil Crusts: Structure, Function, and Management*. Berlin, Heidelberg: Springer, 431–455.

Kelcey, J. and Lucieer, A., 2012. Sensor Correction of a 6-Band Multispectral Imaging Sensor for UAV Remote Sensing. *Remote Sensing*, 4 (5), 1462–1493.

Knox, N.M., 2004. An assessment of techniques used for mapping Lichen Fields, RSA. Masters of Science in Geo-information Science and Earth Observation (Environmental Systems Analysis and Management). International Institute for Geo-information Science and Earth Observation, Enschede, Netherlands.

Knox, N.M., Rsa, F., and Knox, N.M., 2004. *An assessment of techniques used for mapping Lichen Fields, RSA Nichola Knox April, 2004 An assessment of techniques used for mapping Lichen Fields, RSA*.

Lalley, J.S. and Viles, H.A., 2005. Terricolous lichens in the northern Namib Desert of Namibia: distribution and community composition. *The Lichenologist*, 37 (01), 77–91.

Lalley, J.S. and Viles, H.A., 2006. Do Vehicle Track Disturbances Affect the Productivity of Soil-Growing Lichens in a Fog Desert? *Functional Ecology*, 20, 548–556.

Lalley, J.S. and Viles, H.A., 2008. Recovery of lichen-dominated soil crusts in a hyper-arid desert. *Biodiversity and Conservation*, 17, 1–20.

Lalley, J.S., Viles, H.A., Copeman, N., and Cowley, C., 2006. The Influence of Multi-Scale Environmental Variables on the Distribution of Terricolous Lichens in a Fog Desert. *Journal of Vegetation Science*, 17, 831–838.

Lange, O.L., Green, A.T.G., Melzer, B., Meyer, A., and Zellner, H., 2006. Water Relations and Co2 Exchange of the Terrestrial Lichen Teloschistes Capensis in the Namib Fog Desert: Measurements During Two Seasons in the Field and Under Controlled Conditions. *Flora*, 201, 268–280.

Lange, O.L., Green, A.T.G., Meyer, A., and Zellner, H., 2007. Water relations and carbon dioxide exchange of epiphytic lichens in the Namib fog desert. *Flora*, 202, 479–487.

Lange, O.L., Green, A.T.G., Meyer, A., and Zellner, H., 2008. Epilithic Lichens in the Namib Fog Desert: Field Measurements of Water Relations and Carbon Dioxide Exchange. *Sauteria*, 15, 283–302.

Lange, O.L., Meyer, A., Zellner, H., and Heber, U., 1994a. Photosynthesis and water relations of lichen soil crusts: field measurements in the coastal fog zone of the Namib desert. *Functional Ecology*, 8, 253–264.

Lange, O.L., Meyer, A., Zellner, H., and Heber, U., 1994b. Photosynthesis and Water Relations of Lichen Soil Crusts: Field Measurements in the Coastal Fog Zone of the Namib Desert. *Functional Ecology*, 8, 253–264.

Loris, K., Pfiz, M., Erb, E., Wirth, V., and Küppers, M., 2009. Lichen vegetation in the Central Namib as influenced by geomorphological and edaphic conditions, climate and wind erosion. *In*: A. Thell, M.R.D. Seaward, and T. Feuerer, eds. *Diversity of Lichenology - Anniversary Volume*. Berlin Stuttgart: J. Cramer / Gebrüder Borntraeger Verlagsbuchhandlung.

Macander, M.J., Frost, G.V., and Palm, E., 2018. Lichen Cover Mapping for the Range of the Fortymile Caribou Herd, Alaska and Yukon Territory.

Maphangwa, K.W., Musil, C.F., Raitt, L., and Zedda, L., 2012. Experimental climate warming decreases photosynthetic efficiency of lichens in an arid South African ecosystem. *Oecologia*, 169 (1), 257–268.

Michael, P., Kurt, L., Elke, E., Wirth, V., and Küppers, M., 2010. Changing patterns of lichen growth form distributions within the lichen fields of the Central Namib. 107–111.

Oldeland, J., Große-Stoltenberg, A., Naftal, L., and Strohbach, B.J., 2017. The Potential of UAV Derived Image Features for Discriminating Savannah Tree Species. *In*: R. Díaz-Delgado, R. Lucas, and C. Hurford, eds. *The Roles of Remote Sensing in Nature Conservation: A Practical Guide and Case Studies*. Cham: Springer International Publishing, 183–201.

Parrot Sequoia manual [online], 2022. Available from: https://www.manualscat.com/en/parrot-sequoia-manual [Accessed 28 Jul 2022].

R Core Team, 2021.

Rasmussen, J., Ntakos, G., Nielsen, J., Svensgaard, J., Poulsen, R.N., and Christensen, S., 2016. Are vegetation indices derived from consumer-grade cameras mounted on UAVs sufficiently reliable for assessing experimental plots? *European Journal of Agronomy*, 74, 75–92.

Reiter, R., Hoftberger, M., Green, A.T.G., and Turk, R., 2008. Photosynthesis of Lichens from Lichen-dominated Communities in the Alpine/Nival Belt of the Alps – II: Laboratory and Field Measurements of Co2 Exchange and Water Relations. *Flora*, 203, 34–46.

Rieser, J., Veste, M., Thiel, M., and Schönbrodt-Stitt, S., 2021. Coverage and Rainfall Response of Biological Soil Crusts Using Multi-Temporal Sentinel-2 Data in a Central European Temperate Dry Acid Grassland. *Remote Sensing*, 13 (16), 3093.

Rodríguez-Caballero, E., Knerr, T., and Weber, B., 2015. Importance of biocrusts in dryland monitoring using spectral indices. *Remote Sensing of Environment*, 170, 32–39.

Rodríguez-Caballero, E., Paul, M., Tamm, A., Caesar, J., Büdel, B., Escribano, P., Hill, J., and Weber, B., 2017. Biomass assessment of microbial surface communities by means of hyperspectral remote sensing data. *The Science of the Total Environment*, 586, 1287–1297.

Román, J.R., Rodríguez-Caballero, E., Rodríguez-Lozano, B., Roncero-Ramos, B., Chamizo, S., Águila-Carricondo, P., and Cantón, Y., 2019. Spectral Response Analysis: An Indirect and Non-Destructive Methodology for the Chlorophyll Quantification of Biocrusts. *Remote Sensing*, 11 (11), 1350.

SASSCAL WeatherNet - Weather stations in Namibia [online], 2022. Available from: http://www.sasscalweathernet.org/index.php?MIsoCode=NA [Accessed 1 Aug 2022].

Schieferstein, B. and Loris, K., 1992. Ecological Investigations on Lichen Fields of the Central Namib: I. Distribution Patterns and Habitat Conditions. *Vegetatio*, 98, 113–128.

Schultz, C., 2006. Remote sensing the distribution and spatiotemporal changes of major lichen communities in the Central Namib Desert. PhD. University of Kaiserslautern, Kaiserslautern, Germany.

Smith, G.M. and Milton, E.J., 1999. The use of the empirical line method to calibrate remotely sensed data to reflectance. *International Journal of Remote Sensing*, 20 (13), 2653–2662.

Stow, D., Nichol, C.J., Wade, T., Assmann, J.J., Simpson, G., and Helfter, C., 2019. Illumination Geometry and Flying Height Influence Surface Reflectance and NDVI Derived from Multispectral UAS Imagery. *Drones*, 3 (3), 55.

Trajkovski, K., Grigillo, D., and Petrovič, D., 2020. Optimization of UAV Flight Missions in Steep Terrain. *Remote Sensing*, 12, 1293.

Tu, Y.-H., Phinn, S., Johansen, K., and Robson, A., 2018. Assessing Radiometric Correction Approaches for Multi-Spectral UAS Imagery for Horticultural Applications. *Remote Sensing*, 10 (11), 1684.

Turner, D., Lucieer, A., Malenovsky, Z., King, D., and Robinson, S., 2014. Spatial co-registration of ultra-high resolution visible, multispectral and thermal images acquired with a micro-UAV over Antarctic moss beds. *Faculty of Science, Medicine and Health - Papers: part A*, 4003–4024.

Wessels, D.C.J. and van Vuuren, D.R.J., 1986a. Landsat imagery - its possible use in maping the distribution of major Lichen Communities in the Namib Desert, South West Africa. *Madoqua*, 14(4), 369–373.

Wessels, D.C.J. and van Vuuren, D.R.J., 1986b. Landsat imagery - its possible use in mapping the distribution of major Lichen Communities in the Namib Desert, South West Africa. *Madoqua*, 14, 6.

Whitehead, K. and Hugenholtz, C., 2014. Remote sensing of the environment with small unmanned aircraft systems (UASs), part 1: A review of progress and challenges. *Journal of Unmanned Vehicle Systems*, 02, 69–85.

Wirth, V., J., M., M., P., K., L., and Küppers, M., 2010a. Lichen distribution along an ocean-inland transect in the fog zone of the Central Namib. 112–117.

Wirth, V., J., M., M., P., K., L., and Küppers, M., 2010b. Lichen distribution along an ocean-inland transect in the fog zone of the Central Namib. 112–117.

Yu, X., Liu, Q., Liu, X., Liu, X., and Wang, Y., 2017. A physical-based atmospheric correction algorithm of unmanned aerial vehicles images and its utility analysis. *International Journal of Remote Sensing*, 38 (8–10), 3101–3112.

Zietara, A.M., 2017. Creating Digital Elevation Model (DEM) based on ground points extracted from classified aerial images obtained from Unmanned Aerial Vehicle (UAV).

Appendices

Appendix 1 Field Sheet for Data Collection

FIELD SHEETS

Observer:

Date/time:

Weather:

Site number:

Site locality (& lat/long; alt):

Quadrat number:

Slope:

Dominant lichen species	Total lichen count	Cover: < 5% =1; 5—25% =2; 25—50% =3; 50–75% = 4; > 75%= 5	Substrate (soil, rock)	Road track/no track	Other Characteristics

Appendix 2 UAV flight campaign

Site	Date	Time	Platform	Fog	Wind Speed max (m/s) (Coastal Met station)	Incoming radiation (W/m^2) (Coastal)
Swartbank	23-08-2020	12	DJI Phantom 4		2.5	
Swartbank	31-08-2020	**8**	DJI Phantom 4			
Swartbank	31-08-2020	**9**	DJI Phantom 4			
Utuseb	02-09-2020	**9**	DJI Phantom 4	**No**	2.5	**698.1**
Utuseb	02-09-2020	**10**	DJI Phantom 4	**No**	**5.0**	**840.0**
Utuseb	02-09-2020	**11**	DJI Phantom 4	**No**	**5.2**	**908.0**
Utuseb	02-09-2020	**12**	DJI Phantom 4	**No**	**5.8**	**8996.0**
Utuseb	02-09-2020	**14**	DJI Phantom 4	**No**	**7.7**	**691.1**
Utuseb	02-09-2020	**15**	DJI Phantom 4	**No**	**8.6**	**501.5**
Utuseb	02-09-2020	**16**	DJI Phantom 4	**No**	**9.5**	**264.5**
Utuseb	02-09-2020	**17**	DJI Phantom 4	**No**	**9.5**	**52.5**
Utuseb	05-09-2020	**8**	DJI Phantom 4			
Utuseb	05-09-2020	**15**	DJI Phantom 4			
Utuseb	05-09-2020	**16**	DJI Phantom 4			
Utuseb	05-09-2020	**17**	DJI Phantom 4			
Swartbank	**07-09-2020**	**8**	DJI Phantom 4	**Yes**	**6.4**	**3.27.7**
Swartbank	**07-09-2020**	**9**	DJI Phantom 4	**Yes**	**7.7**	**658.2**
Swartbank	**07-09-2020**	**11**	DJI Phantom 4	**Yes**	**8.6**	**877.0**
Swartbank	**07-09-2020**	**13**	DJI Phantom 4	**Yes**	**7.6**	**765.0**
Swartbank	**07-09-2020**	**15**	DJI Phantom 4	**Yes**	**7.1**	**439.1**
Swartbank	**07-09-2020**	**16**	DJI Phantom 4	**Yes**	**7.4**	**222.8**

Swartbank	**07-09-2020**	**17**	DJI Phantom 4	**Yes**	**7.0**	**36.0**
Swartbank	**12-09-2020**	**8**	DJI Phantom 4			
Swartbank	**12-09-2020**	**15**	DJI Phantom 4			
Swartbank	**12-09-2020**	**16**	DJI Phantom 4			
Swartbank	**12-09-2020**	**17**	DJI Phantom 4			
Swartbank	**16-09-2020**	**8**	DJI Phantom 4			
Swartbank	**16-09-2020**	**9**	DJI Phantom 4			
Swartbank	**16-09-2020**	**10**	DJI Phantom 4			
Swartbank	17-09-2020	8	DJI Phantom 4			
Swartbank	17-09-2020	16	DJI Phantom 4			
Swartbank	17-09-2020	17	DJI Phantom 4			
Utuseb	23-07-2020	9	DJI Phantom 4			
Utuseb	23-07-2020	10	DJI Phantom 4			
Utuseb	23-07-2020	11	DJI Phantom 4			
Utuseb	23-07-2020	12	DJI Phantom 4			
Utuseb	23-07-2020	14	DJI Phantom 4			
Utuseb	23-07-2020	15	DJI Phantom 4			
Utuseb	23-07-2020	16	DJI Phantom 4			
Utuseb	23-07-2020	17	DJI Phantom 4			
Utuseb	25-09-2020	10	DJI Phantom 4			
Utuseb	25-09-2020	11	DJI Phantom 4			
Utuseb	25-09-2020	15	DJI Phantom 4			
Utuseb	25-09-2020	16	DJI Phantom 4			
Utuseb	25-09-2020	17	DJI Phantom 4			
Swartbank	03-09-2021	9	Parrot			
Swartbank	03-09-2021	8	Parrot			
Swartbank	03-09-2021	10	Parrot			

Swartbank	03-09-2021	11	Parrot			
Swartbank	03-09-2021	12				
Swartbank	04-09-2021	8	Parrot			
Swartbank	04-09-2021	9	Parrot			
Swartbank	04-09-2021	10	Parrot			
Swartbank	04-09-2021	11	Parrot			
Swartbank	04-09-2021	12	Parrot			
Swartbank	04-09-2021	13	Parrot			
Swartbank	05-09-2021	12	Parrot			
Swartbank	05-09-2021	13	Parrot			
Swartbank	05-09-2021	14	Parrot			
Swartbank	05-09-2021	15	Parrot			
Swartbank	05-09-2021	16	Parrot			
Swartbank	06-09-2021	8	Parrot			
Swartbank	06-09-2021	9	Parrot			
Swartbank	06-09-2021	10	Parrot			
Swartbank	06-09-2021	11	Parrot			
Swartbank	07-09-2021	8	Parrot			
Swartbank	07-09-2021	9	Parrot			
Swartbank	07-09-2021	10	Parrot			
Swartbank	07-09-2021	11	Parrot			
Swartbank	07-09-2021	12	Parrot			
Swartbank	07-09-2021	13	Parrot			
Swartbank	09-09-2021	10	Parrot			
Swartbank	09-09-2021	11	Parrot			
Swartbank	09-09-2021	12	Parrot			
Swartbank	09-09-2021	13	Parrot			

Swartbank	23-09-2021	8	Parrot			

Appendix 3 Figure 1 Fog occurrences at Coastal Met, Sophies Hoogte, and Gobabeb SASSCAL Fognet weather stations, the date of UAV image data collected on August 2020, September 2020 and September 2021.

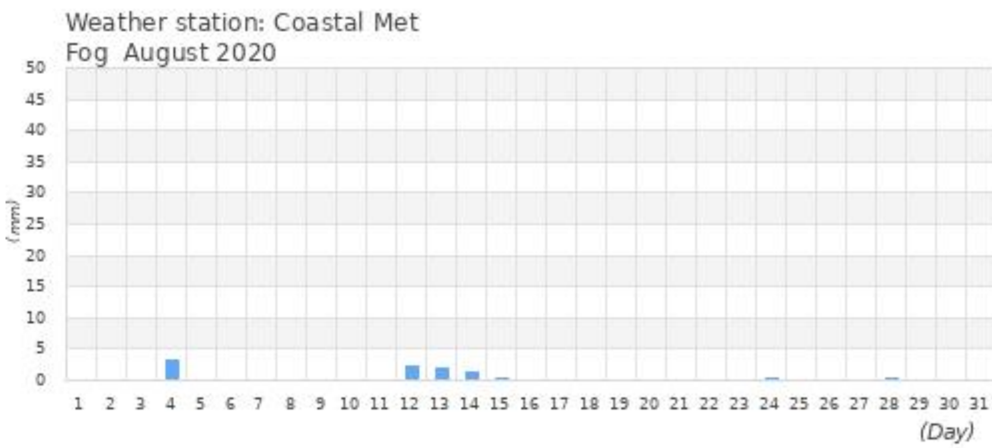

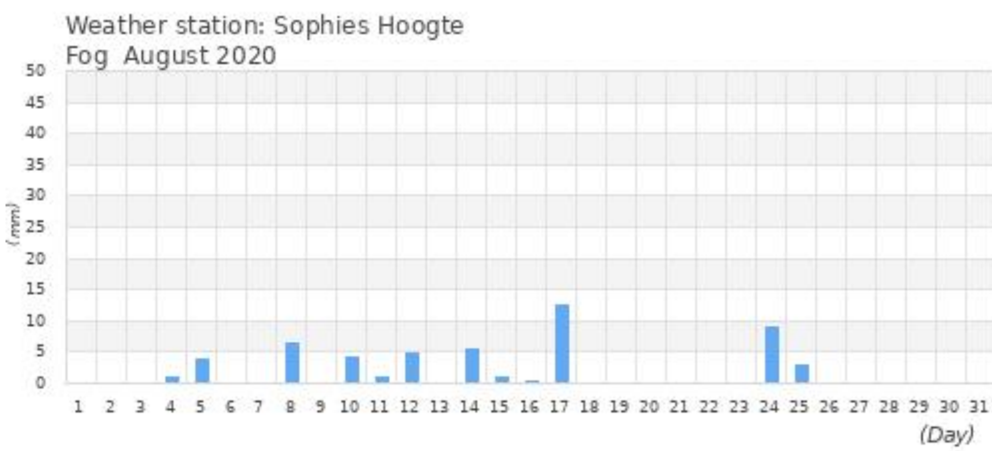

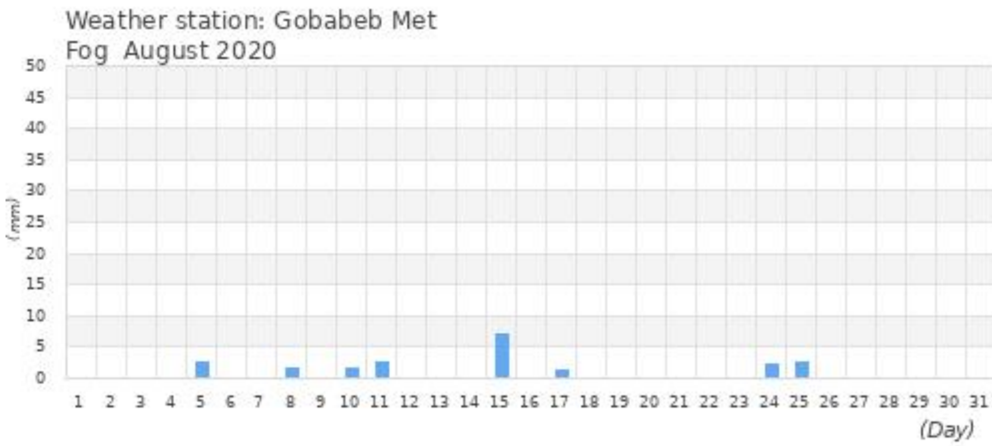
Weather station: Gobabeb Met
Fog August 2020
0 5 10 15 20 25 30 35 40 45 50
(mm)
1 2 3 4 5 6 7 8 9 10 11 12 13 14 15 16 17 18 19 20 21 22 23 24 25 26 27 28 29 30 31
(Day)

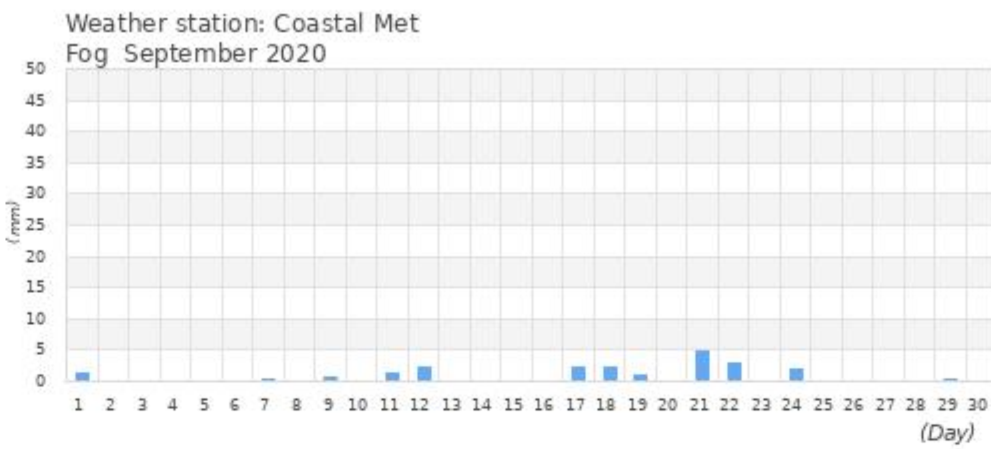
Weather station: Coastal Met
Fog September 2020
0 5 10 15 20 25 30 35 40 45 50
(mm)
1 2 3 4 5 6 7 8 9 10 11 12 13 14 15 16 17 18 19 20 21 22 23 24 25 26 27 28 29 30
(Day)

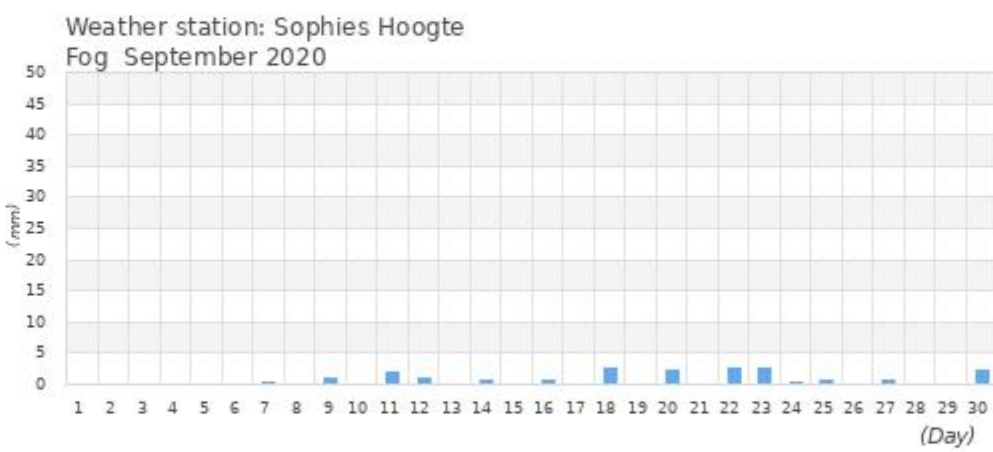
Weather station: Sophies Hoogte
Fog September 2020
0 5 10 15 20 25 30 35 40 45 50
(mm)
1 2 3 4 5 6 7 8 9 10 11 12 13 14 15 16 17 18 19 20 21 22 23 24 25 26 27 28 29 30
(Day)

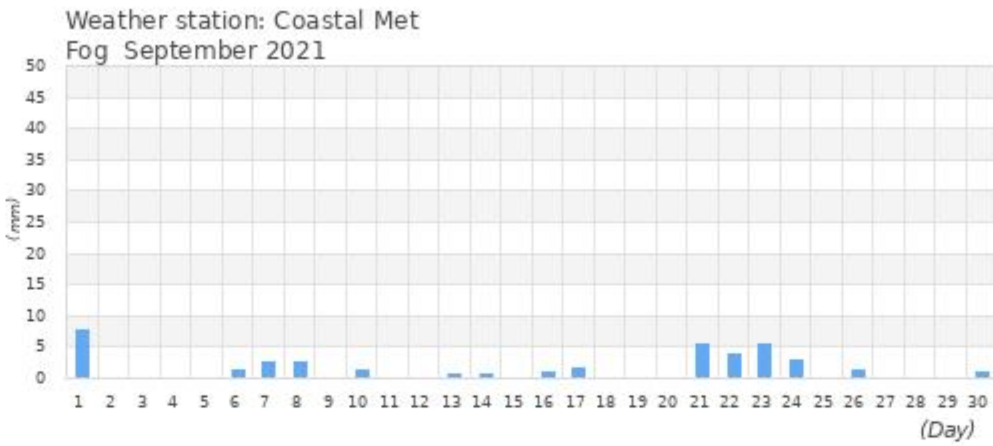
Weather station: Coastal Met
Fog September 2021
(mm)
(Day)

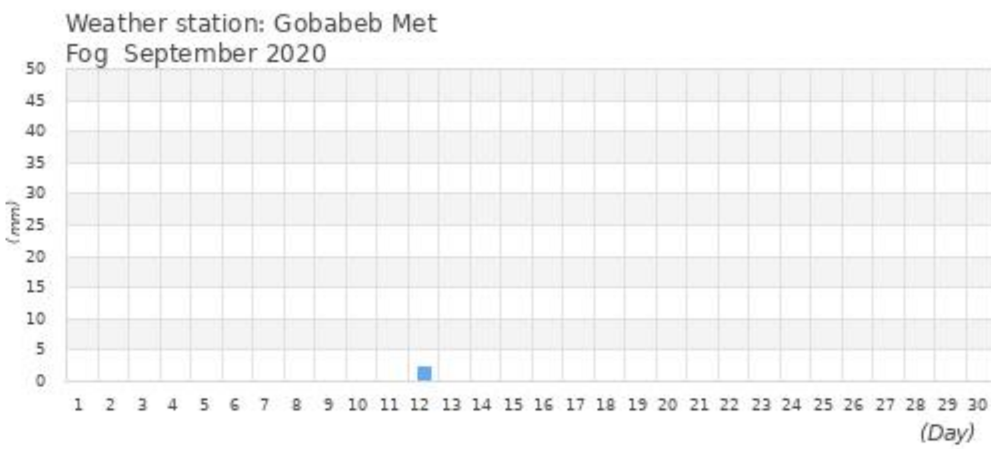
Weather station: Gobabeb Met
Fog September 2020
(mm)
(Day)

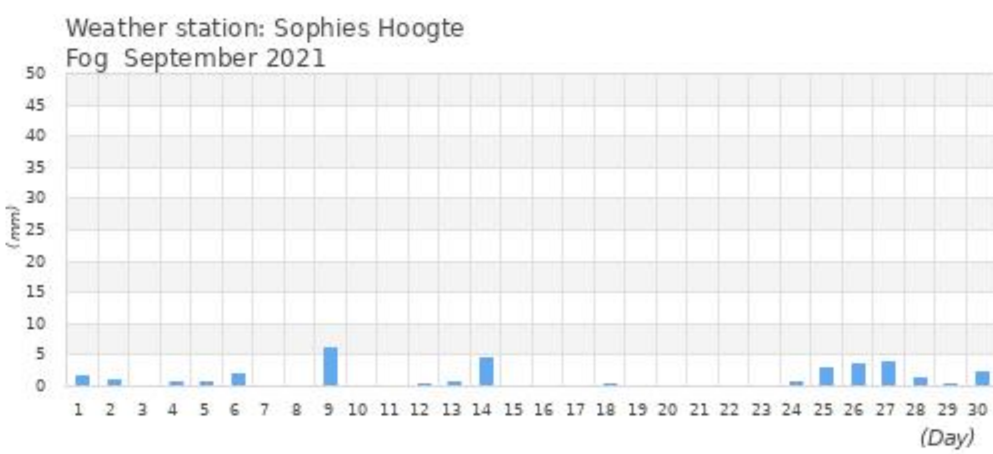
Weather station: Sophies Hoogte
Fog September 2021
(mm)
(Day)

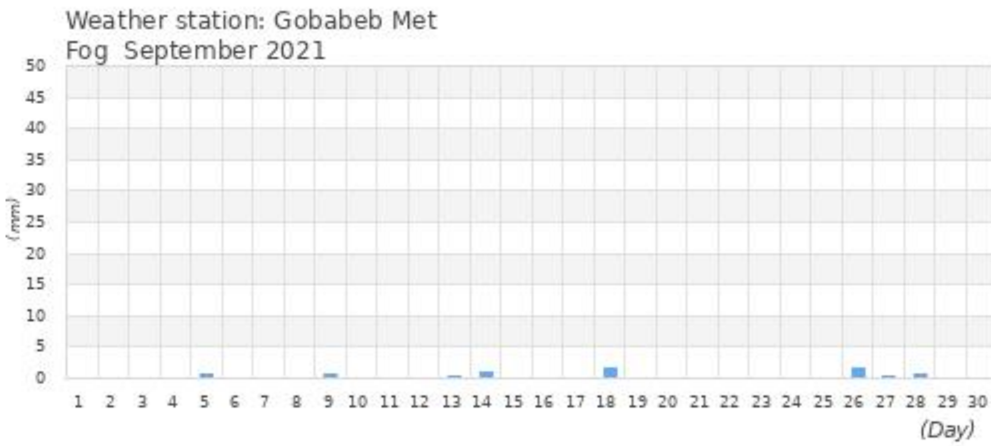

Appendix 4 Digital Photogrammetry Processing in Pix4Dmapper

Appendix 5 Temporal Curves of Lichens' UAV-based NDVI of the West plot 13 at Swartbank site.

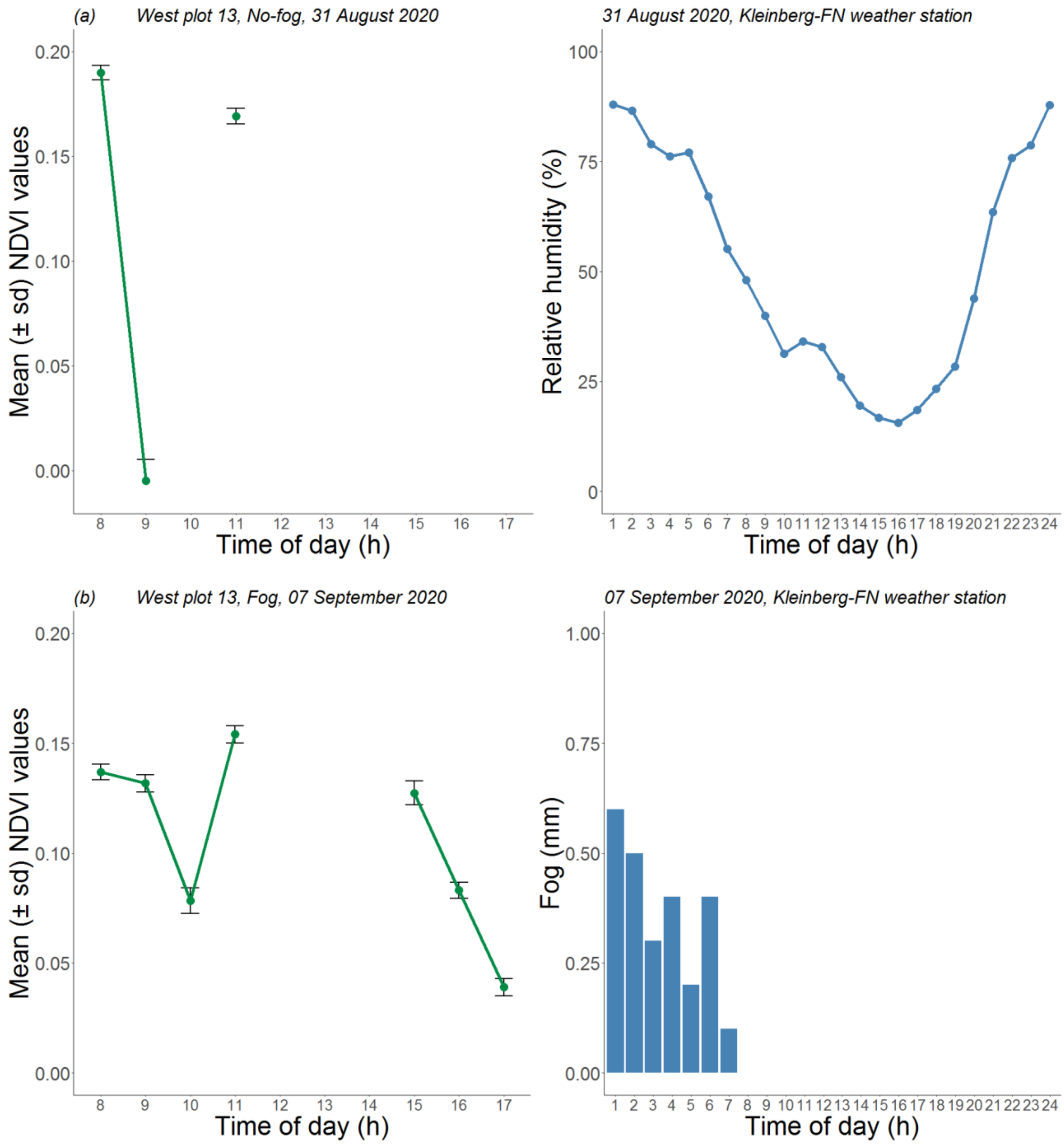

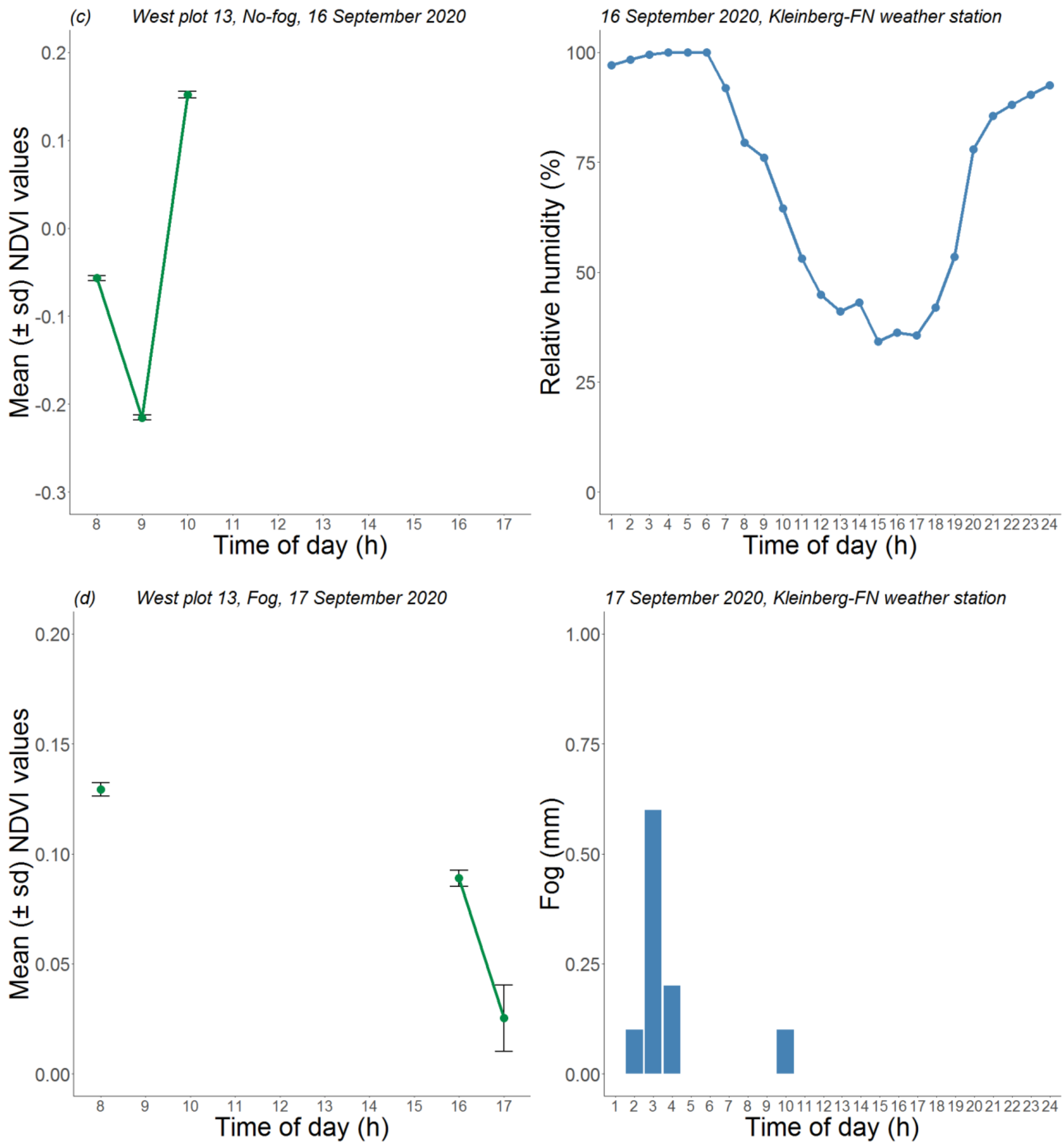
(c)
West plot 13, No-fog, 16 September 2020
Mean (± sd) NDVI values
Time of day (h)
16 September 2020, Kleinberg-FN weather station
Relative humidity (%)
Time of day (h)
(d)
West plot 13, Fog, 17 September 2020
Mean (± sd) NDVI values
Time of day (h)
17 September 2020, Kleinberg-FN weather station
Fog (mm)
Time of day (h)

Appendix 6 Temporal Curves of Lichens' UAV-based NDVI of the East plot 1 at Swartbank site.

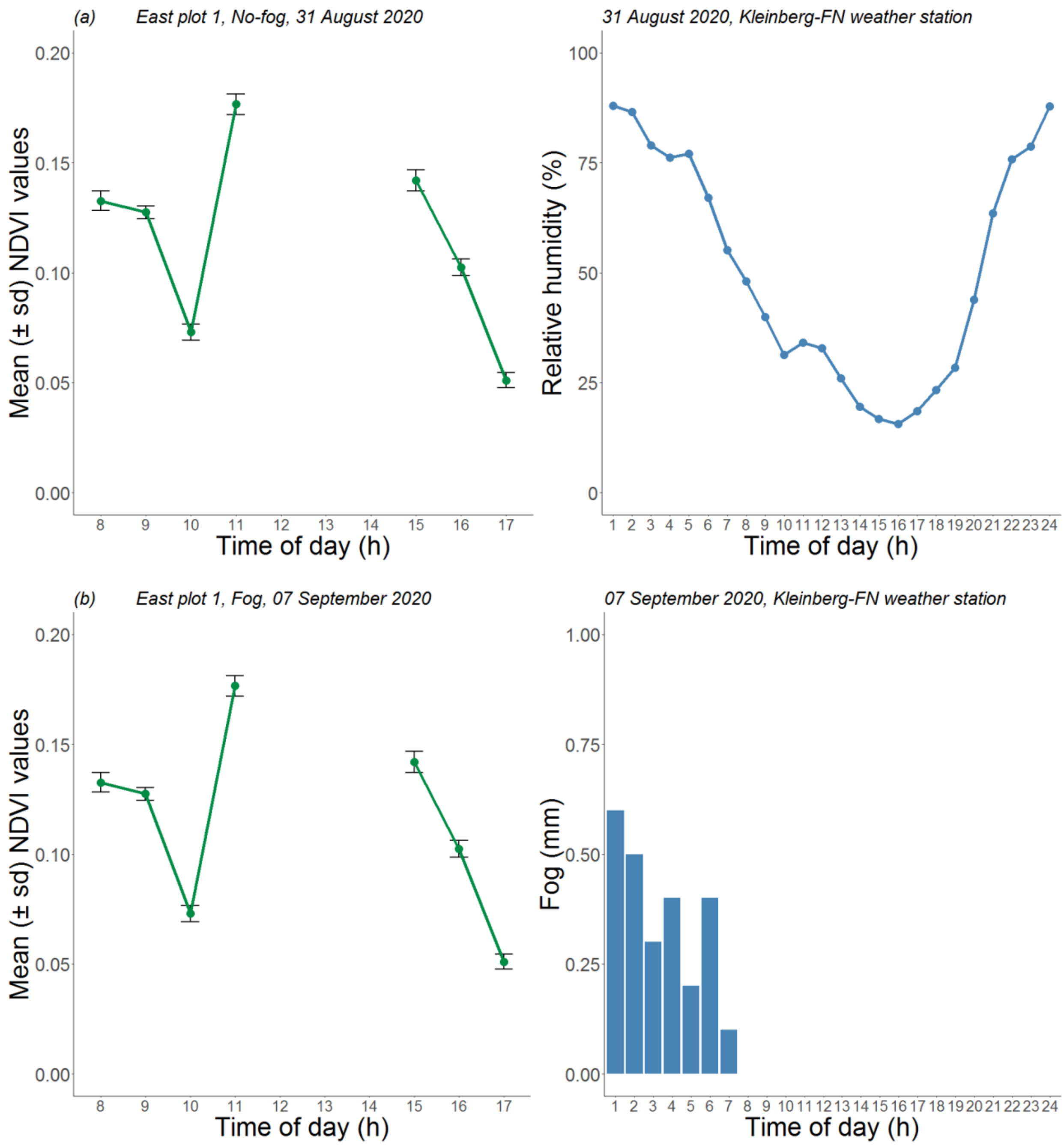

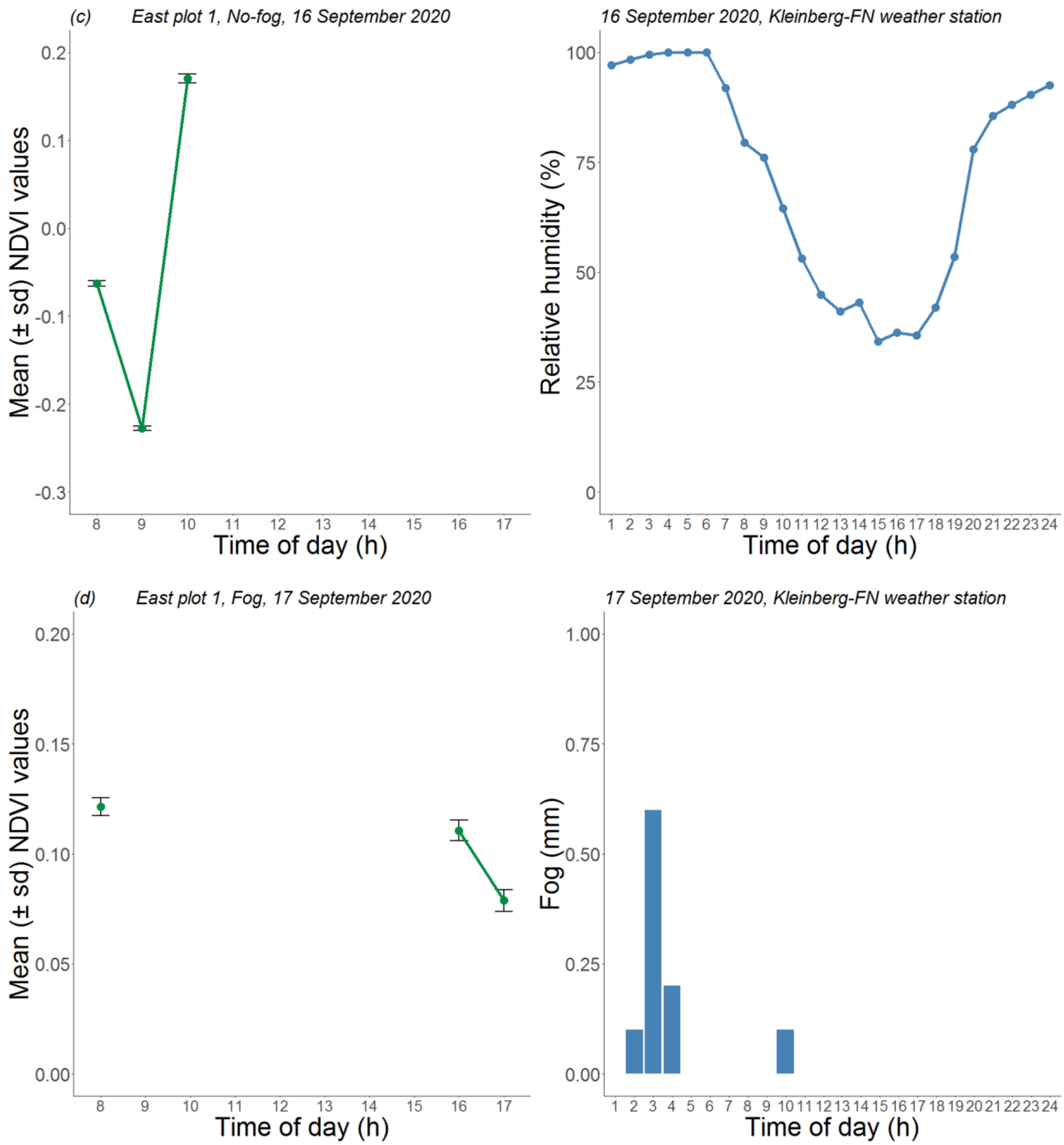

(c)
East plot 1, No-fog, 16 September 2020
Mean (± sd) NDVI values
0.2
0.1
0.0
-0.1
-0.2
-0.3
8 9 10 11 12 13 14 15 16 17
Time of day (h)
16 September 2020, Kleinberg-FN weather station
Relative humidity (%)
100
75
50
25
0
1 2 3 4 5 6 7 8 9 10 11 12 13 14 15 16 17 18 19 20 21 22 23 24
Time of day (h)
(d)
East plot 1, Fog, 17 September 2020
Mean (± sd) NDVI values
0.20
0.15
0.10
0.05
0.00
8 9 10 11 12 13 14 15 16 17
Time of day (h)
17 September 2020, Kleinberg-FN weather station
Fog (mm)
1.00
0.75
0.50
0.25
0.00
1 2 3 4 5 6 7 8 9 10 11 12 13 14 15 16 17 18 19 20 21 22 23 24
Time of day (h)

Appendix 7 Temporal Curves of Lichens' UAV-based NDVI of Plot 2 at Utuseb site.

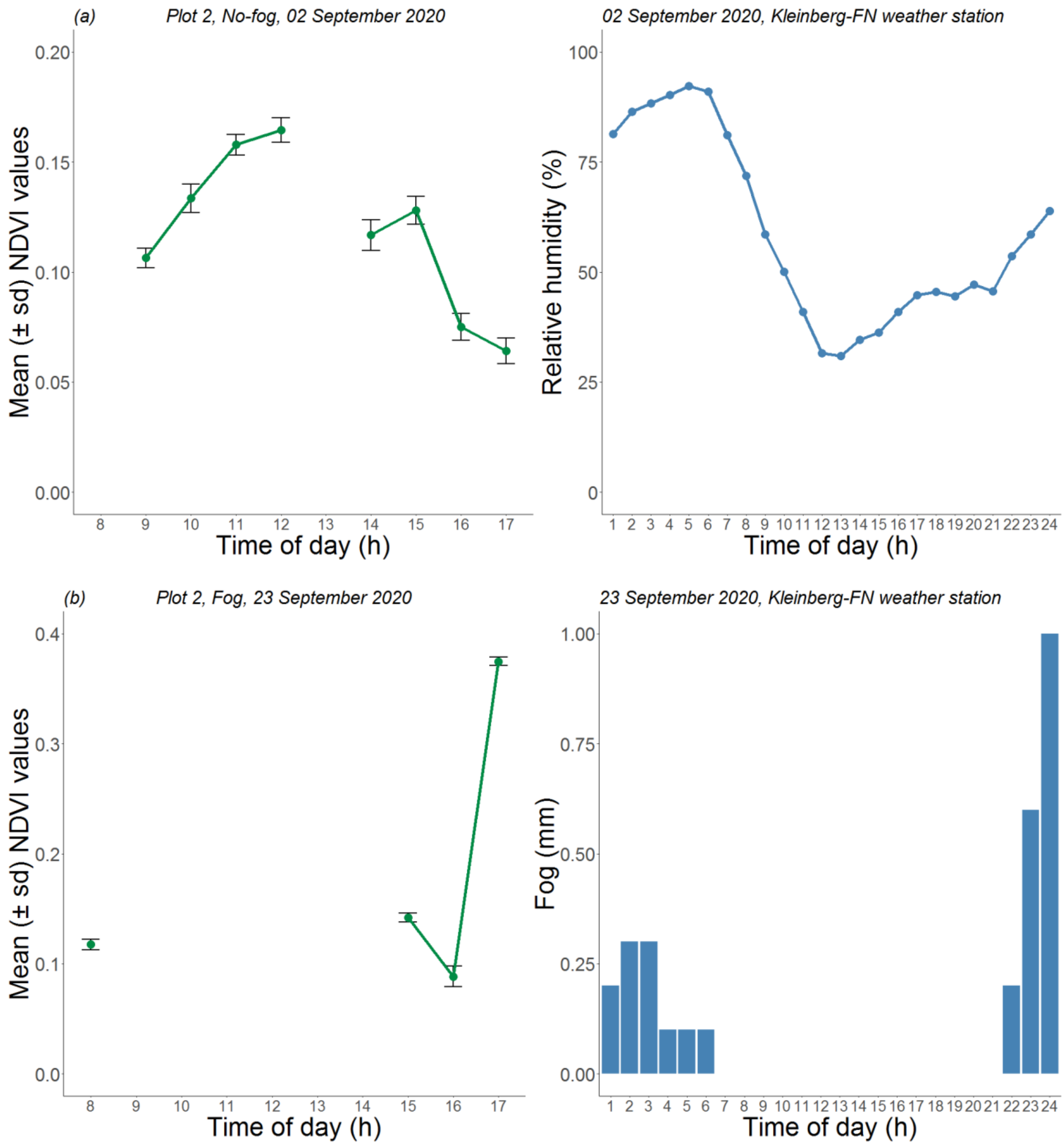

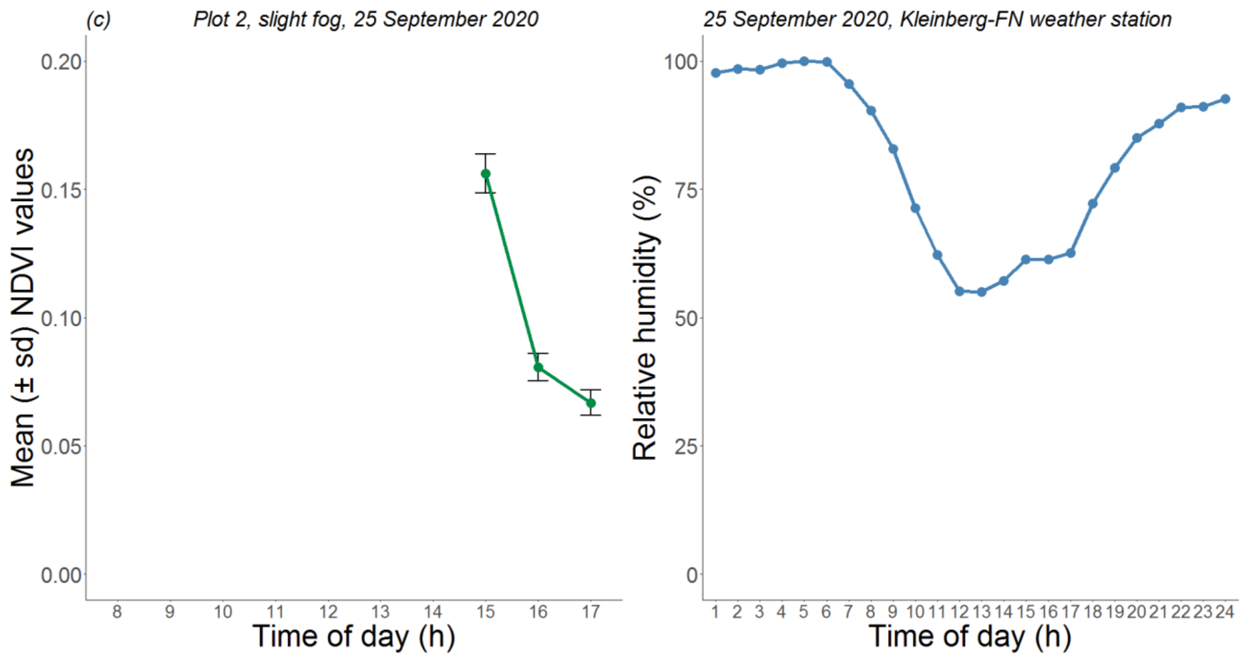

Appendix 8 Temporal Curves of Lichens' UAV-based NDVI of Plot 3 at Utuseb site.

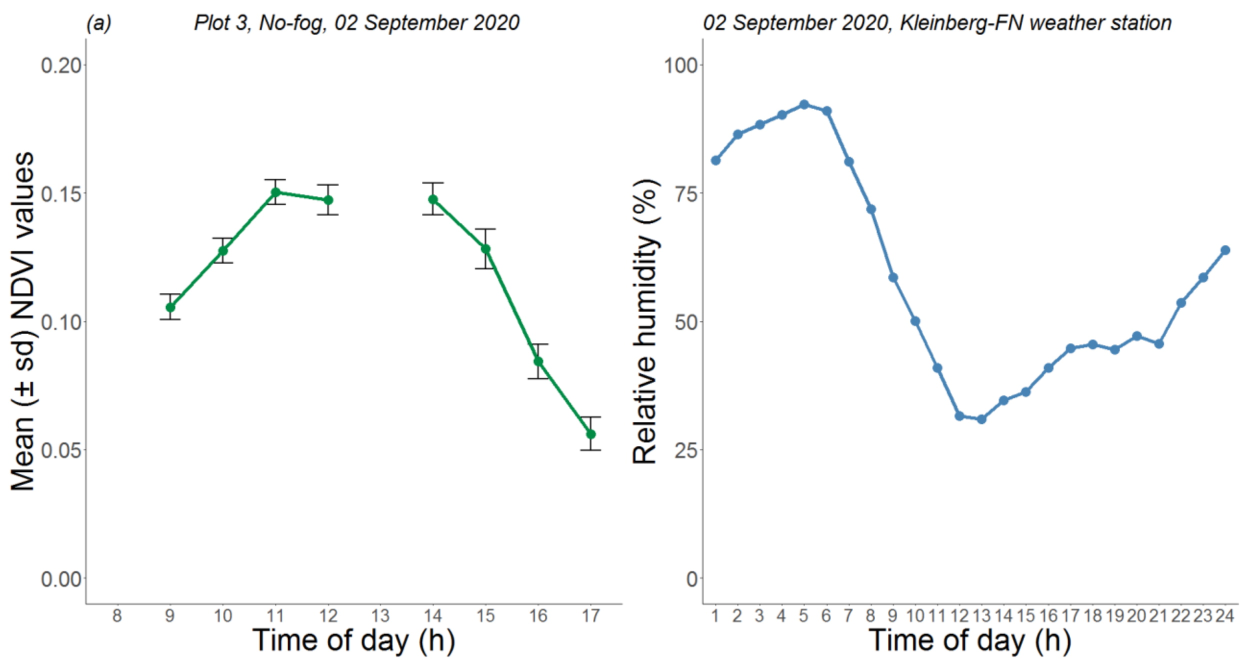

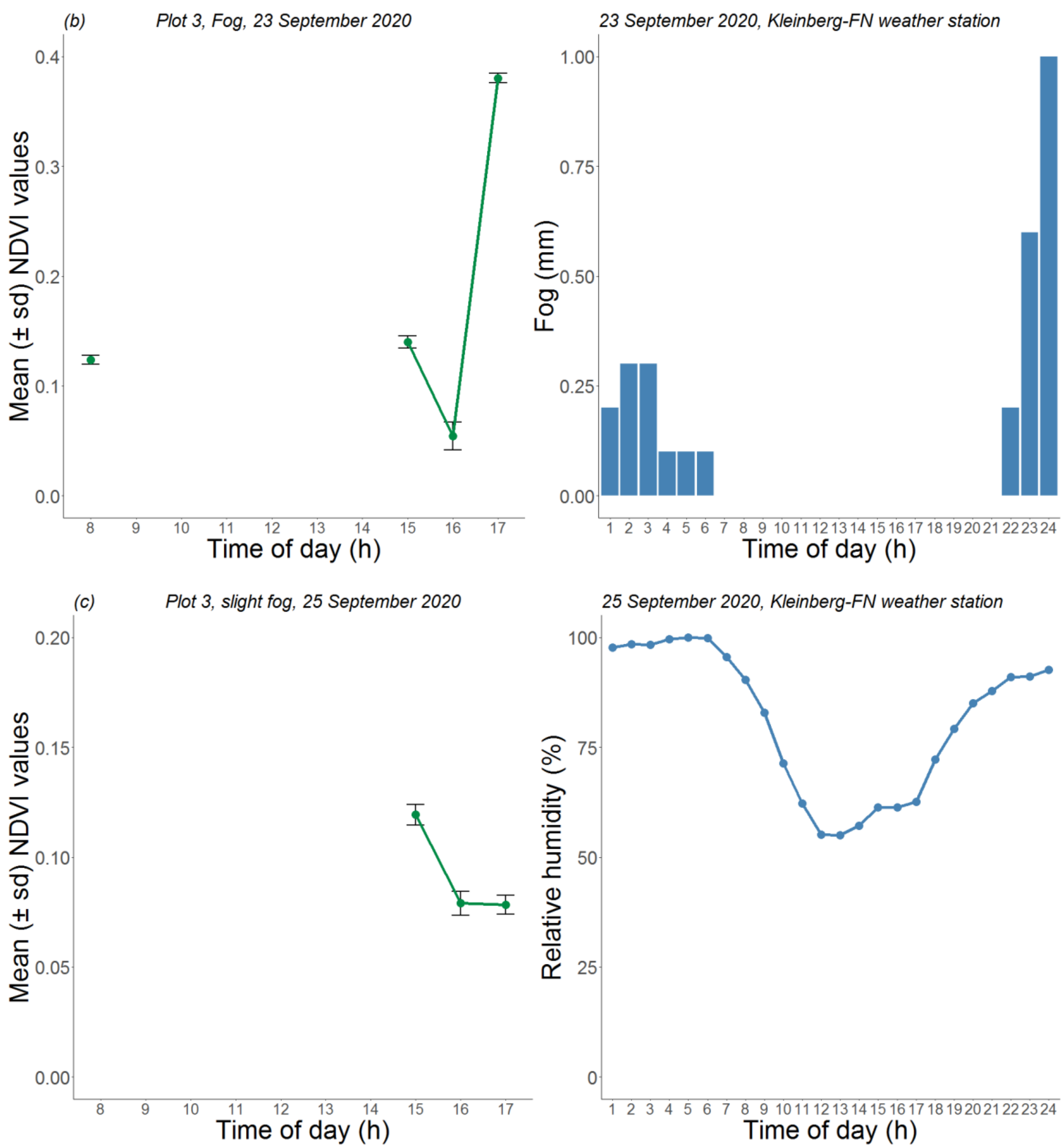
(b)
Plot 3, Fog, 23 September 2020
Mean (± sd) NDVI values
0.0
0.1
0.2
0.3
0.4
Time of day (h)
8 9 10 11 12 13 14 15 16 17
23 September 2020, Kleinberg-FN weather station
Fog (mm)
0.00
0.25
0.50
0.75
1.00
Time of day (h)
1 2 3 4 5 6 7 8 9 10 11 12 13 14 15 16 17 18 19 20 21 22 23 24
(c)
Plot 3, slight fog, 25 September 2020
Mean (± sd) NDVI values
0.00
0.05
0.10
0.15
0.20
Time of day (h)
8 9 10 11 12 13 14 15 16 17
25 September 2020, Kleinberg-FN weather station
Relative humidity (%)
0
25
50
75
100
Time of day (h)
1 2 3 4 5 6 7 8 9 10 11 12 13 14 15 16 17 18 19 20 21 22 23 24